ELSEVIER

Contents lists available at ScienceDirect

Earth-Science Reviews

journal homepage: www.elsevier.com/locate/earscirev



Astronomical time scale for the Paleozoic Era

Huaichun Wu^{a,b,*}, Qiang Fang^{a,b}, Linda A. Hinnov^c, Shihong Zhang^a, Tianshui Yang^a, Meinan Shi^a, Haiyan Li^a

- ^a State Key Laboratory of Biogeology and Environmental Geology, China University of Geosciences, Beijing 100083, China
- ^b School of Ocean Sciences, China University of Geosciences, Beijing 100083, China
- ^c Department of Atmospheric, Oceanic, and Earth Sciences, George Mason University, Fairfax, VA 22030, USA

ARTICLE INFO

Keywords: Astronomical time scale Paleozoic Era Geochronology Astronomical forcing

ABSTRACT

Milankovitch cycles are quasi-periodic fluctuations in insolation forced by variations in the Earth's astronomical parameters, inducing climate change, and in turn affecting sedimentation and the formation of cyclostratigraphy. Astronomical calibration of the cyclostratigraphy can be exploited as a high-resolution (0.02–0.4 Myr) astronomical time scale (ATS), facilitating the reconstruction of Earth's evolutionary history. The ATS is already an important geochronometer for the Cenozoic and Mesozoic eras, however, the ATS for the Paleozoic Era has yet to be fully constructed. Radioisotopic age-calibrated Milankovitch cycles have been detected in Paleozoic strata, linked to the hierarchy of sedimentary cycles deposited in the continental, paralic, and marine environments. The orbital eccentricity metronome (i.e., 405-kyr cycle) has already been used to construct the ATS for the timing of Paleozoic geological and climatic events. Here, we review Paleozoic cyclostratigraphy and develop a provisional ATS from published paleoclimatic proxy time series, which results in revisions to the timing of key geological events in the Paleozoic Era.

1. Introduction

The Paleozoic Era, named after the Greek word for "ancient life" (Sedgwick, 1838), is the earliest and longest-lasting era of the Phanerozoic Eon. It began with the Cambrian explosion at ~538.8 Ma, a major diversification of marine animals, and ended at 251.9 Ma with the end-Permian extinction, the greatest mass extinction in Earth's history (Fig. 1). The Cambrian (~538.8–486.9 Ma), Ordovician (~486.9–443.1 Ma), Silurian (~443.1–419.0 Ma), Devonian (~419.0–359.3 Ma), Carboniferous (~359.3–298.9 Ma), and Permian (~298.9–251.9 Ma) periods are all part of the Paleozoic Era (Gradstein et al., 2020).

The Paleozoic Era saw a series of geologic events covering the Earth system. Continental collisions ended in the latest Precambrian, and Pannotia began to disintegrate (Murphy et al., 2009; Scotese, 2009, 2021). The breakup of Pannotia resulted in the formation of new ocean basins such as the Iapetus and Rheic Oceans (Dalziel, 1977), and sustained sea-level transgression occurred (Haq and Schutter, 2008). Increased seafloor spreading released a large amount of $\rm CO_2$ into the atmosphere, resulting in one of the Paleozoic warmest intervals (Scotese, 2021), when sea level may have been the highest of the Phanerozoic, even higher than that of the Cretaceous (Munnecke et al., 2010).

The Cambrian period witnessed the explosive emergence of animals, marking a revolutionary shift in Earth's life system from the one dominated by microbial life in the Precambrian to the one characterized by animals in the modern period (Zhu et al., 2018). The Great Ordovician Biodiversification Event (GOBE) resulted in three times the diversity of the Cambrian, a diversification rate over four times that of the Mesozoic radiation, and a 700% increase in the number of families of marine organisms until the Late Ordovician (Sepkoski, 1995; Sepkoski and Sheehan, 1983). The oxygen isotope series indicates that the global climate began to cool during the Middle Ordovician (Trotter et al., 2008), culminating at the end of the Ordovician in the Hirnantian (~445 Ma) (Munnecke et al., 2010). This maximum glacial advance was very short, lasting <1 Myr (Ling et al., 2019). The end-Ordovician mass extinction was the first mass extinction event of the Phanerozoic, wiping out 80% of marine species and destroying the marine communities and ecosystems (Rong and Huang, 2014) (Fig. 1).

The breakup of Pannotia was followed by the assembly of the Gondwana Supercontinent. The Iapetus Ocean closed in Late Silurian, and the Rheic Ocean was between Laurentia and northern South America until the Late Devonian (Scotese, 2021). Sea levels increased slowly throughout the Silurian and Devonian (Haq and Schutter, 2008).

^{*} Corresponding author at: State Key Laboratory of Biogeology and Environmental Geology, China University of Geosciences, Beijing 100083, China. E-mail address: whcgeo@cugb.edu.cn (H. Wu).

The development of a short-lived southern polar ice cap caused a drop in sea level at the end of the Devonian (Caputo et al., 2008). The colonization of the terrestrial landscape by rooted vascular plants is considered to have been a critical factor in driving changes in the Devonian climate (Berner, 2003). The appearance of trees with deep root systems and the establishment of forests may have accelerated silicate weathering and/or organic carbon burial (Joachimski and Buggisch, 2002), resulting in multiple oceanic anoxic events (Algeo et al., 2001) and lower pCO₂ levels (Taylor et al., 2009). The Hangenberg Crisis, which lasted from the late Devonian to the early Carboniferous (Kaiser et al., 2011), eliminated \sim 21% of marine invertebrate genera, including ammonoids, conodonts, trilobites, and corals (Sepkoski, 1996) (Fig. 1).

Continental collisions had formed the supercontinent of Pangaea by the late Paleozoic and had created great mountain chains such as the Appalachians, Ural Mountains, and mountains of Tasmania (Rogers and Santosh, 2004). During the Early Carboniferous, global temperatures dropped dramatically, and the Earth's climate system entered icehouse condition (Montañez and Poulsen, 2013). At the end of the Carboniferous, the climate in equatorial Pangea became more arid and seasonal (Tabor et al., 2008). The beginning of the Permian coincided with the peak of the "Late Paleozoic Ice Age" (LPIA) (Isbell et al., 2003; Montañez and Poulsen, 2013) followed by a climatic transition from an icehouse to a greenhouse (Fielding et al., 2008). Equatorial and high-latitude surface temperatures increased substantially toward the very end of the Permian, contributing to the largest bio-crisis in Earth's history (e.g., Kump, 2018), when 95% of marine and 70% of terrestrial life disappeared from Earth (Erwin, 1994; Fan et al., 2020) (Fig. 1).

High-precision geochronology is essential to investigate and test hypotheses about the global correlation of events, the driving mechanisms for change in the Earth system, and rates of geological, biological, geophysical, and geochemical processes (Erwin, 2006). Biostratigraphy (biozones) provides rough age controls for most Paleozoic geological events, but the low temporal resolution (million-year scale) and strong bio-provincialism obstruct global correlation. High-precision radioisotopic geochronology can provide ages with 0.1% error in the Paleozoic (Burgess et al., 2014; Shen et al., 2011), but a large number of layers of volcanic ash in sedimentary strata is not forthcoming.

The insolation received on Earth's surface varies with latitudes and seasons due to (quasi-) periodic variations in Earth's orbital parameters (e.g., eccentricity, obliquity, and precession) (Milanković, 1941). Insolation-driven changes have been recorded in many sedimentary environments. Cyclostratigraphy is recognized as a subdiscipline in stratigraphy that identifies sedimentary cycles in strata caused by Earth's astronomical parameters. Comparison between the identified cycles preserved in strata and astronomical solutions has led to the development of a continuous astronomical time scale with a resolution of ~20-400 kyr. This is a revolutionary advancement for the determination of rates, causes, and consequences of environmental and faunal changes throughout geological history (Hinnov, 2013). Astronomical forcing has been suggested as one of the main drivers of climate change and some important biological, environmental, and geological events during the Paleozoic (Crampton et al., 2018; Fang et al., 2021, 2022). In this paper, we review the basic theory of cyclostratigraphy, systematically summarize the current state of Paleozoic cyclostratigraphy research, and provide future research prospects.

2. Milankovitch Theory and 405-kyr Astronomical Metronome

2.1. Milankovitch Theory

Milutin Milanković (1879–1958), a Serbian mathematician and atmospheric scientist, devoted a large part of his life to computing Earth's insolation back through time by linking the Earth's astronomical parameters to the insolation equation and proposed that climate responded to what are now known as "Milankovitch cycles" (Milanković, 1941). Milankovitch cycles include precession index, obliquity, and

eccentricity cycles and their long-term modulations, which are controlled by the Earth's orbital parameters.

Models of the Solar System's dynamic parameters involve the fundamental secular frequencies g_i and s_i of the planetary orbits (i = 1 to 8, refer to Mercury, Venus, Earth, Mars, Jupiter, Saturn, Uranus, and Neptune) (Laskar, 2020; Laskar et al., 2004, 2011). The Earth's precession index or climatic precession is defined as $e\sin(\varpi)$, where ϖ is the Earth's moving longitude of perihelion and e is orbital eccentricity (Berger, 1978; Fig. 2). The frequencies of the precession index may be expressed in terms of $k + g_i$, where k is the precession rate of the Earth's inclined rotational axis. For the time of 0 Ma, k = 50.48 arcsec/year (period of 25.7 kyr; Laskar et al., 2004). The precession rate k was faster in the geologic past, which depends on what the Earth's spin rate and dynamical ellipticity were (e.g., Eq. 7 in Berger et al., 1992). Models of k take into account the past state of the Earth-Moon system as the result of tidal dissipation (Fig. 3). The model by Laskar et al. (2004) assumes a constant tidal time lag based on present-day tidal dissipation; this leads to an unrealistic Earth-Moon distance at the Roche limit at <2 Ga. The model by Waltham (2015) instead assumes the Roche limit at 4.5 Ga and a smooth-change tidal dissipation through time. For the Cambrian (500 Ma), for example, Waltham's Milankovitch calculator, http://nm2.rhul. ac.uk/Milankovitch1.html, predicts a length-of-day of 22.2 h, k = 58.9arcsec/year (period of 22 kyr; Waltham, 2015). The model by Farhat et al. (2022) accounts for ocean tidal dissipation affected by three phases: an initial global ocean (4.5 Ga to 3.25 Ga) followed by a hemispherical ocean (3.25 Ga to 1 Ga) and finally a hemispherical ocean coupled to plate tectonics. This evolution results in an Earth experiencing multiple resonant states, with more resonances occurring toward the present day. A lookup table provided by the AstroGeo Project, https ://www.astrogeo.eu/?page_id=553, indicates, for the Cambrian at 500 Ma, a length-of-day of 21.62 h, k = 62.21 arcsec/year (period of 20.8 kyr). We can obtain the main frequencies of precession indexes by setting the Milankovitch Calculator to 0 Ma, 500 Ma, and 700 Ma (corresponding to k = 62.21 arcsec/year) respectively. The precession rate *k*, main frequencies of the precession indexes of these three models are shown in Table 1.

The obliquity or axial tilt (ϵ) of the Earth is the angle between the Earth's equatorial plane and orbital plane, and presently has an angle of 23.44° (Fig. 2). The obliquity angle oscillates between 22.5° and 24.5°, with frequencies that may be expressed in terms of $k + s_i$ (Laskar et al., 2004, 2011). As with the precession index, in the past the obliquity frequencies were higher than in the present day. The Milankovitch Calculator outputs only one obliquity frequency, and so here we use astrotarget.m (see Supplemental Materials) to obtain estimates for all four obliquity frequencies. By setting the precession rate k = 50.48, 58.9, and 62.21 arcsec/year, respectively in the Matlab function above, we can obtain the obliquity frequencies of these three models. And all of these values are shown in Table 1. Obliquity determines the angle of incidence of insolation and has a significant impact at high latitudes. During obliquity maxima, high-latitude areas receive more summer insolation and less winter insolation, resulting in large annual temperature differences. During obliquity minima, high-latitude areas receive less summer insolation but more winter insolation, resulting in small annual temperature differences (Imbrie and Imbrie, 1979).

Earth's orbital eccentricity *e* (a measure of the degree of ellipticity of the Earth's orbit around the Sun; a value of "0.0" indicates a circular orbit) is currently 0.016 (Laskar et al., 2004). Orbital eccentricity determines the Earth-Sun distance, and the total insolation (Berger, 1978). High orbital eccentricity favors high seasonality, and low orbital eccentricity favors low seasonality.

The frequency of the orbital eccentricity is expressed in terms of g_i - g_j , and they show some characteristics of chaotic drift, especially g_1 , g_3 , and g_4 (divided as unstable frequencies in Laskar, 2020), but it's not like the long monotone evolution with k. Eccentricity varies between 0.00021318 and 0.066957 due to the interaction of the Earth with the gravitational pull of the other planets (0–40 Ma solution in Laskar et al.,

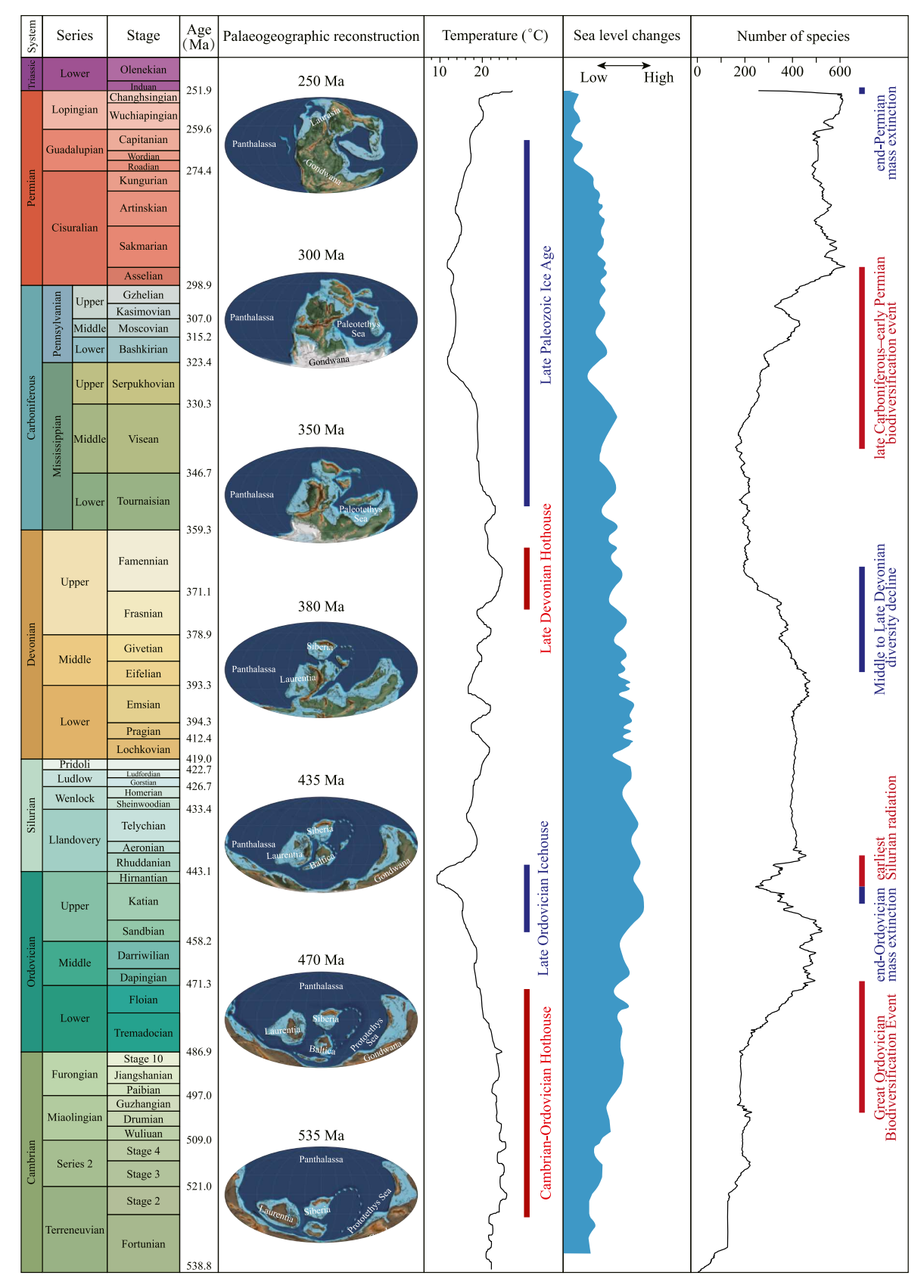


Fig. 1. Overview of tectonic Scotese et al. (2021), climate (Scotese et al., 2021), sea-level changes (Gradstein et al., 2012), and biological events (Fan et al., 2020) of the Paleozoic Era. The ages for the series boundaries were based on Gradstein et al. (2020).

2004) with the main frequencies (Laskar et al., 2004) in Table 1. The magnitude of the orbital eccentricity strongly modulates the amplitude of the climatic precession (precession index); if Earth's orbit is circular, the climatic precession will not change seasonal contrasts through that cycle. The \sim 100-kyr and \sim 405-kyr cycles have remained relatively stable throughout geologic time, particularly the 405-kyr orbital eccentricity cycle, which is controlled by frequencies g_2 and g_5 representing the precession of the perihelion of Jupiter and Venus, respectively (Laskar, 2020). Because of Jupiter's huge mass, and the gravitational interactions between the orbital perihelia of Venus and Jupiter, the 405-kyr orbital eccentricity cycle has remained stable over at least the past 250 Myr and is less influenced by the Solar System's chaotic diffusion than the \sim 100-kyr eccentricity cycles (Laskar et al., 2011).

2.2. Cyclostratigraphy

As a branch of stratigraphy, cyclostratigraphy is concerned with the sedimentary record of astronomically-caused paleoclimatic change (Fischer et al., 1990; Hilgen et al., 2004; Hinnov and Hilgen, 2012). Cyclostratigraphy is defined as "the subdiscipline of stratigraphy concerned with the identification, characterization, correlation, and interpretation of cyclic (periodic or quasi-periodic) variations in the stratigraphic record and, particularly their application to geochronology by improving the accuracy and resolution of time-stratigraphic frameworks" (Hilgen et al., 2004). The cyclic oscillations of the Earth's orbit around the Sun control the seasonal insolation obtained at a specific latitude on the Earth's surface, which drives cyclical fluctuations in the climate system. Temperature, runoff, productivity, sea level, or other climate-sensitive elements within the sedimentary deposits can all have impacts on the record of these periodic fluctuations in climate. The cyclostratigraphic study utilizes high-resolution paleoclimate proxies such as lithological changes, colour, sediment composition, isotopic ratios, environmental magnetic parameters, and paleontological abundances to extract cyclic climate fluctuations through stratigraphic successions. The aim was to identify these cyclic fluctuations in strata and determine if they were brought about by the Milankovitch cycles (Weedon, 2003).

Once the climatic cycle signals have been recovered and shown to be linked to specific Milankovitch cycles, the duration of those cycles may then be used to calibrate the geologic time. The "tuning" process involves connecting and pattern-matching cyclostratigraphic interpretations to an astronomical solution, an astronomically forced climate model, or specific astronomical terms (Meyers, 2019). A strict definition of "tuning" limits the pattern matching and correlation to astronomical solutions only. The astronomical solution for planetary orbital dynamics (orbital eccentricity and inclination) is consistent for different numerical algorithms and initial conditions for the $\sim \! 50$ Ma but diverges rapidly beyond that age (Laskar et al., 2004, 2011; Zeebe and Lourens, 2022; Zeebe, 2017). When an astronomical solution is unreliable, the astronomically forced signals are typically extracted from the sedimentary record, and their cyclic pattern is interpreted in terms of astronomical forcing using a variety of approaches to construct a "floating" astronomical time scale (FATS). Cycles in the data can be identified using ratios of detected spectral peak periods in the spatial (stratigraphic depth) domain, frequently in conjunction with independent age/duration estimates based on bio-/magnetostratigraphic and/ or radioisotopic dating (Li et al., 2018; Meyers and Sageman, 2007).

2.3. Achievements in methodology in cyclostratigraphy

Achievements in cyclostratigraphy cannot be separated from the consistent development of the methodology. The origins of cyclostratigraphy can be traced back to the pioneering work of Hays et al., 1976 in Science, who found that the oxygen isotope data exhibited significant periodicities at frequencies corresponding to cycles of

 $\sim\!23,\!000,\,\sim\!41,\!000,$ and $\sim\!100,\!000$ years, and these cycles were interpreted as reflecting variations in the Earth's orbit and rotation. To establish the cyclical patterns in the oxygen isotope data above, the authors used a mathematical technique known as spectral analysis. It involves the decomposing of a time series (in this case, the oxygen isotope data) into a series of sinusoidal components with different frequencies. Spectral analysis has become the most fundamental method for cyclostratigraphy.

Numerous innovative techniques have been developed to refine and extend the traditional cyclostratigraphic analysis. One of the most widely known techniques is the Average Spectral Misfit (ASM, Meyers and Sageman, 2007). This method uses the ratio of the periods of the astronomical orbital parameters to test spectra under different sedimentation rates. ASM provides a standardized framework for comparing different orbital timescales, allowing for the quality of a timescale to be evaluated based on its average spectral misfit and null hypothesis significance level. This approach enables a formal assessment of the quality of an orbital timescale. The development of ASM represents a milestone in the quantitative identification of astronomical signals in geological records.

Time Scale Optimization (TimeOpt, Meyers, 2015, 2019) and Correlation Coefficient (COCO, Li et al., 2018) are often considered as extensions and improvements to the ASM, and are now widely used in cyclostratigraphy. Similar to ASM, both methods employ a null hypothesis significance test for detecting astronomical signals and estimating the sedimentation rate of geological records. TimeOpt method incorporates a constraint on the modulation relationship between eccentricity and precession as an additional objective test for the existence of astronomical signals. COCO employs correlation as the estimation criterion, yielding effectiveness in signal detection.

Various other mathematical and statistical methods have been incorporated into cyclostratigraphy research to facilitate its progress toward specialization and quantification. Bayesian methods, for instance, have been introduced into cyclostratigraphy research and have

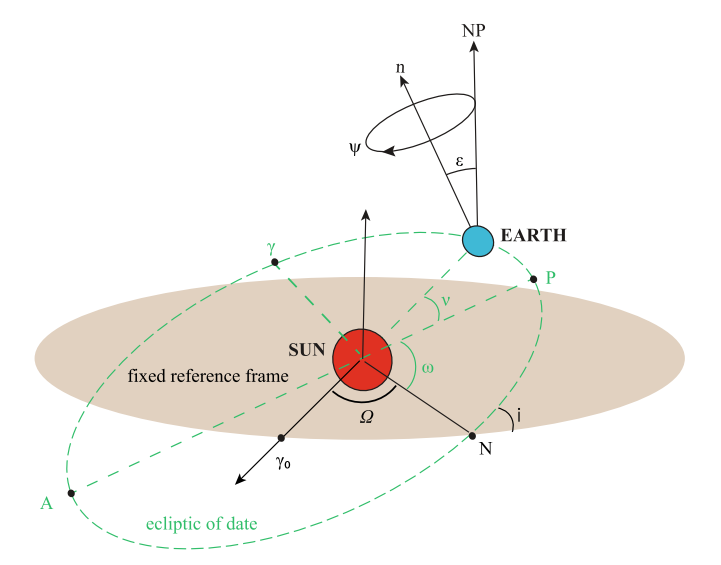


Fig. 2. Earth's astronomical parameters. Earth's orbit is elliptical and the Sun occupies one of the two foci. This orbit has a perihelion P and an aphelion A. NP is Earth's rotation axis ("North Pole"), and n is normal to the ecliptic of date. ϵ is the angle between NP and n, which is also the obliquity of the earth. ψ describes the rotation of NP, which cause vernal equinoctial point's precession. The instantaneous orbital plane of the Earth, the ecliptic of date, is referred with respect to a fixed reference frame. It has a fixed origin γ_0 , and define the ecliptic of date by the longitude of the ascending node N (Ω) , and the inclination i. The argument of perihelion ω is the angle from the line of node N to the perihelion, and the true anomaly ν the angle from the perihelion to the position of the Earth. The equinox of date γ is the intersection of the equator with the ecliptic of date.

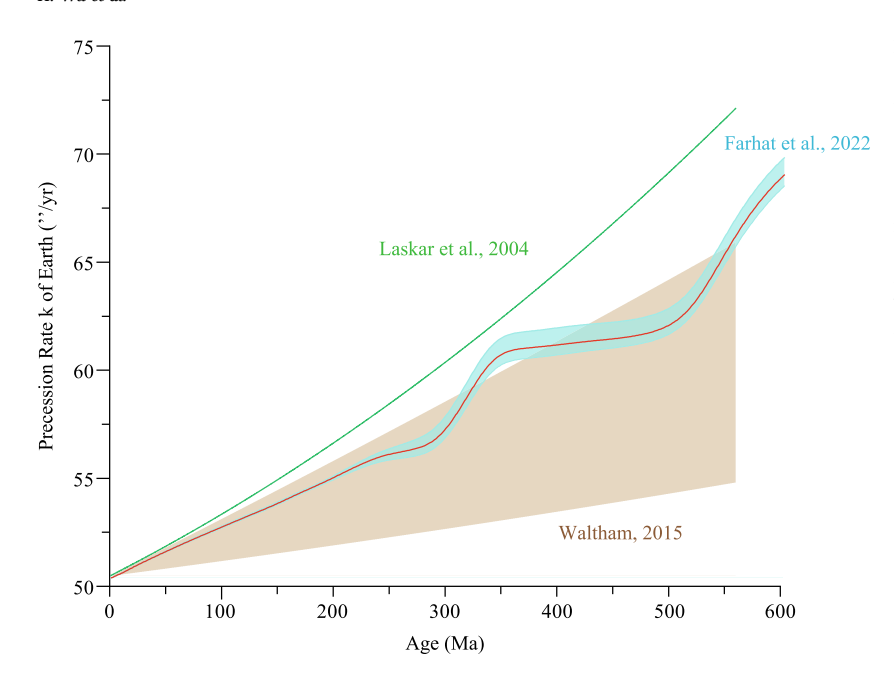


Fig. 3. The continuously changed precession rates of Earth are shown in different theoretical models. The green line shows the results of eq. (40) in Laskar et al. (2004). The orange area shows the range of estimates provided by Waltham (2015). The former may have a large error in ancient times because it is according to the current time delay of tides. The latter is deduced to be the correct lunar age, providing a reasonable margin of error. The latest model from Farhat et al. (2022) gives new estimates of it in a light blue area with a red median line (available at: https://www.astrogeo.eu/?page_id=553), which is probably closer to the truth. (For interpretation of the references to colour in this figure legend, the reader is referred to the web version of this article.)

led to the development of Bayesian Monte Carlo (Malinverno et al., 2010) and Time Scale Optimization Markov Chain Monte Carlo (Time-OptMCMC, Meyers and Malinverno, 2018). These approaches differ from ASM, TimeOpt, and COCO in that they do not provide a singular optimal solution or optimal sedimentation rate. Rather, they optimize the prior distribution based on Bayesian formula and provide the mean and standard deviation of the posterior distribution, reasonably offering the error range of the solution. Other methods, such as Spectral Moments (Sinnesael et al., 2018), have similar applications. The evolution of cyclostratigraphy has been characterized by the development of increasingly sophisticated and powerful techniques. These methods improve the reliability and scalability of cyclostratigraphy research, allowing cyclostratigraphers to identify periodicity without solely relying on a subjective interpretation of data.

2.4. Stability of the 405-kyr orbital eccentricity during the Paleozoic Era

The stability of the 405-kyr orbital eccentricity cycle has inspired its

Table 1 Precession rate k, Precession index $(k+g_i)$, Obliquity frequencies $(k+s_i)$, orbital eccentricity frequencies in the three models.

Parameter	Laskar et al., 2004	Waltham, 2015	Farhat et al., 2022				
	0 Ма	500 Ma	500 Ma				
k (arcsec/year)	50.48	58.9	62.21				
Precession indexes (kyr ⁻¹)							
$k + g_1$	1/23.67	1/20.5	1/19.5				
$k + g_2$	1/22.37	1/19.5	1/18.6				
$k + g_3$	1/19.10	1/17.0	1/16.2				
$k + g_4$	1/18.95	1/16.9	1/16.1				
Obliquity frequencies (kyr ⁻¹)							
$k + s_1$	1/54	1/39.8	1/36.1				
$k + s_2$	1/41	1/32.4	1/29.9				
$k + s_3$	1/39.5	1/31.5	1/29.5				
$k + s_4$	1/29	1/25.0	1/23.5				
Orbital eccentrici	ty frequencies						
g ₄ -g ₃	$\sim 1/2.4 \ {\rm Myr^{-1}}$	_	_				
g ₁ -g ₅	~1/1.0 Myr-1	_	_				
g ₂ -g ₅	$\sim 1/405 \; \mathrm{kyr}^{-1}$	_	_				
g ₃ -g ₂	$\sim 1/131 \; \mathrm{kyr}^{-1}$	_	_				
g ₄ -g ₂	$\sim 1/124 \text{ kyr}^{-1}$	_	_				
83-8 ₅	$\sim 1/99 \; kyr^{-1}$	-	-				
8 4 -8 5	\sim 1/95 kyr $^{-1}$	_	-				

use as a fundamental calibration period for cyclostratigraphy (Hinnov, 2018; Hinnov and Hilgen, 2012; Laskar, 2020). For the Paleozoic records, it is difficult to verify that the astronomical forcing caused cyclic deposition in stratigraphy. Radioisotopic dating techniques have been improved to provide independent chronological constraints on Paleozoic Milankovitch cycle records. The Permian of South China and the Carboniferous of Ukraine are used here as examples of the stability of the Milankovitch cycles constrained by high-resolution radioisotopic ages.

The Meishan section, located in Changxing County, Zhejiang Province, South China, is the stratotype section for the Changhsingian stage with the Global Stratotype Section and Point (GSSP) for the Permian-Triassic and the Changhsingian/Wuchiapingian boundaries (Jin et al., 2006a, 2006b). The Meishan section comprises the Longtan, Changxing, and Yinkeng formations. The Longtan Formation consists of dolomitized calcirudite with limestone, siltstone, and phosphate fragments. Changxing Formation includes siliceous bioclastic lime mudstone with thinly interbedded cherts. Yinkeng Formation mainly consists of laminated calcareous shales with minor intercalations of thin-bedded limestones. Wu et al. (2013) used the cyclostratigraphy method to obtain a high-resolution series of magnetic susceptibility (MS) of Meishan and anhysteretic remanent magnetization (ARM) at Shangsi. MS and ARM showed significant cyclic variations, with high values associated with high clay or mud contents and low values associated with carbonate-rich strata. High-precision U—Pb ID-TIMS ages of 252.10 \pm 0.06 Ma, 252.28 \pm 0.08 Ma, 252.50 \pm 0.11 Ma, 252.85 \pm 0.11 Ma, 253.45 \pm 0.08 Ma, and 253.49 \pm 0.07 Ma were obtained at Meishan, and eight were obtained from the Shangsi section (Shen et al., 2011). An age of 252.28 Ma was used to anchor the cyclicity to absolute time. The 405-kyr tuning resulted in FATS ages that are consistent with the other U-Pb dates, confirming that the constructed FATS for the late Permian is faithful.

The Carboniferous successions, particularly upper Mississippian to Pennsylvanian shallow marine deposits, are characterized by "cyclothem" (Wanless and Shepard, 1936) that represents repetitive stratigraphic stacking depositional sequences with thicknesses ranging from meters to a few tens of meters (Cecil et al., 2014; Heckel, 2008). The sequence stratigraphic, biostratigraphic, and radiometric ages have helped to constrain these widespread strata rhythms (Davydov et al., 2010; Izart et al., 1996, 2003a, 2003b; Schmitz and Davydov, 2012). Cyclothems in Carboniferous stratigraphy are thought to have formed as a result of the growth and decay of Gondwanan glaciation (Heckel, 1994, 2013; Heckel et al., 2007). Based on stratigraphic stacking

patterns and high-precision radiometric ages, studies on the late Paleozoic cyclothemic successions in the Donets Basin presented the onlap-offlap history from late Visean to Gzhelian, and recognized scales of sequences as ~140 kyr and ~ 480 kyr (Eros et al., 2012). It suggests the teleconnection between the high-latitude ice sheet and low-latitude climate pacing with astronomical cycles. Sedimentary patterns and U—Pb zircon ages of intercalated volcanic tuffs from the Ostrava Formation in the foreland Upper Silesian Basin along the Czech-Polish border, show ~100-kyr eccentricity forcing (Jirásek et al., 2018). When combining biostratigraphic and radiometric ages, the eccentricity-forced cyclothems have the potential to estimate the timing of major global events, correlate stratigraphy from different regions, and refine the geological time scale (Fielding, 2021), which is an important part of Carboniferous cyclostratigraphic studies.

2.5. Construction of a 405-kyr timescale for the Paleozoic geochronological framework

Modeling of the 405-kyr metronome from 0 to 249 Ma was accomplished by filtering a down-sampled version of the La2004 orbital eccentricity solution in GTS2012; 614 orbital eccentricity cycles were delineated using this method through the Cenozoic and Mesozoic eras (Hinnov and Hilgen, 2012; Huang, 2018). Based on the relatively stable 405-kyr period, a geochronological framework was tentatively established through artificial calculations due to the lack of precise astronomical solutions for the Paleozoic Era. The average duration of the 614 long eccentricity cycles from 0 to 249 Ma, 405.5 kyr, was used as the period for the orbital eccentricity metronome for the Paleozoic Era. The interval of 249-249.41 Ma was classified as E615 and 715 long eccentricity cycles from E615 to E1329 were constructed back in geologic time to 538.93 Ma. These cycles were plotted using a simple sinusoidal curve, with each cycle beginning and ending in a trough. Although this method does not accurately reflect the true orbital eccentricity cycles, it is useful for incrementalizing the Paleozoic time scale and establishing a geochronological framework in the absence of a precise astronomical solution. Re-analysis of the selected Paleozoic sections using 405-kyrtuning was shown in Table 2.

3. The current status of the FATS for the Paleozoic Era

3.1. Permian

The Permian Period comprises the Lopingian, Guadalupian, and Cisuralian three epochs, spanning from artificially constructed E622 to E737 (Fig. 4). The Lopingian comprised the Changhsingian and Wuchiapingian, lasting 7.6 Myr from 259.5 to 251.9 Ma (Henderson et al., 2020). The Capitanian, Wordian, and Roadian stages are included in the Guadalupian Epoch with a duration of 14.9 Myr (274.4–259.5 Ma). The Cisuralian Epoch lasted for 24.4 Myr (298.9–274.4 Ma) and is subdivided into the Kungurian, Artinskian, Sakmarian, and Asselian stages. A total of 41 conodonts zonations, 27 fusulinid, and benthic foraminifer zonations, and 24 ammonoid zonations were used in GTS2020 for subdividing the Permian, in which conodont zonations are the favored fossils for the Permian correlation and have a reference to the GSSP (Henderson et al., 2020).

3.1.1. The Lopingian Epoch

3.1.1.1. Changhsingian and Wuchiapingian stages. The Changhsingian Stage is the last stage of the Permian, one of the shortest stages in the Phanerozoic, with a 2.3-Myr duration from 254.2 ± 0.4 Ma to 251.9 ± 0.3 Ma. The top of the Changhsingian witnessed the bleak final act of the Permian, characterized by a mass extinction, dramatic negative carbon isotope and strontium isotope shifts, and major sea-level regression (Payne et al., 2004; Shen et al., 2011; Song et al., 2013). The GSSP for

PTB is defined by the first appearance datum (FAD) of *Hindeodus parvus* at the base of Bed 27c at Meishan, and has an interpolated age of 251.902 \pm 0.024 Ma (Burgess et al., 2014; Ogg and Chen, 2020). The base of the Changhsingian Stage was defined by the FAD of conodont *Clarkina wangi* and its GSSP was within Bed 4 in Section D at Meishan, Changxing County, China (Jin et al., 2006b). Wuchiapingian Stage started at 259.5 \pm 0.4 Ma and ended at 254.2 \pm 0.4 Ma, lasting $\sim\!5.3$ Myr (Henderson et al., 2020). Significant global sea-level regression at the end of the Guadalupian Series resulted in the absence of marine sediment in many regions, while a few sections contained a continuous sequence across the Capitanian/Wuchiapingian boundary. The GSSP for Wuchiapingian Stage is located in the Penglaitan section and is defined by the FAD of conodont *C. postbitteri postbitteri* (Jin et al., 2006a).

The FATS for the Lopingian Series was constructed by Wu et al. (2013). The combined 405-kyr cycles identified from the MS and ARM series with the U-Pb age from the Meishan and Shangsi sections in South China (Fig. 4A). FATS indicated a 7.793-Myr duration for the Lopingian series. A comparable age for the PTB (~252.10 Ma) was estimated in both studied sections, while the age for the Wuchiapingian/ Changhsingian boundary varied in different sections, resulting in 1.87 Myr and 2.015 Myr for the Changhsingian Stage in the Meishan and Shangsi sections, respectively (Wu et al., 2013). Cyclostratigraphic analysis of GR and non-U GR data from South China's GFD-1 revealed long and short eccentricity, obliquity, and precession Milankovitch cycles (Wang et al., 2020). Third-order sea-level changes are controlled by long-term modulations. During the Wuchiapingian greenhouse, thirdorder sea-level variations were mainly forced by the 2.4-Myr eccentricity cycle, whereas the 1.2-Myr obliquity cycle forcing was stronger during the Changhsingian cooling interval (Wang et al., 2020).

FATS was used to constrain the duration of the $\delta^{13}C_{carb}$ shifts. The maximum extinction interval in the end-Permian was constrained in the Meishan section. According to the FATS, the maximum extinction interval at Meishan lasted 83 kyr (Wu et al., 2013), which is shorter than the 700 kyr previously estimated at Shangsi (Huang et al., 2011), but close to the result of <60 kyr from Rampino et al. (2000). The duration of the end-Permian mass extinction at Meishan was estimated to be <40 kyr and a < 6 kyr duration for the sharp $\delta^{13}C_{carb}$ negative shift from Bed 24e to Bed 25 in the Meishan section (Li et al., 2016). Recently, the end-Permian carbon isotope excursions were re-constrained using the FATS from the continuous deposits with a high sedimentation rate (~22.4 cm/kyr), with an onset duration of 15 kyr and a total duration of 109 kyr, which are slightly longer than those from South China (Cui et al., 2021).

3.1.2. The Guadalupian Epoch

3.1.2.1. Capitanian, Wordian and Roadian stages. According to GTS2020, the bases of the Capitanian, Wordian, and Roadian stages were defined by the FAD of the conodont Jinogondolella postserrata, J. aserrata and J. nankingensis (Glenister et al., 1999; Mei and Henderson, 2001). The Capitanian Stage, Wordian Stage, and Roadian Stage started from 264.3 \pm 0.4 Ma, 269.2 \pm 0.4 Ma, and 274.4 \pm 0.4 Ma, with a duration of 4.8 Myr, 4.9 Myr, and 5.2 Myr in GTS2020, respectively (Henderson et al., 2020) (Fig. 4).

Based on the results from South China, the duration of the Capitanian Stage was assigned as 2.62 Myr (Fang et al., 2017), shorter than the 3.85 Myr in the Tieqiao section (Xue et al., 2015) and 5.3 \pm 0.8 Myr in GTS2012. While the Capitanian stage in the Shangsi section was estimated with a duration of 1 \pm 0.4 Myr, far less than the 5.3 \pm 0.8 Myr in GTS2012, which may be attributed to the absence of marine sediment at the top of Capitanian (Fang et al., 2015) (Fig. 4B). Using the 405-kyr eccentricity cycles identified in the ARM series from the Maokou Formation of the Shangsi section, the durations of Wordian Stage were estimated as 2.9 \pm 0.4 Myr (Fang et al., 2015). An \sim 580-kyr FATS was constructed for the Wordian–Capitanian interval on the Apache Mountains B section using the MS data, and the ages were also projected onto

this GSSP at Nipple Hill by comparing the magnetostratigraphy susceptibility datasets (Ellwood et al., 2012). Spectral analysis of lithologic rank data from the chert-mudstone sequences in the Upper Chert-Mudstone Member of the Gufeng Formation (Roadian-Capitanian), Chaohu region, South China, revealed orbital forcing in the formation of chert-mudstone couplets (Yao and Hinnov, 2019; Yao et al., 2015). The durations of three radiolarian assemblages and chert sequences were estimated using the 32-kyr obliquity tuning series (Yao et al., 2015). The Fourier transform and multi-taper analyses of the MS data on Roadian GSSP in the Stratotype Canyon section show long eccentricity, short eccentricity, obliquity, and precession signals, allowing the construction of ~1.32-Myr FATS for the Roadian GSSP intervals (Ellwood et al., 2012). The duration of Roadian was estimated to be 3.7 \pm 0.4 Myr using the constructed FATS on Shangsi section, in agreement with the ~ 3.5 Myr in GTS2012 (Fang et al., 2015), but much shorter than 5.2 Myr in GTS2020, which can be attributed to the variation of the age of basal

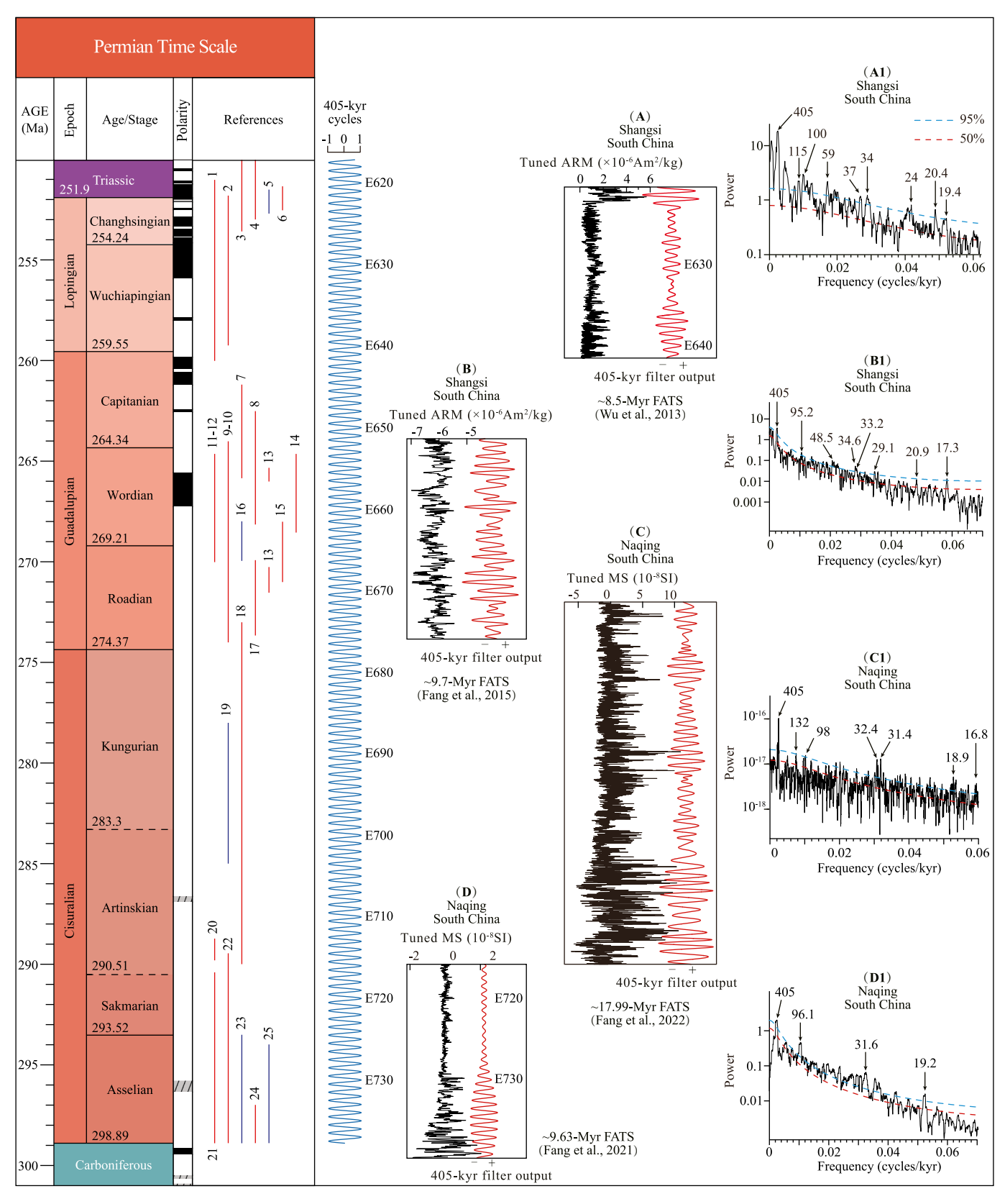
The cyclostratigraphic study was limited to the continental records. Spectral analyses of the GR series from a mid-latitude lacustrine sequence of the Lucaogou Formation ($\sim\!268{-}270$ Ma) in the Junggar Basin reveal the Milankovitch cycles, including long eccentricity, short eccentricity, obliquity, and precession cycles (Huang et al., 2020). A duration of $\sim\!3$ Myr has been estimated for the Lucaogou Formation in

the Jimusar Sag of the eastern Junggar Basin (Huang et al., 2020). The evidence for the orbital forcing from the fluvial succession, Abrahamskraal Formation (~264.6–268.5 Ma), in the Karoo Basin of the Northern Cape Province, South Africa, further confirmed the astronomical theory and suggested that monsoonal control in precipitation could even influence the mid-latitude climate (Lanci et al., 2022).

The third-order sea-level sequence was suggested to be controlled by the 1.2-Myr long-term obliquity modulation cycle. Based on lithological cycles and spectral analysis of grain size and GR, the cyclicities in the Kennedy Group (~267–270 Ma) of the Carnarvon Basin, Western Australia, may be attributed to eustatic sea-level changes forced by Milankovitch cycles (Lever, 2004). Comparing the durations of long-term obliquity cycles from the Maokou Formation, Shangsi Section, South China, with the durations of third-order sea-level sequences in GTS2012, Fang et al. (2015) proposed that global third-order sea-level sequences were astronomically paced by long-term obliquity cycle at the end of the LPIA. Furthermore, the sedimentary records from the Lucaogou Formation, Junggar Basin, also suggested that this cycle forced the basin sedimentary processes, showing a link between middle-latitude lacustrine depositional systems and astronomically paced high-latitude continental ice volume (Huang et al., 2020).

Table 2Re-analysis of the selected Paleozoic sections using 405-kyr-tuning and MTM power-spectra analysis. Span (Myr) and age Limits (Ma) are based on the tuning results.

		•	-				
Location	Geological time	Proxy	Span (Myr)	Spectral cycles (kyr)	AssignedE-cycles	Age limits (Ma)	References
Shangsi (China)	Latest Capitanian–earliest Triassic	ARM	8.5	E: 405 (tuned); e: 115, 100, 95; O: 34; P: 20.4, 19.4	E620-E641	259.8–251.3	Wu et al. (2013)
Shangsi (China)	Early Roadian–earliest Capitanian	ARM	9.7	E: 405 (tuned); e: 95.2; O: ~44, ~33; P: 20.9, 17.3	E651-E675	273.9–264.2	Fang et al. (2015)
Naqing (China)	Artinskian–early Roadian	MS	18.0	E: 405 (tuned); e: 132, 105, 98; O: 32.4, 31.4; P: 18.9, 16.8	E671–E715	290.0-272.0	Fang et al. (2022)
Naqing (China)	Latest Gzhelian–earliest Artinskian	MS and GR	9.6	E: 405 (tuned); e: 99, 96.1; O: 31.6; P: 19.2, 17.8, 15.8	E715 -E739	299.7–290.0	Fang et al. (2021)
Naqing (China)	Latest Visean–Gzhelian	MS	33.9	E: 405 (tuned); e: 136, 122, 96; O: 31; P: 22.9, 19.7	E737-E821	332.5–298.6	Wu et al. (2019)
Luokun (China)	Serpukhovian and Moscovian	MS	8.3 and 5.1	E: 405 (tuned); e: 136, 104, 100; O: ~34; P: 19, 18.7, 17.8, 15.9	E765–E777 and E797–E817	331.6–323.2 and 315.3–310.2	Fang et al. (2018a)
Lali (China)	Famennian	Ca (%)	14.4	E: 405 (tuned); e: 134, 100	E879-E915	371.9–357.5	Ma et al. (2020)
Alberta (Canada)	Frasnian	MS	6.5	E: 405 (tuned); e: 114, 83.6	E918-E934	378.9–372.4	De Vleeschouwer et al. (2012a)
Dinant Synclinorium (Belgium)	Givetian	MS	4.4	E: 405 (tuned); e: 100; O: 33	E938-E949	385.3–380.9	De Vleeschouwer et al. (2015)
Appalachian Basin (USA)	Eifelian	Ti (%)	4.2	E: 405 (tuned); e: 95; O: 33	E961-E971	393.9-389.7	Pas et al. (2020)
Pod Barrandovem (Czech Republic)	Lochkovian–earliest Emsian	MS	13.4	E: 405 (tuned); e: 95; O: 33.4, 27.8; P: 21.1	E999-E1032	419.0–405.6	Da Silva et al. (2016)
Shuanghe (China)	Aeronian	TOC	1.3	E: 405 (tuned); e: 111.7; O: 34.3, 29.8; P: 23.3	E1083-E1087	440.5–439.2	Jin et al. (2020)
Shuanghe (China)	Rhuddanian–early Aeronian	TOC	3.7	E: 405 (tuned); e: 80.6; O: 30; P: 22.1, 18.5	E1087-E1096	444.2–440.5	Jin et al. (2020)
Wanhe (China)	Early Katian–early Hirnantian	ARM	7.4	E: 405 (tuned); e: 125, 95; O: 33.8; P: 21.2, 19.8, 18.3, 17.9	E1095–E1113	451.6–444.2	Zhong et al. (2020)
Core EHD1 (China)	Late Katian–Hirnantian	Fe (%)	5.0	E: 405 (tuned); e: 128; O: 38; P: 21.3, 20.4	E1096-E1108	448-443.07	Lu et al. (2019)
Dawangou (China)	Late Darriwilian–early Sandbian	MS	4.9	E: 405 (tuned); e: 100; O: 31.5; P: 21.2, 20	E1132-E1140	462.2–457.3	Fang et al. (2019)
Huangnitang and Core CJ-3 (China)	Late Floian–late Darriwilian	MS	12.4	E: 405 (tuned); e: 130, 101; O: 33.7, 31 P: 21.3, 20, 18.8	E1143-E1173	473.4–461.0	Zhong et al. (2018)
Liangjiashan and Huanghuachang (China)	Late Tremadocian–Dapingian	Ca (%)	9.5	E: 405 (tuned); e: 100, 91; O: 33, 31; P: 21, 19.6, 17.5	E1163–E1181	478.4–469.1	Ma et al. (2019a)
Core Albjära-1 (Sweden)	Guzhangian–early Tremadocian	Al (%)	16.0	E: 405 (tuned); e: 108, 94; O: 30.9; P: 20.8	E1194-E1233	499.9–483.9	Zhao et al., (2022)
Luoyixi (China)	Late Drumian–earliest Guzhangian	MS	1.4	E: 405 (tuned); e: 100.9; O: 30.7; P: 19.2, 18.2	E1235-E1237	501.2–499.8	Fang J et al., (2020)
Leshan (China)	Early Stage 2–Late Stage 3	GR	10.8	E: 405 (tuned); e: 131,114, 85; O: 31.9; P: 20	E1271-E1298	526.2-515.4	Zhang et al., (2022)



(caption on next page)

Fig. 4. Our reanalysis and 405 kyr tuning of selected series for the Permian FATS. Chronostratigraphy columns on the left were modified from the GTS2020 integrated stratigraphy (Henderson et al., 2020). (A) ARM series and the 405 kyr filter output (red curve, passband: 0.002469 ± 0.00075 cycles/kyr) of the Shangsi Section, South China (the original data is from Wu et al., 2013). (B) ARM series and the 405-kyr filter output (red curve, passband: 0.00246 ± 0.0015 cycles/kyr) of the Shangsi Section, South China (the original data is from Fang et al., 2015). (C) MS series and the 405 kyr filter output (red curve, passband: 0.00247 ± 0.00033 cycles/kyr) of the Naqing Section, South China (the original data is from Fang et al., 2022). (D) MS series and the 405 kyr filter output (red curve, passband: 0.00247 ± 0.00033 cycles/kyr) of the Naqing Section, South China (the original data is from Fang et al., 2022). (D) MS series and the 405 kyr filter output (red curve, passband: 0.00246 ± 0.0003 cycles/kyr) of the Naqing Section, South China (the original data is from Fang et al., 2021). (A1) is 3π MTM power spectra of series in A. (B1) and (C1) are 2π MTM power spectra of series in B and C, respectively. (D1) is 4π MTM power spectra of series in D. References are listed as 1—Wu et al. (2013), 2—Wang et al. (2020), 3—Huang et al. (2011), 4—Li et al. (2016), 5—Peng et al. (2008), 6—Rampino et al. (2000), 7—Xue et al. (2015), 8—Fang et al. (2017), 9—Fang et al. (2015), 10—Fang et al. (2018b), 11—Yao et al. (2015), 12—Yao and Hinnov (2019), 13—Ellwood et al. (2012), 14—Lanci et al. (2022), 15—Huang et al. (2020), 16—Lever (2004), 17—Li et al. (2018), 18—Fang et al. (2022), 19—Pfeifer et al. (2020), 20—Huang et al. (2021), 21—Fang et al. (2021), 22—Schmitz and Davydov (2012), 23—Ueno et al. (2013), 24—Huang et al. (2021), 25—Gannon et al. (2022). (For interpretation of the references to colour in this figure legend, the reader is referred to the web version of

3.1.3. Cisuralian Epoch

3.1.3.1. Kungurian and Artinskian stages. The Kungurian Stage was proposed to have lasted for 8.9 Myr from 283.3 ± 0.4 to 274.4 ± 0.4 Ma, including 7 conodont zones (Henderson et al., 2020). The GSSP of the basal Kungurian has yet to be defined, which is hampered by poor fossil successions and the lack of additional good makers. This is probably based on the conodont lineage of *Neostreptognathodus* (Chernykh et al., 2020b). The Artinskian Stage lasted for 7.2 Myr, ranging from 290.5 ± 0.4 to 283.3 ± 0.4 Ma, containing 3 conodont zones. Although the base-Artinskian GSSP at the Dal'ny Tulkas section in Russia has not been ratified by IUGS, the FAD of the conodont *Sweetognathus asymmetrica* within the chronomorphocline *S. binodosus* to *S. anceps* to *S. asymmetrica* is regarded as the key reference for the base of the Artinskian (Chuvashov et al., 2013).

A systematic cyclostratigraphic investigation of the late Cisuralian (Artinskian and Kungurian stages) was recently conducted using highresolution GR and MS data from Naqing section, South China (Fang et al., 2022) (Fig. 4C). The ~18-Myr FATS from 290.0 Ma to 272.01 Ma was constructed using the forty-five 405-kyr cycles identified in the MS series, and the uppermost Kungurian Stage (Cisuralian-Guadalupian boundary) was estimated at 272.83 \pm 0.2 Ma, supporting a radioisotopic date (273.01 \pm 0.14 Ma) for this boundary in South China (Wu et al., 2017). Furthermore, cyclostratigraphic analyses of the MS data from a continental succession, the Salagou Formation (late Artinskian to middle Kungurian), south-central France, revealed the astronomical forcing in the climate change recorded in the loessite of low-latitude Pangea (Pfeifer et al., 2020). The Salagou Formation was estimated to have lasted for ~9-10 Myr (Pfeifer et al., 2020). The cyclostratigraphic analyses of the DEN and TOC series from the Lucaogou Formation suggested that the lake level variations and organic matter burial were forced by long-term obliquity cycles and ~ 170 kyr cycles (Wei et al., 2023). By tuning the DEN series to stable 405-kyr long-eccentricity cycles, an ~4.2-Myr FATS was established for the Lucaogou Formation (Wei et al., 2023).

3.1.3.2. Sakmarian Stage. The Sakmarian Stage lasted about 3 Myr, from 293.5 \pm 0.4 to 290.5 \pm 0.4 Ma, including 2 conodont zones. The base-Sakmarian GSSP is defined by the FAD of the conodont Mesogondolella monstra in the Usolka Section (Chernykh et al., 2020a). The widespread glacial eustasy resulted in the stratigraphic cyclicity in shallow marine successions which extended from the Carboniferous to lower Sakmarian, and then is replaced by the third-order sequences, which are attributed to the acme and then the waning of the LPIA. The duration of the Sakmarian Stage was estimated at 4.9 Myr based on the radiometric ages, biostratigraphic correlation, and cyclostratigraphic study (Schmitz and Davydov, 2012). As mentioned above, the cyclostratigraphic study result from Naqing, suggested a 294.1 \pm 0.2 Ma age for the base of the Sakmarian Stage and an estimated duration of 4 ± 0.2 Myr for Sakmarian Stage (Fang et al., 2021) (Fig. 4A). Furthermore, the juxtaposed climatic proxies and indicators across blocks and latitudes suggested that the climatic changes were in pace with 1.2-Myr obliquity cycles during late Paleozoic deglaciation in the early Permian (Fang

et al., 2021).

3.1.3.3. Asselian Stage. The Asselian Stage lasted 5.4 Myr, from 298.9 \pm 0.4 to 293.5 \pm 0.4 Ma, and contained 7 conodont zones. The base-Asselian GSSP is defined by the FAD of the conodont Streptognathodus isolatus in Aidaralash Creek, Atobe region, northern Kazakhstan, representing the boundary between the Carboniferous and Permian (Davydov et al., 1998). Both marine (Schmitz and Davydov, 2012; Ueno et al., 2013) and continental successions (Huang et al., 2021) have been achieved. The relatively complete FATS of the Asselian Stage was constructed using high-resolution MS and GR data from a deep-marine succession in Naging, South China (Fang et al., 2021). The top of the Asselian Stage has refined to 294.1 \pm 0.2 Ma when an age of 298.57 Ma was adopted for the Carboniferous/Permian boundary in the Naqing. Thus, the duration of the Asselian Stage was estimated at 4.5 \pm 0.2 Ma (Fang et al., 2021) (Fig. 4D). In addition, Huang et al. (2021) constructed an ~5.0-Myr FATS for the Fengcheng Formation (Gzhelian to earliest Asselian), an alkaline lake succession from the Junggar Basin, using 405-kyr eccentricity tuning datasets.

3.2. Carboniferous

The Carboniferous began at 359.3 \pm 0.3 Ma (Aretz et al., 2020), after the mass extinctions at the Frasnian/Famennian boundary (Kellwasser Event) (McGhee, 1996) and end-Devonian (Hangenberg Event) (Kaiser et al., 2016), with a global greenhouse-icehouse transition background, and ended at 298.9 \pm 0.4 Ma with extensive Gondwana ice sheet (Davydov et al., 2012), lasting ~60.4 Myr (from E738 to E885 shown in Fig. 5). The subdivision of the Carboniferous is highly dependent on biostratigraphy. In the marine realm, conodonts and benthic foraminifers are the favored fossils for Carboniferous subdivisions, which have the advantage over invertebrate macrofossils (Davydov et al., 2012). Detailed conodonts and benthic foraminiferal standard zonations have been well-established in Europe, America, and China (Hu et al., 2019; Poty et al., 2006; Wahlman, 2013). Over the last few decades, standard conodont zonation was refined and further developed (Hu et al., 2019; Nemyrovska, 1999). However, provincialism and paleoecological limitations still influence their temporal and spatial distributions (Davydov and Cozar, 2019), which complicates the global correlation.

The Carboniferous is divided into the Mississippian and Pennsylvanian subsystems. The Mississippian is subdivided into three stages: Tournaisian, Visean, and Serpukhovian; while the Pennsylvanian contains four stages: Bashkirian, Moscovian, Kasimovian, and Gzhelian. 47 radioisotopic dates of the Carboniferous were used in GTS2020 to constrain the biozones and stage boundaries (Aretz et al., 2020). To date, only the base of the Tournaisian, Visean, and Bashkirian stages have been defined by fully ratified GSSP (Devuyst et al., 2003; Lane et al., 1999; Paproth et al., 1991; Richards and Aretz, 2009). As one of the first established geological periods, the subdivision of the Carboniferous is a pending issue owing to its complex geological, biological, and climatic settings (Aretz et al., 2020). The cyclostratigraphy based on astronomical tuning of the orbitally forced records provides a reasonable solution for the Carboniferous stratigraphic subdivision.

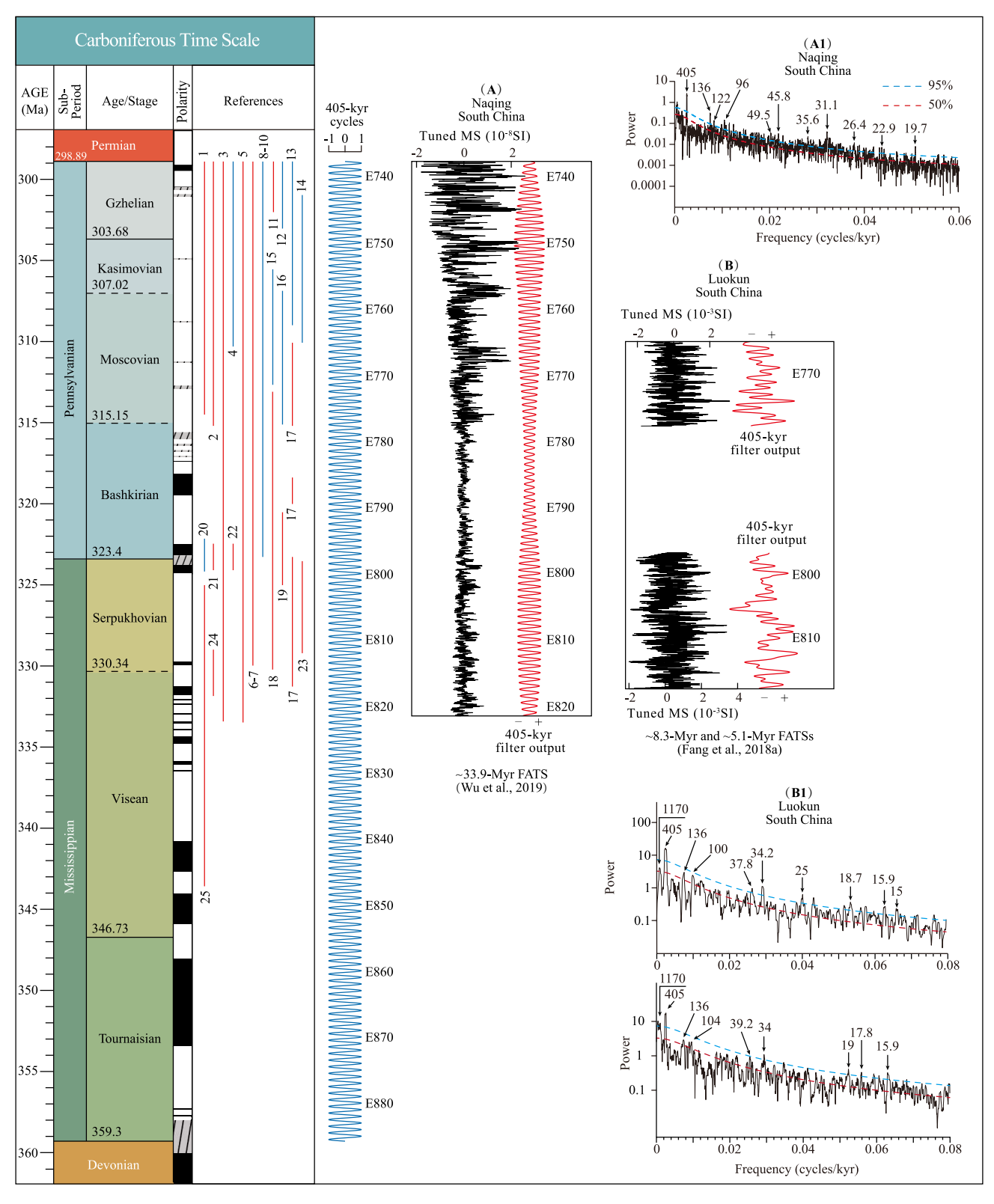


Fig. 5. Our reanalysis and 405 kyr tuning of selected series for the Carboniferous FATS. Chronostratigraphy columns on the left were modified from the GTS2020 integrated stratigraphy (Aretz et al., 2020). (A) MS series and the 405-kyr filter output (red curve, passband: 0.00246 ± 0.0003 cycles/kyr) of the Naqing Section, South China (the original data is from Wu et al., 2019). (B) MS series and the 405-kyr filter output (red curve, passband: 0.003 ± 0.001 cycles/kyr) of the Luokun Section, South China (the original data is from Fang et al., 2018a). (A1) and (B1) is 2π MTM power spectra of series in A and B, respectively. References are listed as 1—Davydov et al. (2010), 2—Schmitz and Davydov (2012), 3—Wu et al. (2019), 4—Ueno et al. (2013), 5—Eros et al. (2012), 6—Birgenheier et al. (2009), 7—Izart et al. (2003b), 8—Grader et al. (2008), 9—Greb et al. (2008), 10—Martin et al. (2012), 11—Huang et al. (2021), 12—Kochhann et al. (2020), 13—Heckel et al. (2008), 14—Heckel (1986), 15—Blomeier et al. (2009), 16—Khodjanyazova et al. (2014), 17—Fang et al. (2018a), 18—Waters and Condon (2012), 19—Pointon et al. (2012), 20—Atakul-Özdemir et al. (2011), 21—Ellwood et al. (2007), 22—Barnett and Wright (2008), 23—Jirásek et al. (2018), 24—Kodama (2019), 25—Liu (2012). (For interpretation of the references to colour in this figure legend, the reader is referred to the web version of this article.)

3.2.1. Pennsylvanian Subsystem (Upper Carboniferous)

The Pennsylvanian Subsystem is divided into four stages, and only the GSSP for the Bashkirian stage is defined. During the Pennsylvanian subsystem, Gondwana land was characterized by extensive ice sheets, and the glacial-interglacial cycles dominated the global climate and sealevel fluctuations (Montañez and Poulsen, 2013), resulting in cyclothems sedimentation and sedimentological and stratigraphic gaps. The widespread major cyclothems across Euramerica were tuned to the long eccentricity cycles using high-precision radiometric ages, biostratigraphic correlation, and sedimentary sequences, establishing a comparable chronostratigraphic framework for the majority of the Pennsylvanian and Early Permian (Davydov et al., 2010; Schmitz and Davydov, 2012). As mentioned above, the FATS for the Pennsylvanian was constructed using the 405-kyr-tuned MS series from the Naqing section (Wu et al., 2019).

3.2.1.1. Gzhelian Stage. The Gzhelian is the youngest Carboniferous stage, with a 4.8 Myr duration from 303.7 \pm 0.4 to 298.9 \pm 0.4 Ma (Fig. 5). The FAD of the conodont Idiognathodus simulator (s.s.) in the chronocline I. eudoraensis-I. simulator defines the base of the Gzhelian stage (Heckel et al., 2008; Villa et al., 2009). To determine the potential stratotype candidates free from the exposed surfaces and major facies changes is the current work of a task group for defining the Kasimovian-Gzhelian (Aretz et al., 2020). The deep-water Usolka section in the southern Urals and Naqing section in South China were selected as candidates. The top of the Gzhelian is consistent with the base of the Permian (base of the Asselian stage), and it is defined by the FAD of the conodont Streptognathodus isolatus (Davydov et al., 1998). Cyclostratigraphic analysis of MS from Naqing section helped to estimate the duration of Gzhelian as 4.83 Myr (Wu et al., 2019) (Fig. 5A), inconsistent with the 4.8 Myr in GTS2020, which further confirms the reliability of FATS.

3.2.1.2. Kasimovian Stage. The duration of Kasimovian stage, the shortest stage of Carboniferous, is 3.3 Myr, from 307 \pm 0.4 Ma to 303.7 \pm 0.4 Ma (Fig. 5). The Moscovian/Kasimovian boundary in the Moscow Basin coincides with the eustatic sea-level lowstand and with disconformities in several sections around the world (Davydov et al., 2012). However, the criterion for the base of Kasimovian has yet to be determined. Compared to fusulinids, the current task group favors a conodont-based boundary, and proposed two candidate sections as potential boundary stratotypes (the Usolka section in the Russian Urals and the Naqing in South China) (Aretz et al., 2020). According to the cyclostratigraphic result of MS from Naqing, the duration of Kasimovian is estimated as 2.99 Myr, showing some differences compared to that in GTS2020 and GTS2012, which can be attributed to the uncertainty of the basal Kasimovian (Wu et al., 2019) (Fig. 5A). Five major depositional sequences have been recognized in Kasimovian shallow marine succession from Zongdi section South China, which correspond to the major cyclothems in the Midcontinent, USA. and Moscow basin, probably forced by 405-kyr eccentricity cycle (Ueno et al., 2013).

3.2.1.3. Moscovian Stage. The Moscovian stage lasted about 8.2 Myr from 315.2 ± 0.4 Ma to 307 ± 0.4 Ma (Fig. 5). To date, the base of the global Moscovian stage has not been defined. The strong endemism of fusulinids between the western and eastern hemispheres hampers the global correlation. Thus, conodont species are considered potential index fossils by the task group for establishing the Moscovian GSSP. Despite several proposals (Alekseev and Goreva, 2013; Qi et al., 2016), a final decision on the reference for the base of the Moscovian stage has not been made.

According to the high-precision ID-TIMS U—Pb zircon ages, the fourth-order sequences in the Donets Basin were tuned to the \sim 400-kyr eccentricity cycle, constructing a continuous age model for Moscovian–Kasimovian–Gzhelian strata (Davydov et al., 2010). The bases of

the Moscovian, Kasimovian, and Gzhelian Stages were calibrated as 314.6 Ma (the FAD of conodont *Declinagnathodus donetzianus*), 306.7 Ma (FADs of fusilinid *Protriticites pseudomontiparus* and conodont *Streptognathodus subexcelsus*), and 303.2 Ma (the FAD of the conodont *S. simulator*), respectively (Davydov et al., 2010). The cyclostratigraphy analysis of MS from the Naqing section, estimated the duration of Moscovian as 8.38 Myr (Wu et al., 2019) (Fig. 5A), showing differences with the 8.2 Myr in GTS2020. The uncertainty of the basal Kasimovian may contribute to these slight differences (Wu et al., 2019). The facies arrangement and cyclostratigraphic architecture of shallow-marine, warm-water deposits from the Ny Friesland Platform in the eastern Spitsbergen and Zongdi section on the Yangtze Carbonate Platform, South China, suggested that eccentricity forced the glacio-eustatic sealevel fluctuation during the Pennsylvanian (Blomeier et al., 2009; Ueno et al., 2013).

3.2.1.4. Bashkirian Stage. The Bashkirian stage is the first stage in Pennsylvanian, lasting 8.2 Myr from 323.4 ± 0.4 Ma to 315.2 ± 0.4 Ma (Fig. 5). The base of the Bashkirian (Mississippian–Pennsylvanian transition) coincides with significant stratigraphic gaps in many sections and an important marine extinction caused by a major glacio-eustatic sea-level lowering (McGhee et al., 2012, 2013). The FAD of the conodont Declinognathodus noduliferus s.l. is used as the reference for the base of the Bashkirian, and the GSSP is defined in Arrow Canyon, United States (Lane et al., 1999). Though Declinognathodus inaequalis (a former subspecies of *D. noduliferus*) was suggested to define the GSSP level by Manger (2017), *D. noduliferus* s.l. currently defines the base of the Bashkirian in the absence of a formal decision.

The duration of the Bashkirian stage was estimated as 8.1 Myr by Wu et al. (2019) (Fig. 5A), which is close to 8.2 Myr in GTS2020 which confirms the astronomical calibration results. The cyclostratigraphy analysis of MS from the Luokun section of South China estimated Idiognathoides sulcatus sulcatus, I. sinuatus, I. sulcatus parvus, and "Streptognathodus" expansus M1 conodont zones in the Bashkirian periods of 520 \pm 370 kyr, 480 \pm 320 kyr, 230 \pm 190 kyr, and 260 \pm 160 kyr, respectively (Fang et al., 2018a) (Fig. 5B). Detailed sedimentological and cyclostratigraphic studies of the shallow-water carbonate succession in the lower part of the Bird Spring Formation hosts the Mississippian-Pennsylvanian GSSP in Arrow Canyon, Nevada, USA. It indicates that a large number of glacio-eustatic sea-level fluctuations are missing and over 25 beats of the Milankovitch band were not recorded. This equates to a gap of >1 Myr or possibly over 2.5 Myr (Barnett and Wright, 2008). Time-series analysis of the MS series from the Mississippian-Pennsylvanian GSSP at the Arrow Canyon and two additional sections indicated the 405-kyr eccentricity forcing in glacio-eustatic cyclicity (Ellwood et al., 2007).

3.2.2. Mississippian Epoch

3.2.2.1. Serpukhovian Stage. The Serpukhovian stage lasted 6.9 Myr from 330.3 ± 0.4 Ma to 323.2 ± 0.4 Ma (Fig. 5), shorter than the Tournaisian and Visean stages. In many regions, the Visean–Serpukhovian boundary is characterized by incomplete stratigraphic records or major facies changes, leading to widespread fossil gaps that complicate the global correlation (Kabanov et al., 2016). Dramatic global climate change related to the LPIA and plate configurations resulted in significant changes in the biosphere and depositional sequences. Although the conodont *Lochriea ziegleri* has been tested as a reference for the base of the Serpukhovian for many years, a formal decision on the definition of the global Serpukhovian stage has not been made.

The cyclostratigraphy analysis of the MS, covering the Serpukhovian to Moscovian stages, from the Luokun section of South China showed significant Milankovitch cycles with 405 kyr long eccentricity, 136 and 100 kyr short eccentricity, 34 kyr obliquity, and 19 and 15.9 kyr precession cycles (Fang et al., 2018a) (Fig. 5B). The duration of the

Serpukhovian stage is estimated as 7.68 ± 0.15 Myr (Fang et al., 2018a) (Fig. 5B) similar to the result of Wu et al. (2019) (7.6 Myr; Fig. 5A) and GTS2012/2016 (7.7 \pm 0.2 Myr). The little discrepancy may be induced by the missing of one 405-kyr-long eccentricity cycle in the Donets Basin and Urals during interpolation of the ages of the base of the stages (Fang et al., 2018a). The higher sediment accumulation rate (SAR) events relating to glaciation records suggest glacial events may be controlled by orbital forcing (Fang et al., 2018a). Kodama (2019) estimated a 1.75 Myr duration for the normal polarity interval in the terrestrial, fluvial deposits of the Pottsville Mauch Chunk Formation (roughly from late Visean to Serpukhovian) section using cyclostratigraphy analysis of MS, which is much longer than <1 Myr as previously suggested by the biostratigraphy.

3.2.2.2. Visean Stage. The Visean Stage was 16.4-Myr long, occurring from 346.73 ± 0.4 Ma to 330.34 ± 0.4 Ma (Fig. 5). There was no significant faunal turnover in the pelagic realm during the Tournaisian/Visean boundary; thus, the foraminifera genus *Eoparastaffella* was used as the boundary marker. The base of Visean is defined by the FAD of *Eoparastaffella simplex* (morphotype 2) with an outer subangular periphery in bed 83 of the Pengchong section in Liuzhou, South China (Devuyst et al., 2003). Although the final official publication is still missing, the International Commission on Stratigraphy ratified the GSSP proposal for the base of Visean.

Cyclostratigraphic studies on the Visean are rare. Liu (2012) analyzed the GR data from the Karashayi Formation, roughly corresponding to Visean and Serpukhovian. The results of the cyclostratigraphy analysis show that the duration of the Karashayi Formation in Central Tarim Basin varies from 21.87 to 27.06 Myr, and the third-order sequences were controlled by the 2.4-Myr eccentricity cycles. However, the number of cycles and sequences in the Karashayi Formation varies among different wells, and the cyclostratigraphy results have not been correlated to the international geological time scale. Other cyclostratigraphic studies have normally focused on the top of the Visean (Eros et al., 2012; Schmitz and Davydov, 2012; Wu et al., 2019).

3.2.2.3. Tournaisian Stage. The Tournaisian Stage is a 12.6-Myr duration, from 359.3 ± 0.3 Ma to 346.7 ± 0.4 Ma. The current base of the Tournaisian, Devonian/Carboniferous boundary is based on the FAD of the conodont Siphonodella sulcata in the La Serre section (Paproth et al., 1991). While the new data on the FAD of S. sulcata in the La Serre section suggested 0.45 cm below the defined boundary (Kaiser, 2009), which questions the validity of the La Serre GSSP and the Carboniferous time scale. Though the joined task group of the Devonian and Carboniferous subcommissions (Aretz, 2014) is trying to re-define this boundary, the originally proposed FAD of S. sulcata remains the current reference. The Tournaisian conodont zones have been well established in Europe, the Midcontinent, and South China. While there is no cyclostratigraphic study on the Tournaisian and the duration of each biological zones and the middle Tournaisian positive δ^{13} C excursion are poorly constrained by FATS.

3.3. Devonian

The base of Devonian is set as the level of the FAD of graptolite *Uncinatograptus uniformis* from $\sim\!419.0$ Ma, and the top as the level of the FAD of the conodont *Siphonodella* (*Eosiphonodella*) *sulcata* at 359.3 \pm 1.8 Ma, spanning $\sim\!59.7$ Myr (Kaufmann, 2006) and corresponding to the 405-kyr cycles from E886 to E1033 (Fig. 6).

During the Devonian, the Earth's climate system underwent major changes, including the rapid decrease in pCO_2 to modern levels for the first time in geological history and a shift from Silurian greenhouse to Carboniferous icehouse conditions (Joachimski et al., 2009). Several studies have confirmed that sea-level fluctuations, ocean anoxia, and biological extinction (e.g., Frasnian and Famennian crisis and the

Hangenberg crisis) may be associated with the astronomically-forced climate changes during the Devonian (De Vleeschouwer et al., 2013; Huang and Gong, 2016; Myrow et al., 2014). The identification of the FADs of graptolite or conodont with global correlation significance prompted the International Subcommission on Devonian Stratigraphy to divide the Devonian into 7 stages grouped in the Early, Middle, and Late Devonian series (Fig. 6). Cyclostratigraphy studies have been conducted on Devonian strata, but only a few FATSs have been established due to the lack of high-precision geochronological data constraints.

3.3.1. Late Devonian

The Late Devonian Epoch includes the Famennian and Frasnian stages, spanning ~19.6 Myr from 378.9 to 359.3 Ma. The lower boundary of Famennian stage is placed at the stratigraphic level of the FAD of conodont *Palmatolepis subperlobata* or the LAD of *P. bogartensis*, while the upper stage boundary is placed at the conodont *Siphonodella sulcata* (Eva et al., 1991; Maurice and Johannes, 1999), and the Famennian lasted ~11.8 Myr (Fig. 6). The base of the Frasnian Stage is set at the FAD of conodont *Ancyrodella rotundiloba pristina* (Gilbert et al., 1987), while the top is defined at the FAD of the conodont *P. subperlobata* or the LAD of *P. bogartensis* (Klapper et al., 1993), and the Frasnian Stage spanned ~7.8 Myr (Aboussalam and Becker, 2007; Klapper and Kirchgasser, 2016).

3.3.1.1. Famennian Stage. The Famennian Stage cyclostratigraphic analysis focuses on the Midcontinent. and South China. In the Illinois Basin of central North America, astronomical calibration using MS gives an estimated duration of 13.5 \pm 0.5 Myr (Pas et al., 2018). A cyclostratigraphic analysis of the Lali section from South China suggested that the duration of the Famennian Stage was 14.4 \pm 0.28 Myr (Ma et al., 2020) (Fig. 6A). These results are consistent with the 13.3 Myr of the Famennian Stage given in the GTS2012 (Becker et al., 2012), but longer than the time of 11.8 Myr given by GTS2020 (Becker et al., 2020). The difference is mainly ascribed to the uncertainty in the biostratigraphy. In addition, the studied rhythmic sedimentary sequence from the Kowala section of the Holycross Mountains in Poland indicates 400-kyr and 100-kyr eccentricity cycles. The time intervals between the Annulata and Dasberg, and Dasberg and Hangenberg were estimated as 2.2 Myr and 2.4 Myr, respectively, which may be paced by the 2.4-Myr long-term eccentricity cycle (De Vleeschouwer et al., 2013).

The F—F event is one of the five extinction events of the Phanerozoic, and it includes two stages, corresponding to the lower and upper Kellwasser positive δ^{13} C excursion. A previous study focused on cyclostratigraphy based on lithologic changes of limestone and nodular limestone at the four F-F boundary sections in South China and found that the ratio of the lithologic cycles is consistent with that in the Milankovitch cycle (Gong et al., 2001, 2005). A FATS was established based on the MS and carbon isotope collected from six different F-F boundary sections on a global scale (De Vleeschouwer et al., 2017). Onset of the lower Kellwasser was estimated as 800 kyr earlier than the F—F boundary, and the duration of the lower Kellwasser was \sim 200 kyr. The time spans between the lower and upper Kellwasser was ∼600 kyr (De Vleeschouwer et al., 2017). MS, carbon isotope, and chemical element analysis were extracted from the Steinbruch Schmidt section (Kellerwald, Germany) for cyclostratigraphic analysis (Da Silva et al., 2020), and combined with the research profile in De Vleeschouwer et al. (2017). The duration of the lower Kellwasser and upper Kellwasser were estimated to be 80–96 kyr and 100–130 kyr, respectively, equivalent to about one short eccentricity cycle. An age of 371.870 \pm 0.108 Ma was obtained for the F-F boundary (Da Silva et al., 2020). A FATS was established for the F-F transition portion of the Lali and Yangdi sections in South China (Ma et al., 2022). The results reveal that 1000 kyr spans the interval between the LKH and UKH, and $\sim 1600 \; kyr$ separates the maximum values of the LKH and UKH $\delta^{13}\text{C}$ excursions. The estimated duration of the UKH is $\sim \! 150$ kyr, during which the first, second, and

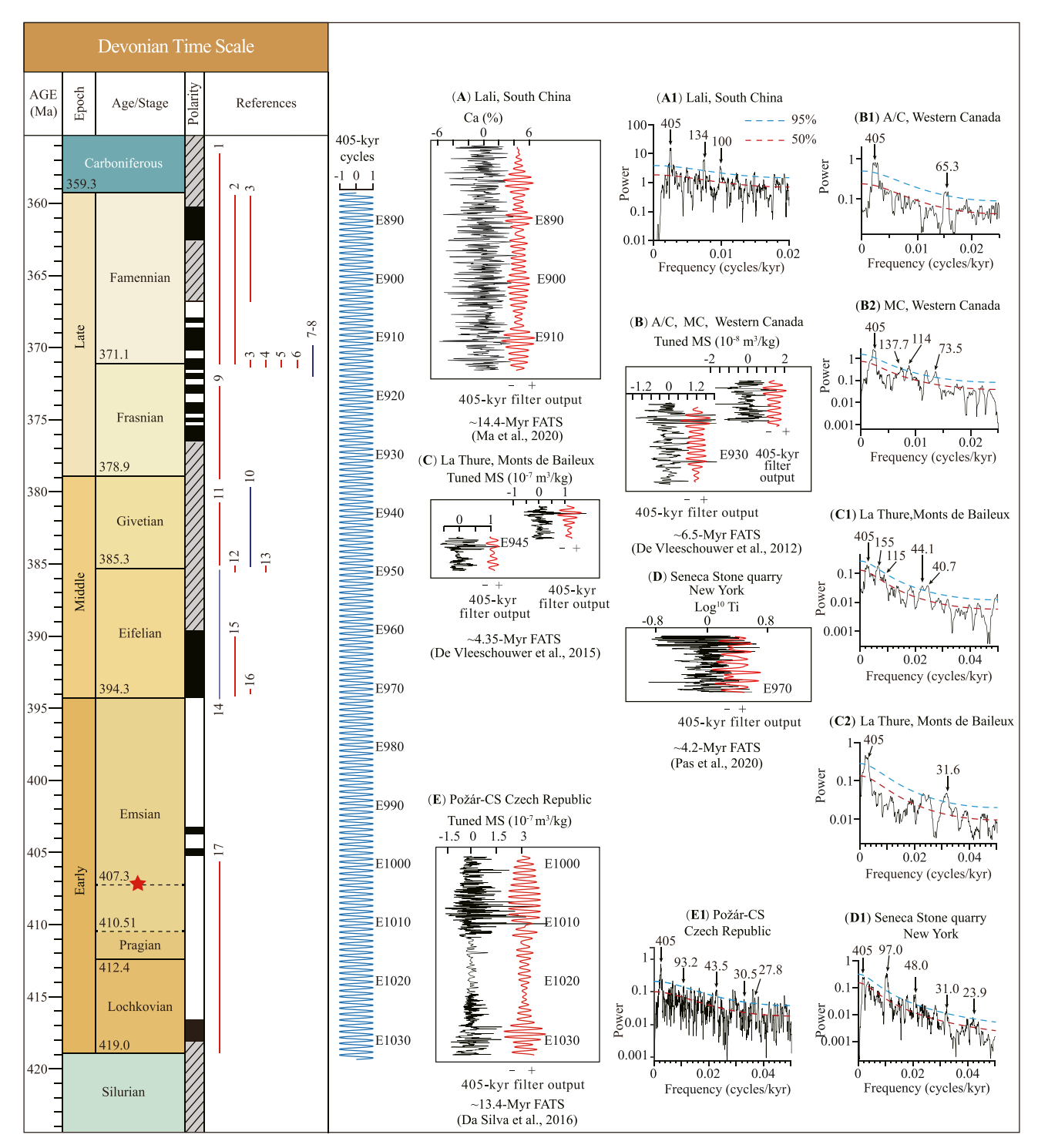


Fig. 6. Our reanalysis and 405 kyr tuning of selected series for the Devonian FATS. Chronostratigraphy columns on the left were generated using the GTS2020 integrated stratigraphy (Becker et al., 2020). (A) Ca series and 405-kyr filter output (red curve, passband: 0.00243 ± 0.000486 cycles/kyr) of the Lali section (South China) (the original data from Ma et al., 2020). (B) MS series and 405-kyr filter output (red curve, passband: M/C section 0.00247 ± 0.00049 cycles/kyr; A/C section 0.00245 ± 0.00049 cycles/kyr) of the Alberta (Canada) (the original data from De Vleeschouwer et al. (2012a)). (C) MS series and 405-kyr filter output (red curve, passband: Monts de Baileux section 0.002456 ± 0.0008 cycles/kyr; La Thure section 0.002692 ± 0.0007 cycles/kyr) from Dinant Synclinorium (Belgium) (the original data from De Vleeschouwer et al., 2015). (D) Ti series and 405-kyr filter output of the Seneca section (USA) (the original Figure from Pas et al., 2020). (E) MS series and 405-kyr filter output (red curve, passband: 0.002478 ± 0.00049 cycles/kyr) of the Pod Barrandovem section (Czech Republic) (the original data from Da Silva et al., 2016). All proxies in the figure have been benchmarked by the corresponding line of each stage at the bottom of the proxies. (A1), (B1), (B2), (C1), (C2), (D1) and (E1) are 2π MTM power spectra of series in A to E, respectively. References are listed as 1—Ma et al. (2020), 2—Pas et al. (2018), 3—De Vleeschouwer et al. (2017), 4—Ma et al. (2022), 5—Da Silva et al. (2020), 6—De Vleeschouwer et al. (2013), 7—Gong et al. (2001), 8—Gong et al. (2013), 14—Ellwood et al. (2011a), 11—De Vleeschouwer et al. (2015), 12—De Vleeschouwer et al. (2015), 13—Da Silva et al. (2013), 14—Ellwood et al. (2015), 15—Pas et al. (2020), 16—De Vleeschouwer et al. (2016). Red star indicates a newly-defined base of Emsian using the FAD of Eocostapolygnathus excavates. (For interpretation of the references to colour in this figure legend, the reader is referred to the web version of this article.)

third extinctions of the F—F bio-crisis lasted \sim 120 kyr, \sim 20 kyr, and \sim 10 kyr, respectively. It was confirmed that the long eccentricity cycle controlled the sea surface temperature, and third-order eustatic sea-level changes were forced by the alignment of eccentricity and obliquity cycles (Ma et al., 2022).

3.3.1.2. Frasnian stage. The establishment of the FATS was completed in the Frasnian stage. A cyclostratigraphic study was conducted using MS on five sections (two of them shown in Fig. 6B) from the Southesk-Cairn carbonate platform (section KC), Miette (section AB/W4), and Ancient Wall platforms (sections A/C and MC) in Alberta, and Western Canada (De Vleeschouwer et al., 2012a) (Fig. 6B). The identified 405-kyr long eccentricity cycle provides the duration of Frasnian as 6.5 ± 0.4 Myr (Fig. 6B). Furthermore, based on FATSs and U—Pb age for the Frasnian/Famennian boundary (Kaufmann, 2006; Kaufmann et al., 2004), the ages of Givetian/Frasnian and Frasnian/Famennian boundaries were calculated as 383.6 ± 3.0 Ma and 376.7 ± 3.0 Ma, respectively (Becker et al., 2020). These results are consistent with the time of 7.8 Myr for the Frasnian stage in GTS2020 (Becker et al., 2020) but slightly shorter than the 10.5 Myr given by GTS2012 (Becker et al., 2012).

3.3.2. Middle Devonian

The Middle Devonian Epoch includes the Givetian and Eifelian stages, which lasted ~15.4 Myr (394.3–378.9 Ma) (Becker et al., 2020). The lower and upper Givetian stage boundaries were placed at the stratigraphic level of the FAD of conodont *Polygnathus hemiansatus* and the conodont *Ancyrodella rotundiloba pristina*, respectively (Davydov et al., 2010; Walliser et al., 1995), and the Givetian lasted ~6.4 Myr. The base of the Eifelian Stage was set at the FAD of conodont *P. partitus* and the top was defined at the FAD of conodont *P. hemiansatus* (Walliser et al., 1995), spanning ~9.0 Myr (Fig. 6).

3.3.2.1. Givetian stage. Time-series analysis of MS data from the Eifelian/Givetian GSSP sequence in Morocco, and the Givetian/Frasnian GSSP in France, shows that eccentricity-band rhythms are well-defined in datasets. The MS cyclicity in the section falls within the 405-kyr eccentricity band, providing a FATS for the Givetian. The duration of the Givetian stage was estimated at ~5.6 Myr based on the MS of the AKZO Core in the New York Tully composite section (Ellwood et al., 2011a; Ellwood et al., 2011b). This result is consistent with the GTS2020 time for the Givetian stage of ~6.4 Myr (Becker et al., 2020). In addition, four sections (La Couvinoise, Monts De Baileux, Fromelenes-Flohimont, and La Thure) in the Dinant Synclinorium, Belgium, were performed the cyclostratigraphic analysis using MS series (De Vleeschouwer et al., 2015) (Fig. 6C). High-precision stratigraphic correlation was conducted based on the oscillation characteristics of lithology and MS series, and the FATS of Givetian with a duration of 4.35 \pm 0.45 Myr was established. The result of Givetian was slightly shorter than GTS2020 but closer to the 5.0 Myr given by GTS2012 (Becker et al., 2012). No radioisotope age has been used to construct the Givetian time scale, and cyclostratigraphy results may serve as a crucial reference for determining its duration.

3.3.2.2. Eifelian stage. A detailed cyclostratigraphic analysis was conducted on the MS of the Bou Tchrafine section in the Tafilalt of southeastern Morocco (Ellwood et al., 2015). They identified periods of the Milankovitch cycle, providing an estimated duration of the Eifelian stage as ~ 6.2 Myr. In addition, the durations of the two bio-events in the Eifelian Stage were estimated based on the FATS: ~ 370 kyr for Kačák bio-events and ~ 600 kyr for Choteč (Ellwood et al., 2015). The FATS was yielded via 100-kyr calibration, which provides an estimated duration of ~ 5.1 Myr for the Eifelian stage in the Appalachian Basin of New York (Pas et al., 2020) (Fig. 6D). According to the calculated sediment accumulation rates, the deposition time of the unmeasured

part of the section is estimated as 0.42 Myr and 0.37 Myr. Therefore, this section's FATS duration should be 4.2 Myr. Based on the high-resolution U—Pb radiometric age (389.58 \pm 0.86 Ma) available for the Tioga F Bentonite (Roden et al., 1990), the numerical ages of the Emsian/Eifelian and Eifelian/Givetian sediments were re-calibrated at 393.39 \pm 0.86 Ma and 388.24 \pm 0.86 Ma, respectively.

3.3.3. Early Devonian

The Early Devonian (419.0–394.3 Ma) includes the Emsian, Pragian, and Lochkovian stages, lasting ~24.7 Myr. The top of the Emsian Stage is set at the FAD of conodont *Eocostapolygnathus kitabicus*, and is defined at the FAD of the conodont *Polygnathus partitus*, spanning ~16.2 Myr (Yolkin et al., 1997b). The lower and upper Pragian stage boundaries are located at the stratigraphic level of the conodont *Eognathodus irregularis* and the conodont *Eocost. kitabicus*, respectively (Ivo and William, 1989), spanning about ~1.89 Myr. Recently, the Emsian/Pragian boundary has been proposed to move up to the FAD of *Eocost. excavatus* M114 (Carls et al., 2008). Lochkovian Stage, spanning ~6.6 Myr, was defined as the base and top at the stratigraphic level of the FAD of the graptolite *Uncinatograptus uniformis* and the conodont *Eogna. irregularis*, respectively (Ivo and František, 2003). The study of the Early Devonian geological records focused on the Lochkovian and Pragian stages (Fig. 6).

3.3.3.1. Emsian Stage. Few studies have focused on the Emsian stage, while Milankovitch cycles have been identified at the Emsian/Eifelian boundary at the Wetteldorf section of the Rhenohercynian basin of Germany (De Vleeschouwer et al., 2018).

3.3.3.2. Pragian Stage and Lochkovian Stage. Cyclostratigraphic studies of the Pragian and Lochkovian stages are less studied. Milankovitch cycles were found in the basal Pragian and Lochkovian stages in the Pod Barrandovem and Požár sections of the Czech Republic (Da Silva et al., 2016). Using the counting of the dominant 405-kyr eccentricity cycles, the estimated total duration for the FATS was $\sim\!13.4$ Myr. The Lochkovian and Pragian stages were estimated to be 7.7 \pm 2.8 Myr and 1.7 \pm 0.7 Myr, respectively (Fig. 6E). Pragian result is consistent with the 3.2 Myr given in the GTS2012 (Becker et al., 2012) but slightly shorter than the 5.1 Myr given by GTS2020 (Becker et al., 2020). The Lochkovian stage result lies between 8.4 Myr in GTS2012 and 6.6 Myr in GTS2020. The uncertainties of the Early Devonian stages may be over-optimistic due to the adopted cubic spline fitting approach used in the GTS2012 (Da Silva et al., 2016; De Vleeschouwer and Parnell, 2014).

3.4. Silurian

The Silurian Period (443.1-419.0 Ma), spanning the 405-kyr cycles from E1034 to E1092, was a time of dramatic changes in climate, ocean chemistry, and biodiversity. It began at the level where the graptolite species Akidograptus ascensus first appeared (Cocks, 1985; Melchin et al., 2020). The topmost Silurian is defined at the FAD of the graptolite Uncinatograptus uniformis uniformis (Jaeger, 1977; Melchin et al., 2020), which can also be identified by a major positive carbon isotope excursion called the Klonk event (Racki et al., 2012). According to chemostratigraphic investigations, seven positive carbon isotope excursions associated with significant bioevents and environmental changes have been identified globally over this period (Cramer and Jarvis, 2020). The Silurian comprises four series: the Llandovery, Wenlock, Ludlow, and Pridoli, in an upward sequence. Goodwin et al. (1986), Yolkin et al. (1997a), Marshall (2000), and others have been recognized fine-scale cyclic sedimentation within the Silurian System, using the assumption that observed cyclicity is related to an astronomical origin (Westphal et al., 2010). However, the Silurian time scale based on astrochronological tuning remains in its infancy (Fig. 7).

Earth-Science Reviews 244 (2023) 104510

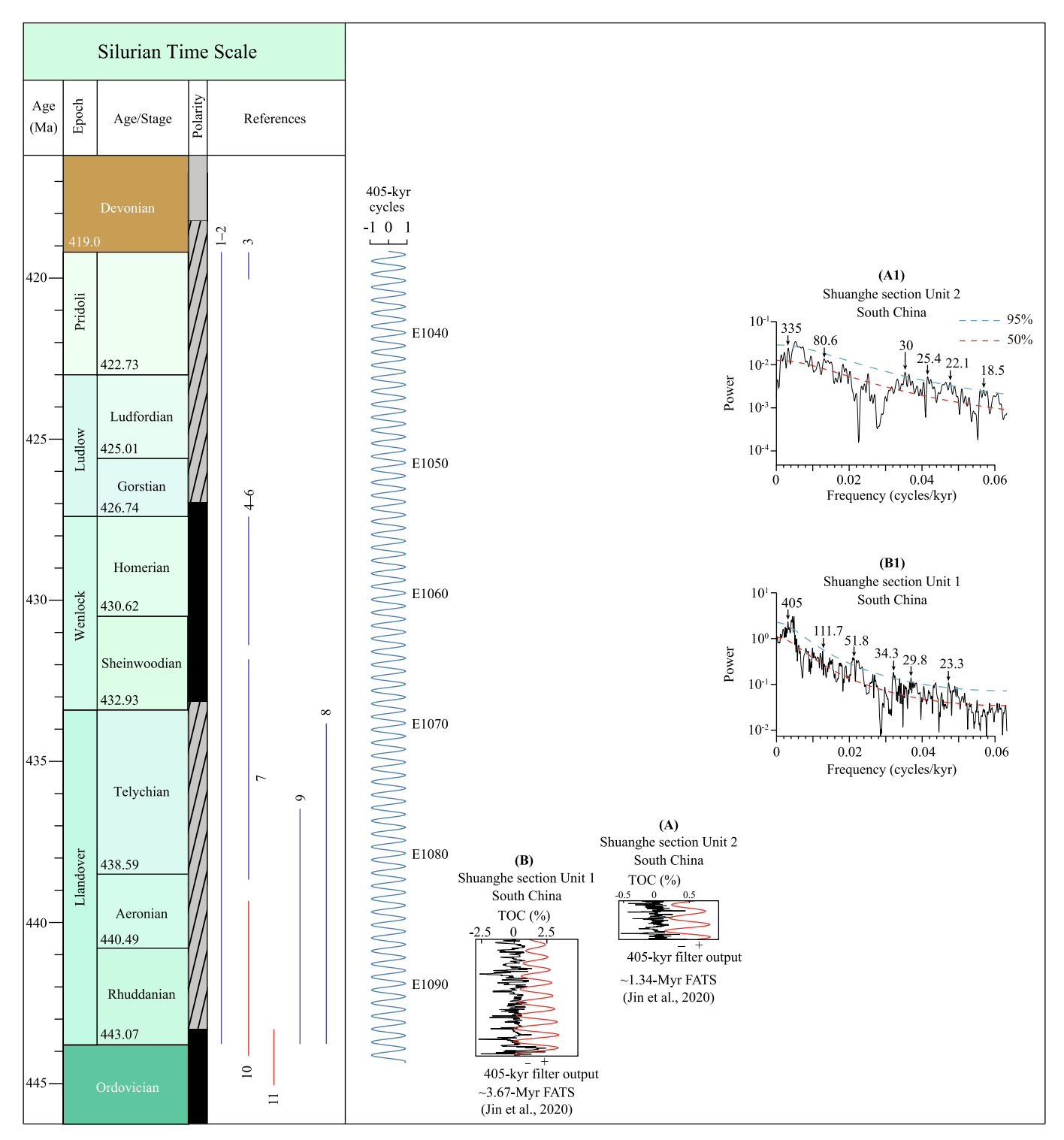


Fig. 7. Our reanalysis and 405 kyr tuning of selected series for the Silurian FATS. Chronostratigraphy columns on the left were modified from the GTS2020 integrated stratigraphy. (A) TOC series and the 405 kyr filter output (red curve, passband: 0.0025 ± 0.001 cycles/kyr) of the Shuanghe Section Unit 2 (South China) (the original data from Jin et al., 2020). (B) TOC series and the 405-kyr filter output (red curve, passband: 0.0022 ± 0.001 cycles/kyr) of the Shuanghe Section Unit 1 (South China) (the original data from Jin et al., 2020). (A1) and (B1) are 2π MTM power spectra of series in A and B, respectively. References are listed as 1—Crampton et al. (2018), 2—Sproson (2020), 3—Crick et al. (2001), 4—Radzevičius et al. (2014), 5—Radzevičius et al. (2017), 6—Spiridonov et al. (2016), 7—Braun et al. (2021), 8—Jia et al. (2018), 9—Gambacorta et al. (2018), 10—Jin et al. (2020), 11—Zhang et al. (2021). (For interpretation of the references to colour in this figure legend, the reader is referred to the web version of this article.)

3.4.1. Ludlow Series and Pridoli Series

The Pridoli stage is estimated as 3.7 Myr, lasting from 422.7 \pm 1.6 to 419.0 \pm 1.8 Ma (Melchin et al., 2020). The MS cyclic nature of the Pridoli–Lochkovian GSSP (Klonk, Prague Basin, Czech Republic) was

developed in response to climate cycles driving erosion, which changed the supply rate of weathered terrigenous paramagnetic grains to the marine system (Crick et al., 2001). These variations in supply occurred due to climate change resulting from the obliquity or eccentricity of the

Earth's orbit during the latest Silurian and earliest Devonian periods. Crampton et al. (2018) reported that a significant component of the variability in graptolite turnover rates in the Silurian could be explained by the 2.6-Myr long-term eccentricity cycles. Variations in the $\sim\!4.5$ Myr eccentricity and obliquity cycles enhanced organic carbon burial or carbon reservoir stability leading to the $\delta^{13}C$ fluctuations. This process led to a decline in atmospheric pCO2 to threshold levels, after which astronomical forcing triggered the onset of glaciation and extensive global cooling associated with multiple positive carbon isotope excursions during the Silurian (Sproson, 2020). There are no reports on cyclostratigraphy for the Ludlow series.

3.4.2. Wenlock Series

The Wenlock ranges from an estimated 432.9 \pm 1.2 Ma to 426.7 \pm 1.5 Ma, with a duration of 6.2 Myr (Melchin et al., 2020), and has been divided into two stages, the Homerian and Sheinwoodian Stages. To date, only a few cyclostratigraphic studies have been published for the middle and upper Wenlock. A previous study (Radzevičius et al., 2014, 2017) presented a cyclostratigraphic analysis of GR logs from four wells located in the deep-water facies belt of the Lithuanian part of the Wenlock (Homerian) Baltic Basin of the Geluva regional stage. The results show remarkable eccentricity cycles and achieved a high-precision intra-basinal cyclostratigraphic correlation of the order of several tens of thousands of years. Spiridonov et al. (2016) present evidence that conodonts and phytoplankton (acritarchs and green algae) from the sedimentary successions of the Wenlock period from two deep cores (Ledai-179 and Viduklė-61) experienced cyclic changes driven by the periodic variations in Earth's orbital eccentricity.

3.4.3. Llandovery Series

The Llandovery includes Telychian, Aeronian, and Rhuddanian stages and lasted $\sim\!10.2$ Myr, from 443.1 \pm 0.9 Ma to 432.9 \pm 1.2 Ma (Ling et al., 2019; Melchin et al., 2020). Attracted by the widespread deposition of organic-rich black shales, Late Ordovician glaciation, and mass extinction, several scholars have attempted to conduct cyclostratigraphic research on the stratigraphic sequence in the Upper Ordovician–Llandovery.

Recently, a continuous core drilled through the Telychian Stage (Llandovery, Silurian) of the Pasłek Formation in the Baltic Basin (Poland) reflected orbitally-driven climatic variations, showing a duration of ~5.46 Myr for the Telychian Stage (Gambacorta et al., 2018). This value is within the range of the estimates provided by Melchin et al. (2012), Ogg et al. (2016), and Melchin et al. (2020). Braun et al. (2021) qualitatively estimated the Aeronian and Telychian stages to be 2.4-Myr long. These results should be re-considered because the resolution is insufficient for identifying astronomical cycles. In the Early Silurian (~439.673-444.681 Ma), Jin et al. (2020) identified the Milankovitch cycles and constructed a FATS via 405-kyr tuning, using the total TOC as a proxy for the spectral analyses at the Shuanghe section in the Changning area of the Sichuan Basin (Fig. 7A, B). This FATS's Rhuddanian Stage duration of 2.80 Myr is slightly shorter than the GTS2012 (3.1 Myr; Melchin et al., 2012) and longer than the GTS2020 (2.6 Myr; Melchin et al., 2020). The uncertainty inherent in deriving these time scales for global time scale (Agterberg et al., 2020) may contribute to these slight differences. Comparatively, the duration of \sim 2.4 Myr for the Rhuddanian from the study carried out by Braun et al. (2021) is significantly shorter. Gambacorta et al. (2018), Jin et al. (2020), and Zhang et al. (2021) proposed that orbital cycle variations might lead to rhythmic variations in organic matter fluxes and benthic anoxic conditions. Astronomical signals significantly influence the cycle thickness of the Silurian Kepingtage Formation deposited in a tidal flat environment in the Tarim Basin. Jia et al. (2018) showed that the Kepingtage Formation, corresponding to the Llandovery series, lasted for 10.4 Myr.

3.5. Ordovician

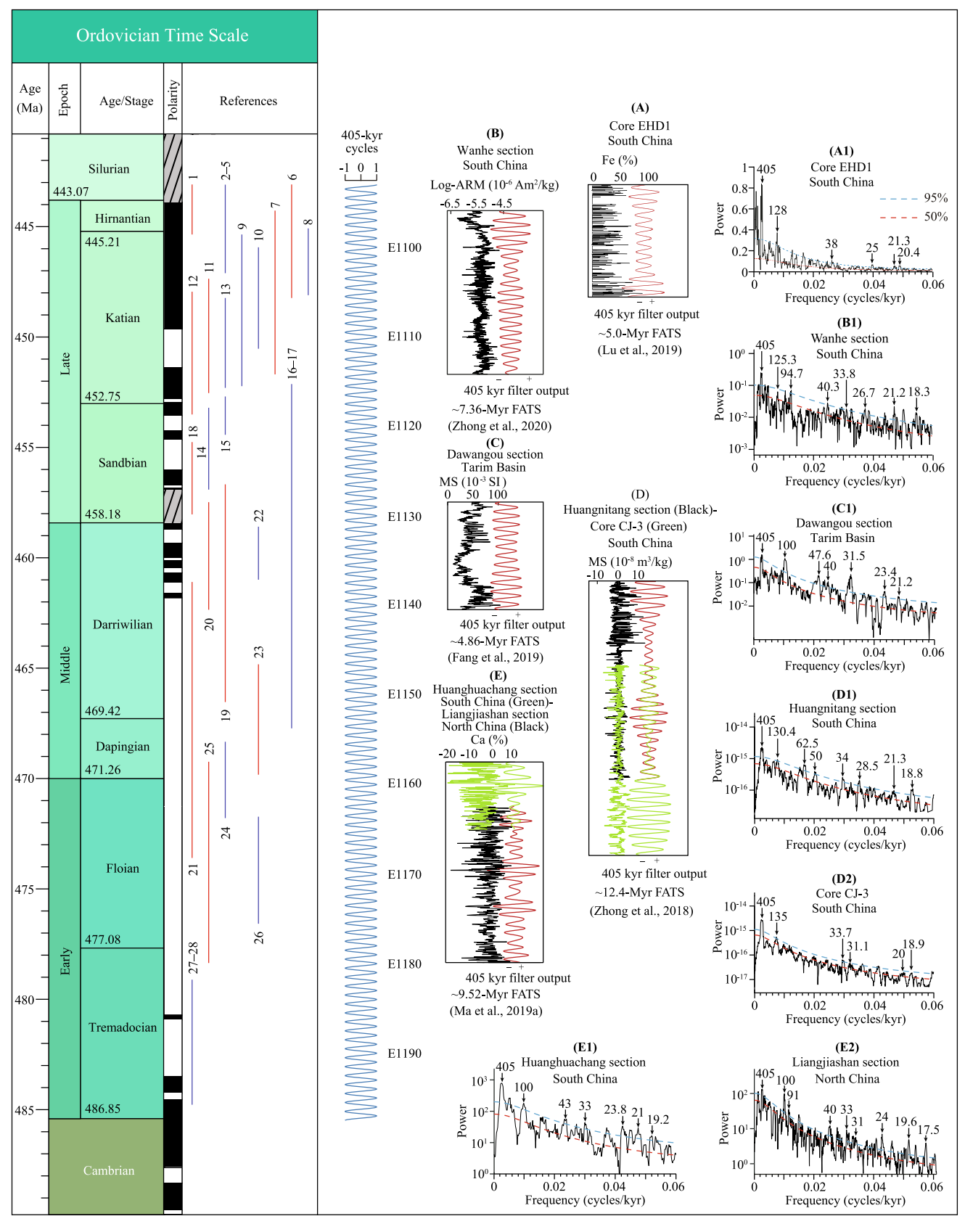
The Ordovician base is set at the FAD of the conodont Iapetognathus fluctivagus corresponding to 486.9 \pm 1.5 Ma, and the top at the FAD of the graptolite Akidograptus ascensus at 443.1 \pm 0.9 Ma (Cocks, 1985; Cooper et al., 2001; Goldman et al., 2020), lasting 43.8 Myr and corresponding to the 405-kyr cycles from E1093 to E1201. Apart from two bio-events (Great Ordovician Biodiversification Event and Late Ordovician extinction) that have been widely reported, the Ordovician period encompasses several isotopic carbon excursions (e.g., Guttenberg Isotope Carbon Excursion, GICE) coinciding with the start of secular shifts in ⁸⁷Sr/⁸⁶Sr (Saltzman et al., 2014; Young et al., 2009). The greenhouse-icehouse transitions and resultant Hirnantian glaciation, which started in the Sandbian or earlier, are probably related to the Late Ordovician extinction (Harper et al., 2014). Based on the identification of graptolite or conodont FADs with global significant correlation, the International Subcommission on Ordovician Stratigraphy divided the Ordovician into 7 stages grouped in the Early, Middle, and Late Ordovician series (Fig. 8).

3.5.1. The Upper Ordovician

The Upper Ordovician includes the Hirnantian, Katian, and Sandbian stages, which lasted ~15.1 Myr (~458.2–443.1 Ma). The Hirnantian Stage, the uppermost stage of the Ordovician, was defined as the base and top at the stratigraphic level of the FAD of the graptolite *Metabolograptus extraordinarius* and the graptolite *Akidograptus ascensus*, respectively (Chen et al., 2006; Cocks, 1985; Goldman et al., 2020). The lower and upper Katian stage boundaries are located at the stratigraphic level of the graptolite *Diplacanthograptus caudatus* and the graptolite *Metabolograptus extraordinarius*, respectively, with a duration of 7.6 Myr for Katian (Chen et al., 2006; Daniel et al., 2007; Goldman et al., 2020). The base of the Sandbian Stage is set at the FAD of the graptolite *Nemagraptus gracilis*, and the top is defined at the FAD of graptolite *Diplacanthograptus caudatus*, spanning ~5.4 Myr (Bergström et al., 2000; Daniel et al., 2007; Goldman et al., 2020) (Fig. 8).

3.5.1.1. Hirnantian Stage. The Hirnantian Stage is estimated to have lasted 0.5–1 Myr based on the equal period (maximum 0.5 Myr) of extraordinarius and persculptus Zones (Barnes, 1992; Brenchley et al., 1994; Harland et al., 1990). The FATS indicates the durations of the Hirnantian Stage of \sim 1225 kyr in the Wanhe section, (Zhong et al., 2020) and 1.77 \pm 0.4 Myr in the EHD1 drill core of Yichang (Lu et al., 2019) in South China (Fig. 8A). These results are consistent within the error of 1.33 \pm 0.2 Myr for the Hirnantian Stage in the GTS2012 (Cooper et al., 2012), but slightly shorter than the time of 2.1 Myr given by GTS2020 (Goldman et al., 2020). This discrepancy may be due to the fewer radioisotopic dates in the Hirnantian used for the construction of the time scale in GTS (Goldman et al., 2020). Comparatively, the Hirnantian Stage duration of \sim 0.88 Myr calculated by Jin et al. (2020) in the Shuanghe Section, Changning area, is much shorter.

The spectral peaks of the distribution of minor chemical components in the Upper Ordovician–Lower Silurian salt deposits of Australia are comparable with those in late Quaternary climatic records influenced predominantly by ~100-kyr eccentricity (Imbrie et al., 1992), suggesting that eccentricity cycles had a significant impact on the Late Ordovician climate (Williams, 1991). Coupled atmosphere–ocean–sea ice models have also shown that the Late Ordovician ice sheet was sensitive to changes in orbital cycles of ~100-kyr eccentricity (Poussart et al., 1999). The decameter-scale variations in the δ^{18} O signal within these transgressive/regressive cycles on Anticosti Island also suggest that orbital-scale (eccentricity) glacioeustasy controlled the water-depth changes (Mauviel et al., 2020). Using this assumption, Sutcliffe et al. (2000) assessed the two cycles (lasted 0.2 Myr) of ice-sheet growth during glaciation and the minimum duration (0.3 Myr) of the first extinction event based on interpretations of Upper Ordovician glacial-



(caption on next page)

Fig. 8. Our reanalysis and 405 kyr tuning of selected series for the Ordovician FATS. Chronostratigraphy columns on the left were modified from the GTS2020 integrated stratigraphy. (A) Fe³⁺ series and the 405 kyr filter output (red curve, passband: 0.00247 ± 0.0008 cycles/kyr) of the Core EHD1 (South China) (the original data from Lu et al., 2019). (B) Log-ARM series and 405-kyr filter output (red curve, passband: 0.00247 ± 0.0008 cycles/kyr) of the Wanhe Section (South China) (the original data from Zhong et al., 2020). (C) MS series and 405-kyr filter output (red curve, passband: 0.00247 ± 0.0008 cycles/kyr) of the Dawangou Section (Tarim Basin) (the original data from Fang et al., 2019). (D) MS series and 405-kyr filter output (passband: 0.0025 ± 0.0005 cycles/kyr) of the Huangnitang Section and Core CJ-3 (South China) (the original data from Zhong et al., 2018). (E) Ca series and 405-kyr filter output (passband: 0.0025 ± 0.001 cycles/kyr) of the Huangnuachang Section (South China) and Liangjiashan Section (North China) (the original data from Ma et al., 2020). A1-E2 are 2π MTM power spectra of the A-E series, respectively. References are listed as 1-Zhang et al. (2021), 2-Long (2007), 3-Mauviel et al. (2020), 4-Williams (1991), 5-Sutcliffe et al. (2000), 6-Lu et al. (2019), 7-Zhong et al. (2020), 8-Sinnesael et al. (2021), 9-Elrick et al. (2013), 10-Brookfield and Hannigan (2021), 11-Ma et al. (2019b), 12-Zhong et al. (2019), 13-Zhao et al. (2019), 13-Zhao et al. (2019), 20-Fang et al. (2019), 21-Zhong et al. (2015), 16-Dabard et al. (2015), 17-Sinnesael et al. (2022), 18-Fang et al. (2016), 19-Rasmussen et al. (2019), 20-Fang et al. (2011), 27-Goldhammer et al. (2018), 22-Rodionov et al. (2003), 23-Rasmussen et al. (2012), 24-Gong and Droser (2001), 25-Ma et al. (2019a), 26-Zhang et al. (2011), 27-Goldhammer et al. (1993), 28-Kim and Lee (1998). (For interpretation of the references to colour in this figure legend, the reader is refer

marine rocks in Africa. Recently, a high-precision FATS established in the Wanhe section, South China, suggests that the first and second pulses of the Late Ordovician mass extinction lasted \sim 440 and \sim 540 kyr, respectively (Zhong et al., 2020) (Fig. 8).

3.5.1.2. Katian Stage. There has not been a continuous record of Katian cyclostratigraphy until now, and most studies have concentrated on the Sandbian-Katian or Katian-Hirnantian stages. Three proxy series (GR, MS, and ¹⁸O data) were used in the time series analysis of cyclostratigraphy for the Pagoda and Linhsiang formations, corresponding to the Sandbian-Katian period, in the YH-1 core drilled in Huanghuachang, South China (Zhong et al., 2018) (Fig. 8). The total duration of the Pagoda and Linhsiang formations are estimated to be 5.98 Myr. Ma et al. (2019b) conducted high-resolution cyclostatigraphic studies on the MS series of the upper Ordovician Pagoda Formation in three sections in the Sichuan basin, South China. They determined the precise durations of the Pagoda Formation to be 4.17 Myr in Qiaoting section, 5.64 Myr in the Sanquan section, and 5.05 Myr in Liangeun section, indicating that the deposition of Pagoda Formation has obvious diachronism. In the Traim Basin, fourth-, fifth-, and sixth-order sequences were developed in the carbonate succession of the Lianglitage Formation of the Upper Ordovician in the Tazhong-Bachu area and have been interpreted to be related to 405-kyr, 100-kyr, and 20-40-kyr cycles, respectively. The Lianglitage Formation can be inferred to comprise eleven or twelve 405kyr cycles (Zhao et al., 2010). Zhong et al. (2020) yielded a FATS via the stepwise 405-kyr and 33.8-kyr calibrations, which provided an estimated duration of ~7.36 Myr for the early Katian through Hirnantian succession at the Wanhe section of the western Yangtze Platform (Fig. 8B).

The Milankovitch cyclicity from δ^{13} C patterns in mid-Cincinnatian samples on the eastern North American passive margin shelf in SW Ontario, Canada, is practically identical to that from magnetic intensities on the contemporary Yangtze Platform (Brookfield and Hannigan, 2021). Several researchers have interpreted the record of eccentricity and long-term obliquity cycles in the Upper Ordovician reference outcrop sections of Anticosti Island, Québec, Canada (Elrick et al., 2013; Ghienne et al., 2014; Long, 2007; Mauviel et al., 2020). Based on these interpreted sedimentation accumulation rates, a total length of tens of millions of years was projected for the upper Katian mixed siliciclastic-carbonate succession, which is incongruous with the integrated stratigraphic constraints showing an estimated duration of 4-5 Myr (Cooper et al., 2012; McLaughlin et al., 2016). The clear imprint of the amplitude modulation of precession and eccentricity constrains the entire succession to only ~3 Myr, representing ~10 times higher accumulation rates than previously suggested (Sinnesael et al., 2021). Moreover, Sinnesael et al. (2021) detected a shift of the dominated orbital cycle that may be related to contemporaneous global cooling before the Hirnantian glacial maximum in the uppermost Vauréal Formation. In addition to providing the duration of stratigraphic intervals, the cyclostratigraphic studies of the Katian have shed light on the major Myr-scale eustatic sea-level cycles, corresponding to third- or fourth-order sea-level fluctuations driven by the 405-kyr eccentricity and 1.2-Myr obliquity cycles (Lu et al., 2019; Sinnesael et al., 2017; Zhang et al., 2021; Zhong et al., 2020).

3.5.1.3. Sandbian Stage. Several studies suggest that Milankovitchband cyclicity, recorded in sedimentary successions from the Sandbian stage, fits well with the expected orbital periodicities for the Ordovician and the radiometric ages. In the Oslo region of southern Norway, Svensen et al. (2015) dated two of the key tephras (the Kinnekulle and upper Grimstorp K-bentonite) and identified cyclicities that represent the 100-kyr short eccentricity and 30.3-kyr obliquity components of the Arnestad Formation. Similarly, a detailed geochronological and cyclostratigraphic study of one of the complete Ordovician K-bentonite sections in Europe was conducted by Ballo et al. (2019) in the Sinsen section with 33 K-bentonite beds in the Olso region of southern Norway. They interpreted significant periodicity peaks of MS as eccentricity (111.6 kyr), obliquity (33.1 kyr), and precession (17.5 kyr and 14.2 kyr) components. In addition, Ballo et al. (2019) presented an age model for the Arnestad Formation with implications for the age determination of the entire sequence of 33 Sandbian K-bentonites, international Kbentonite correlation, and a new age estimate for the Sandbian-Katian boundary of 452.62 \pm 0.39 Ma. This result is very close to the age given by Cooper et al. (2012) in GTS2012 (453.0 \pm 0.7 Ma) and proposed by Goldman et al. (2020) in GTS2020 (452.8 \pm 0.7 Ma). In the Ordos Basin, North China, the Pingliang Formation, comprising rhythmic alternations of shale, limestone, and siliceous beds, indicates possible astronomical forcing preserved in this lithological record. Fang et al. (2016) estimated the middle Pingliang Formation durations as ~3.3 Myr.

3.5.2. Middle Ordovician

The Middle Ordovician includes Darriwilian and Dapingian stages, spans \sim 13.1 Myr from \sim 471.3 Ma to 458.2 Ma (Goldman et al., 2020), including Darriwilian and Dapingian stages. The base of the Darriwilian Stage correlates with the graptolite *Levisograptus austrodentatus*, and the top is defined at the FAD of the graptolite *Nemagraptus gracilis*, which is 11.2-Myr long (Bergström et al., 2000; Goldman et al., 2020; Mitchell et al., 1997). The base and top of the Dapingian Stage are defined at the FAD of conodont *Baltoniodus triangularis* and the graptolite species *Levisograptus austrodentatus*, respectively, lasting 1.9 Myr (Goldman et al., 2020; Mitchell et al., 1997; Wang et al., 2009). Milankovitch cycles were identified in the outcrops and boreholes of South China, Tarim Basin, Siberia, North America, and Europe (Fig. 8).

3.5.2.1. The Darriwilian Stage. Zhong et al. (2018) conducted a detailed cyclostratigraphic analysis of the MS logs from the Huangnitang Darriwilian GSSP section (Fig. 8D). They identified Milankovitch periods and built a FATS for this section by tuning it with the 405-kyr cycles. Based on the FATS, Zhong et al. (2019) gave the durations of 8.38 \pm 0.4 Myr for the Darriwilian Stage, which is close to 8.9 \pm 1.1 Myr in GTS2012 and further confirms the reliability of FATS (Fig. 8).

In the Baltoscandian, high-precision XRF elemental core scanning data from the island of Öland, Sweden, the presence of Milankovitch-scale cyclicity in the records of Kårehamn P4 cores were observed.

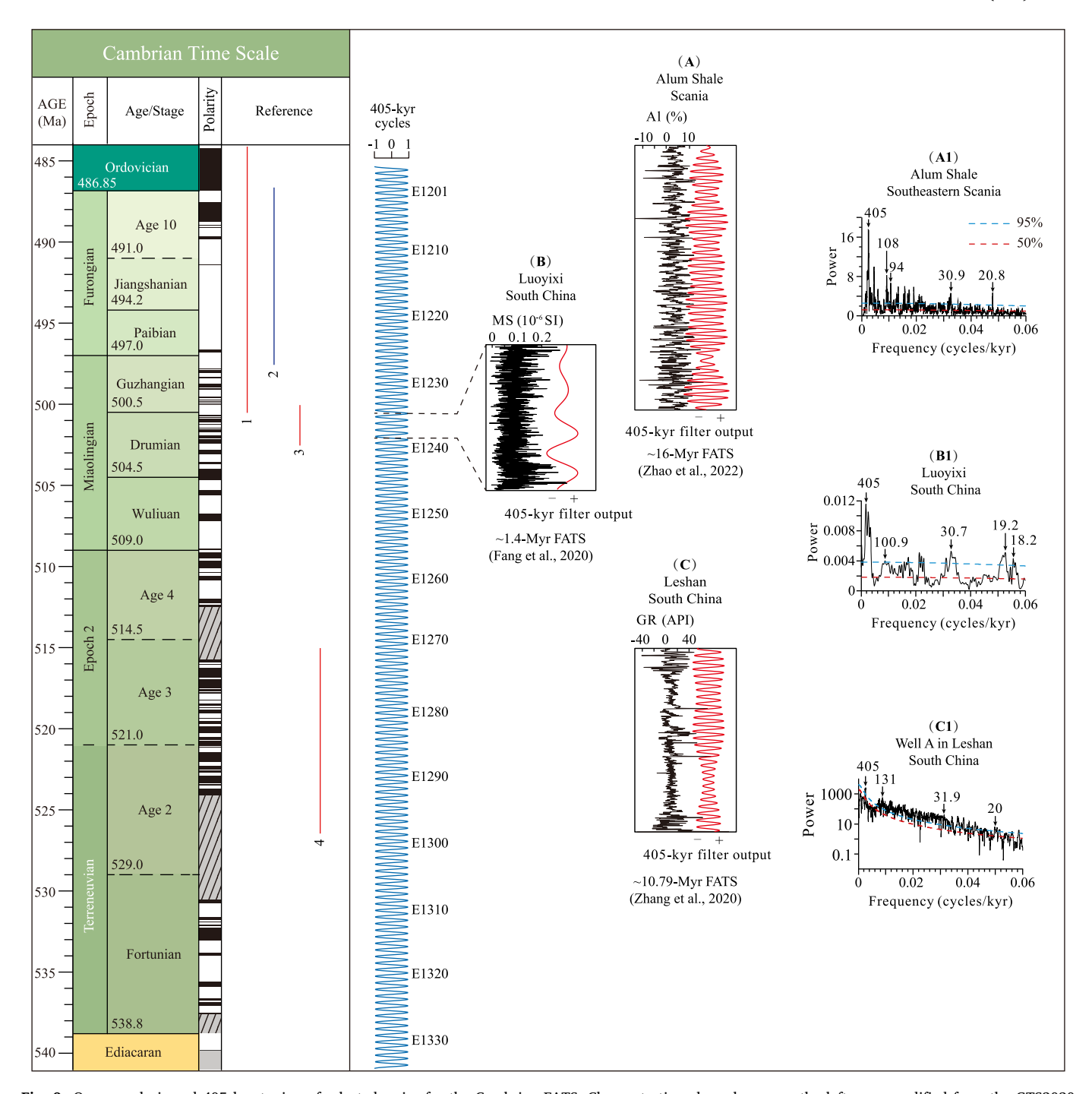


Fig. 9. Our reanalysis and 405 kyr tuning of selected series for the Cambrian FATS. Chronostratigraphy columns on the left were modified from the GTS2020 integrated stratigraphy. (A) Aluminum series. The original data from Zhao et al. (2022) from Albjära-1 drill core (Scania) with 405-kyr filter output (red curve, passband: 0.00247 ± 0.0005 cycles/kyr). (B) MS series. The original data from the Luoyixi section (South China) (Fang et al., 2020) with 405-kyr filter output (red curve, passband: 0.002469 ± 0.001 cycles/kyr). (C) GR series. The original data from Well A (South China) (Zhang et al., 2022) with 405-kyr filter output (red curve, passband: 0.002469 ± 0.0008 cycles/kyr). (A1), (B1), and (C1) are 2π MTM power spectra of series in A, B, and C, respectively. References are listed as 1—Zhao et al. (2022), 2—Sørensen et al. (2020), 3—Fang et al. (2020), 4—Zhang et al. (2022). (For interpretation of the references to colour in this figure legend, the reader is referred to the web version of this article.)

Rasmussen et al. (2019) conducted a spectral analysis of the red spectrum based on high-resolution colour images obtained from the core scanner, and the millimeter-scale data in key elements. 24 long-eccentricity cycles were observed in the Kårehamn core for D2–D3, indicating a total duration of 9.72 Myr. This estimate is supported by a comparison of the revised chronostratigraphy for the Middle Ordovician (Lindskog et al., 2017) with the conodont biozonation in Kårehamn. Considering the inconsistent response of different proxies to climate

change, different sedimentary environments, and the large uncertainty of the isotopic dates used to build the Ordovician time scale, it is still difficult to draw a definite conclusion on the duration of the Darriwilian Stage.

Cyclostratigraphy for Darriwilian has also been studied in Siberia, Tarim Basin, and western France. Spectral analysis using high-field MS showed significant cyclicity in the Krivaya Luka section of southern Siberia. Rodionov et al. (2003) interpreted these spectral peaks as the

precession (17.82 kyr and 16.35 kyr), obliquity (27.9 kyr), and eccentricity (125 kyr) cycles, and estimated an average sediment accumulation rate of ~3.5 cm/kyr. Extrapolating from this, the durations of the Volginsky fossil zone and the entire Krivaya Luka section are 1 Myr and 1.2 Myr, respectively (Rodionov et al., 2003). Fang et al. (2019) identified twelve and seventeen 405-kyr eccentricity cycles in MS series at Dawangou and Yangjikan sections, Tarim, respectively (Fig. 8C). Applying the 405-kyr tuned timescale to the boundaries of graptolite biozones, they estimated the durations of the Pterograptus elegans (1040 kyr), Didymograptus murchisoni (2120 kyr), and Jiangxigraptus vagus (540 kyr) at Dawangou. However, the 405-kyr-tuned duration of the P. elegans biozone in the Huangnitang area, South China, is 0.55 Myr (Zhong et al., 2018). The reconstruction of third to fifth-order eustatic sea-level changes was based on sedimentological interpretations and meter-scale natural GR data, which are hypothesized to correspond to astronomical forcing in the Ordovician sections of the Crozon Peninsula (western France) (Dabard et al., 2015). Subsequently, Sinnesael et al. (2022) performed traditional cyclostratigraphic analyses using centimeter-scale portable X-ray fluorescence and natural GR data in the same section. The results confirm a potential astronomical imprint of some sedimentary cycles in the relatively homogenous lithology.

The Earth experienced a shift from a greenhouse to an icehouse climate during the Darriwilian Stage, which resulted in biotic, atmospheric, and hydrological changes. A growing number of publications have inferred that it is linked to astronomical cycles, for example, ~1.2-Myr obliquity and \sim 2.4-Myr eccentricity cycles. Fang et al. (2019) suggest that the cooling trend was initiated by the alignment of the 2.4-Myr eccentricity and 1.2-Myr obliquity cycles minima ~4.07 Myr before the Darriwilian/Sandbian (D/S) boundary, and was dominated by the obliquity forcing. Recently, a precise FATS was built in the Middle Ordovician Steinsodden section in the Moelv area of southern Norway. Based on the astronomically calibrated cyclostratigraphic framework, Rasmussen et al. (2021) found an energy transfer from precession to 405-kyr eccentricity cycles that coincided with the start of GOBE and succeeded the onset of icehouse conditions by 200,000 years at \sim 469 Ma. The FATS indicates that an asteroid break-up, postulated to facilitate the icehouse with increased extra-terrestrial dust, post-dated the onset of icehouse conditions by 800,000 years. These decoupled the asteroids break up from glacially induced biotic radiations and deciphered the orbital control in modulating climate and even biodiversity accumulation over time. Despite the lack of identified glacial deposits at present, 1.2-Myr obliquity cycles were confirmed to be the main driver of the third-order glacio-eustatic sequences in South China, Tarim Basin, and Western France (Dabard et al., 2015; Fang et al., 2019; Sinnesael et al., 2022; Zhong et al., 2018).

3.5.2.2. Dapingian Stage. The Dapingian Stage has a duration of \sim 1.97 Myr according to the astronomically calibrated MS series from the Huangnitang section and the core Changjin 3 (CJ-3), Zhejiang Province, South China (Zhong et al., 2018). In comparison, the duration of the Dapingian stages in GTS2012 was \sim 2.7 Myr. The GTS2020 scale for the Dapingian Stage provides a duration of 1.9 Myr (Goldman et al., 2020). The duration of the Dapingian compares well with the FATS, which confirms the calibration results. Moreover, Zhong et al. (2019) estimated the durations of two graptolite zones in the Dapingian Stage based on the FATS as follows: Isograptus caduceus imitatus Zone (2.89 Myr) and Exigraptus clavus Zone (0.5 Myr).

3.5.3. Early Ordovician

The Early Ordovician includes Floian and Tremadocian stages and spans ~15.6 Myr from ~486.9 Ma at Cambrian/Ordovician boundary (COB) to ~471.3 Ma at the Early/Middle Ordovician boundary (Goldman et al., 2020). The Floian Stage from the stratigraphic level at the FAD of the graptolite *Tetragraptus approximates*, to the FAD of the conodont *Baltoniodus triangularis*, which is 5.8-Myr long (Bergström et al.,

2004; Goldman et al., 2020; Wang et al., 2009). The Tremadocian Stage, which lasted 9.8 Myr, is marked by the FAD of the conodont species *Iapetognathus fluctivagus* as the base and is defined as the FAD of the graptolite *Tetragraptus approximates* (Bergström et al., 2004; Cooper et al., 2001; Goldman et al., 2020). Only a few cyclostratigraphic studies have been published for the Early Ordovician.

3.5.3.1. Floian Stage. The Floian Stage has a composite FATS constraint that is mainly derived from marine carbonates in South and North China (Ma et al., 2019a) (Fig. 8E). Ma et al. (2019a) built the FATS for the Floian Stage based on an analysis of the Ca of the Liangjiashan Formation (North China) and Huanghuachang section (South China). According to the FATS, the duration of the Serratognathus bilobatus Zone, Serratog. extensus Zone, Oepikodus communis Zone, O. evae Zone, and Baltoniodus triangularis Zone are 1.0 Myr, 5.1 Myr, 0.2 Myr, 0.8 Myr, and 0.2 Myr, respectively (Ma et al., 2019a). Approximately fifteen 405-kyr cycles span the Floian in North China, indicating a duration of the partly Floian Stage of $\sim\!6.07$ Myr. At Huanghuachang, South China, two and a half 405-kyr cycles are recognized in the Floian, providing an estimated duration of ~ 1.01 Myr for the Late Floian. With constraints of conodont biostratigraphy and cyclostratigraphy between the Liangjiashan and Huanghuachang sections, Ma et al. (2019a) estimated duration of 7.08 \pm 0.40 Myr for the Floian Stage (Fig. 8E). In comparison, high-precision U-Pb dates combined with the biostratigraphic framework of the Canning Basin indicate that the duration of the Floian Stage is >6.95 \pm 0.21 Myr (Normore et al., 2018).

In Tarim, NW China, Zhang et al. (2011) recognized the obliquity (37 kyr), short-eccentricity (95 kyr), and long-eccentricity (413 kyr) cycles in the Yingshan Formation of the Floian Stage, and opined that these orbitally forced the fourth- to sixth- order sequences. Moreover, the duration of the Yingshan Formation was estimated to be $\sim\!4.92$ Myr (Zhang et al., 2011). For the Early–Middle Ordovician (Ibexian–Whiterockian) transition, Gong and Droser (2001) identified 100-kyr eccentricity sedimentary cycles in the Low–Middle Ordovician in western Utah, USA, and postulated a duration of 3.4 Myr for the periodic anoxic event.

3.5.3.2. Tremadocian Stage. Only two cyclostratigraphic studies have been conducted in North America and North Korea. Goldhammer et al. (1993) interpreted the remarkable sedimentary cycles in the Lower Ordovician strata on the Diablo platform, Texas, USA, as precession cycles. In North Korea, the meter-scale sedimentary cycles of the Lower Ordovician Dumugol Formation were estimated to be \sim 96-kyr eccentricity cycle, and Kim and Lee (1998) proposed that this may correspond to high-frequency fourth- to fifth-order sea level sequences. The research mentioned above only judged whether the Earth's orbit parameters affected the deposition process through the combination of characteristics, mode, and hierarchical structure of the lamina/layer, laminar beam, laminar beam group, and superlayer beam group.

3.6. Cambrian

The marker for the Cambrian base is the FAD of the trace fossil, *Treptichnus pedum* (Linnemann et al., 2019). The Cambrian base should lie between ash beds 5 and 6 in the Spitskopf Member of the Urusis Formation, which have calculated ages of 538.99 ± 0.21 Ma and 538.58 ± 0.19 Ma, respectively (Linnemann et al., 2019). These ash beds are below the last occurrence of *Swarpuntia germsi* and *Pteridinium simplex* in the Ediacaran biota. The current best estimated radioisotopic date for the base of the Cambrian is 538.8 ± 0.60 Ma (Linnemann et al., 2019). Therefore, the duration of the Cambrian is regarded as ~ 51.9 Myr. The bases of the five international Cambrian stages assigned to GSSPs or candidate definitions are at levels corresponding to the FAD of trilobites. Only four cyclostratigraphic studies have been published for the Cambrian in recent years (Fig. 9). The Cambrian period spans E1201 to

E1329.

3.6.1. The Furongian and Miaolingian

From the Miaolingian/Furongian boundary (\sim 497 Ma) to the Cambrian/Ordovician boundary (\sim 486.9 Ma), the Furongian contains Stage 10, Jiangshanian, and Paibian and covers a total duration of \sim 10 Myr. The Miaolingian consists of the Guzhangian, Drumian, and Wuliuan stages and spans \sim 12 Myr between the Series 2/Miaolingian boundary at \sim 509 Ma and the Miaolingian/Furongian boundary at \sim 497 Ma. Only three Furongian and Miaolingian cyclostratigraphic investigations have been published (Fang et al., 2020; Sørensen et al., 2020; Zhao et al., 2022).

For the Miaolingian/Furongian boundary, Sørensen et al. (2020) constructed an 8.7-Myr FATS based on the recognition of 405-kyr cycles in the drilled core from the Alum Shale Formation in the Baltica Basin (Bornholm, Denmark). The Parabolina superzone spans ~4.8405-kyr cycles, suggesting a 1.9 ± 0.3 Myr duration. In contrast, a shorter duration was interpreted in the Albjära-1 drill core of the Alum Shale Formation by Zhao et al. (2022), who collected Al data measured by XRF from the 77.37 m succession and detected four 405-kyr cycles in Para*bolina* Superzone. After anchoring the numerical ages of 486.78 \pm 0.53 Ma and 488.71 \pm 1.17 Ma, the constructed 16-Myr FATS spans from 499.9 ± 0.9 Ma to 483.9 ± 0.7 Ma (Zhao et al., 2022) (Fig. 9A). Fang et al. (2020) found the Milankovitch cycles from the basal Guzhangian Stage in Luoyixi section, which mainly consists of cyclic argillaceous/ ribbon limestone and limestone of shallow marine facies (Fig. 9B). Using the counting of the dominant 405-kyr eccentricity cycles, the estimated total duration for the whole succession was ~1.4 Myr. The durations of the agnostoid trilobite biozones of G. nathorsti and L. armata were estimated to be \sim 524 and \sim 152 kyr, respectively.

3.6.2. Series 2 and Terreneuvian

The Series 2 includes Stage 4 and Stage 3 stages and spans \sim 12 Myr from the Terreneuvian/Series 2 boundary at \sim 521 Ma to the Series 2/Miaolingian boundary at \sim 509 Ma. The Terreneuvian includes Stage 2 and Fortunian stages and lasted \sim 18 Myr from the Precambrian/Cambrian boundary at \sim 538.8 Ma to the Terreneuvian/Series 2 boundary at \sim 521 Ma. Only one Series 2 and Terreneuvian cyclostratigraphic study has been published in 2022 (Zhang et al., 2022) (Fig. 9C).

Zhang et al. (2022) interpreted Milankovitch cycles for the interval of Stages 2–3 from the 358 m (Well A) in Leshan City, southwestern Sichuan Province, South China. The analyses were based on 2864 spectral GR measurements and 1071 geochemical data points. The predominant $\sim\!14.9$ m cycles and $\sim\!11.6$ m cycles were assumed to be the stable 405-kyr eccentricity cycle, and tuning to this 405-kyr period produced an $\sim\!10.8$ -Myr FATS for the Stages 2–3. The age assignment to the cyclostratigraphy was based on a U—Pb zircon age of 526.2 \pm 1.9 Ma, interpreting this series as spanning $\sim\!526.2$ Ma (early Stage 2) to $\sim\!515.41$ Ma (late Stage 3).

4. Concluding remarks and research prospects

Astronomically calibrated cyclostratiraphy provides an unprecedented opportunity to recognize and understand the Earth system at a kiloyear scale. Results on cyclostratigraphy could not only construct the high-resolution time scale for the sedimentary record but also provide evidence for the relationship between the astronomical forcing and the climatic and biological evolution, which may improve the understanding of the coupling between forcing outside the Earth and Earth's surface systems. The International Commission on Stratigraphy is about to complete its work on the establishment of sequences in the Mesozoic of the International Geological Time Scale, and future work will focus on the Paleozoic Era. The established FATS for the whole Paleozoic Era would benefit from the efforts in other stratigraphy studies. Future cyclostratigraphy studies have great potential to improve the temporal

resolution on the Paleozoic strata.

Paleozoic cyclostratigraphic studies have largely relied on stable long eccentricity cycles as calibration target. The constructed FATS would be further refined by identifying short eccentricity, precession, and obliquity cycles, which would lead to unprecedented highresolution timescales. Identification of these short-period signals has important paleoclimatological, geochronological, and astronomical implications. The preliminary empirical reconstruction of Earth-Moon and Solar System dynamical parameters has proved the importance of high-resolution cyclostratigraphy records in Paleozoic and even Proterozoic (e.g., Meyers and Malinverno, 2018; Rodrigues et al., 2019; J. Fang et al., 2020; Huang et al., 2020; Sørensen et al., 2020; Zhong et al., 2020; Lantink et al., 2022; Mitchell and Kirscher, 2023; Zhou et al., 2022). Earth's orbital parameters will get more precise with the advancements in astronomical solutions and dating technologies, and it will be feasible to apply astronomical tuning over the whole Phanerozoic in the future. Expanding the cyclostratigraphy to the Paleozoic and using radiometric ages with a higher precision will provide crucial geological evidence for validating the Paleozoic solar system planetary dynamics model and establishing Paleozoic Earth orbit astronomical solutions (Wu et al., 2013; Zeebe and Lourens, 2022).

Cyclostratigraphy is still a developing discipline, and its research methods and related terminology still need to be further standardized. For now, there is still no uniform approach for the expression of uncertainty of astronomical calibration results. An effort should be made to compare the various astrochronological interpretations in a robust and comprehensive stratigraphic framework that takes into account multiple sources of uncertainty. Besides, deciphering the temporal variations of the deep-time climate systems is strongly dependent on interpreting indirect climate proxies from the local or regional records. Paralleling the astronomically calibrated records across successions from different continents and latitudes is still difficult for the deep-time cyclostratigraphy study. The orbital forcing behind climate evolution should also be paid attention to the research, which calls upon the comparison between the time series results with various paleoenvironmental indicators and numerical modeling. As more stratigraphers apply cyclostratigraphic methodologies, the details of astrochronological information will increase. Unprecedented high-resolution records will help us understand the dynamics of the Paleozoic world and the history of the Solar System.

Declaration of Competing Interest

The authors declare that they have no known competing financial interests or personal relationships that could have appeared to influence the work reported in this paper.

Data availability

Data will be made available on request.

Acknowledgements

We express our sincere appreciation to Editor Prof. Timothy Kusky, and Guest Editors Profs. Zhongwu Lan and Huaiyu He, and two reviewers for their comments that significantly improved the manuscript. We also thank Anne-Christine da Silva for her instructive suggestion. Wentao Huang, Chuanzhen Ren, Maoyang Zhou, Shan Li, and Yifei Zhang helped to collect the published data. This work was supported by the National Natural Science Foundation of China (grant no. 41925010, 42072039), the Chinese 111 project (grant no. B20011), and the Fundamental Research Funds for the Central Universities (2-9-2022-201). LAH was partially supported by the Heising Simons Foundation (grant no. 2021-2796).

Appendix A. Supplementary data

Supplementary data to this article can be found online at https://doi.org/10.1016/j.earscirev.2023.104510.

References

- Aboussalam, Z.S., Becker, R.T., 2007. New upper Givetian to basal Frasnian conodont faunas from the Tafilalt (Anti-Atlas, Southern Morocco). Geol. Quart. 51 (4), 345–374. https://doi.org/10.1111/j.1468-0459.2007.00319.x.
- Agterberg, F.P., Da Silva, A.C., Gradstein, F.M., 2020. Chapter 14A–Geomathematical and statistical procedures. In: Gradstein, F.M., Ogg, J.G., Schmitz, M.D., Ogg, G.M. (Eds.), Geologic Time Scale 2020. Elsevier, pp. 401–424. https://doi.org/10.1016/ B978-0-12-824360-2.00020-6.
- Alekseev, A.S., Goreva, N.V., 2013. The conodont *Neognathodus bothrops* Merrill, 1972 as the marker for the lower boundary of the Moscovian Stage (Middle Pennsylvanian). In: Lucas, S.G., DiMichele, W.A., Barrick, J.E., Schneider, J.W., Spielmann, J.A. (Eds.), The Carboniferous–Permian Transition. New Mexico Museum of Natural History and Science Bulletin, pp. 1–6.
- Algeo, T.J., Scheckler, S.E., Maynard, J.B., 2001. Effects of the Middle to Late Devonian spread of vascular land plants on weathering regimes, marine biotas, and global climate. In: Plants Invade the Land. Columbia University Press, pp. 213–236.
- Aretz, M., 2014. Redefining the Devonian–Carboniferous boundary: an overview of problems and possible solutions. In: Rocha, R., Pais, J., Kullberg, J., Finney, S. (Eds.), STRATI 2013, Springer Geology. IUGS, pp. 227–231. https://doi.org/10.1007/978-3-319-04364-7 46.
- Aretz, M., Herbig, H.G., Wang, X.D., Gradstein, F.M., Agterberg, F.P., Ogg, J.G., 2020.
 The Carboniferous Period. In: Geologic Time Scale 2020. Elsevier, pp. 811–874.
- Atakul-Özdemir, A., Altıner, D., Özkan-Altıner, S., Yılmaz, İ.Ö., 2011. Foraminiferal biostratigraphy and sequence stratigraphy across the mid-Carboniferous boundary in the Central Taurides, Turkey. Facies 57, 705–730. https://doi.org/10.1007/s10347-010-0260-y.
- Ballo, E.G., Augland, L.E., Hammer, O., Svensen, H.H., 2019. A new age model for the Ordovician (Sandbian) K-bentonites in Oslo, Norway. Palaeogeogr. Palaeoclimatol. Palaeoecol. 520, 203–213. https://doi.org/10.1016/j.palaeo.2019.01.016.
- Barnes, C.R., 1992. The uppermost series of the Ordovician System. In: Webby, B., Laurie, J.(Eds.) (Eds.), Global Perspectives on Ordovician Geology. Balkema, Rotterdam, pp. 185–192.
- Barnett, A.J., Wright, V.P., 2008. A sedimentological and cyclostratigraphic evaluation of the completeness of the Mississippian–Pennsylvanian (Mid-Carboniferous) Global Stratotype Section and Point, Arrow Canyon, Nevada, USA. J. Geol. Soc. Lond. 165, 859–873. https://doi.org/10.1144/0016-76492007-122.
- Becker, R.T., Gradstein, F.M., Hammer, O., 2012. Chapter 22–The Devonian Period. In: Gradstein, F.M., Ogg, J.G., Schmitz, M.D., Ogg, G.M. (Eds.), The Geologic Time Scale. Elsevier, Boston, pp. 559–601. https://doi.org/10.1016/B978-0-444-59425-0.0023.6
- Becker, R.T., Marshall, J.E.A., Da Silva, A.C., Agterberg, F.P., Gradstein, F.M., Ogg, J.G., 2020. Chapter 22–The Devonian Period. In: Gradstein, F.M., Ogg, J.G., Schmitz, M. D., Ogg, G.M. (Eds.), Geologic Time Scale 2020. Elsevier, pp. 733–810. https://doi.org/10.1016/B978-0-12-824360-2.00022-X.
- Berger, A.L., 1978. Long-term variations of caloric insolation resulting from the Earth's orbital elements. Quat. Res. 9, 139–167. https://doi.org/10.1016/0033-5894(78)
- Berger, A., Loutre, M.F., Laskar, J., 1992. Stability of the astronomical frequencies over the Earth's history for paleoclimate studies. Science 255 (5044), 560–566. https://doi.org/10.1126/science.255.5044.560.
- Bergström, S.M., Finney, S.C., Chen, X., Palsson, C., Wang, Z.H., Grahn, Y., 2000.

 A proposed global boundary stratotype for the base of the Upper Series of the Ordovician System: the Fågelsång section, Scania, southern Sweden. Episodes 23 (2), 102–109. https://doi.org/10.18814/epiiugs/2000/v23i2/003.
- Bergström, S.M., Lofgren, A., Maletz, J., 2004. The GSSP of the second (Upper) stage of the lower Ordovician series: Diabasbrottet at Hunneberg, province of Vastergotland, southwestern Sweden. Episodes 27 (4), 265–272. https://doi.org/10.18814/epiiugs/ 2004/v27i4/005
- Berner, R.A., 2003. The long-term carbon cycle, fossil fuels and atmospheric composition. Nature 426 (6964), 323–326. https://doi.org/10.1038/nature02131.
- Birgenheier, L.P., Fielding, C.R., Rygel, M.C., Frank, T.D., Roberts, J., 2009. Evidence for dynamic climate change on sub-10⁶-year scales from the late Paleozoic glacial record, Tamworth Belt, New South Wales, Australia. J. Sediment. Res. 79, 56–82. https://doi.org/10.2110/jsr.2009.013.
- Blomeier, D., Scheibner, C., Forke, H., 2009. Facies arrangement and cyclostratigraphic architecture of a shallow-marine, warm-water carbonate platform: the late Carboniferous Ny Friesland Platform in eastern Spitsbergen (Pyefjellet Beds, Wordiekammen Formation, Gipsdalen Group). Facies 55 (2), 291–324. https://doi.org/10.1007/s10347-008-0163-3.
- Braun, M.G., Daoust, P., Desrochers, A., 2021. A sequential record of the Llandovery delta δ¹³C_{carb} excursions paired with time-specific facies: Anticosti Island, eastern Canada. Palaeogeogr. Palaeoclimatol. Palaeoecol. 578, 110566 https://doi.org/ 10.1016/j.palaeo.2021.110566.
- Brenchley, P.J., Marshall, J.D., Carden, G.A.F., Robertson, D.B.R., Long, D.G.F., Meidla, T., Hints, L., Anderson, T.F., 1994. Bathymetric and isotopic evidence for a short-lived late Ordovician glaciation in a greenhouse period. Geology 22 (4), 295–298. https://doi.org/10.1130/0091-7613(1994)022<0295:BAIEFA>2.3.CO;2.

- Brookfield, M.E., Hannigan, R.E., 2021. Carbon and oxygen isotope variations in shell beds from the Upper Ordovician (mid-Cincinnatian: Maysvillian to early Richmondian) of Ontario: evaluation of the warm Saline Deep Ocean hypothesis, paleoceanographic changes, and Milankovitch orbital cycles in the transition to the Hirnantian glaciation. Palaeogeogr. Palaeoclimatol. Palaeoecol. 577, 110528 https://doi.org/10.1016/j.palaeo.2021.110528.
- Burgess, S., Bowring, S., Shen, S.Z., 2014. High-precision timeline for Earth's most severe extinction. Proc. Natl. Acad. Sci. U.S.A. 111 (13), 5060. https://doi.org/10.1073/ pnas.1403228111.
- Caputo, M.V., de Melo, J.H.G., Streel, M., Isbell, J.L., 2008. Late Devonian and early Carboniferous glacial records of South America. Geol. Soc. Am. Spec. Pap. 441, 161–173. https://doi.org/10.1130/2008.2441(11).
- Carls, P., Slavik, L., Valenzuela-Rios, J.I., 2008. Comments on the GSSP for the basal Emsian stage boundary: the need for its redefinition. B. Geosci. 83 (4), 383–390. https://doi.org/10.3140/bull.geosci.2008.04.383.
- Cecil, B.C., DiMichele, W.A., Elrick, S.D., 2014. Middle and late Pennsylvanian cyclothems, American Midcontinent: Ice-age environmental changes and terrestrial biotic dynamics. Compt. Rendus Geosci. 346 (7), 159–168. https://doi.org/10.1016/ icste.2014.03.008
- Chen, X., Rong, J.Y., Fan, J.X., Zhan, R.B., Mitchell, C.E., Harper, D.A.T., Melchin, M.J., Peng, P., Finney, S.C., Wang, X.F., 2006. The Global boundary Stratotype Section and Point (GSSP) for the base of the Hirnantian Stage (the uppermost of the Ordovician System). Episodes 29 (3), 183–196. https://doi.org/10.18814/epiiugs/ 2006/w2913/004
- Chernykh, V., Chuvashov, B., Shen, S.Z., Henderson, C., Yuan, D.X., Stephenson, M., 2020a. The Global Stratotype Section and Point (GSSP) for the base-Sakmarian Stage (Cisuralian, lower Permian). Episodes 43 (4), 961–979. https://doi.org/10.18814/ eniiues/2020/020059.
- Chernykh, V.V., Kotlyar, G.V., Chuvashov, B.I., Kutygin, R.V., Filimonova, T.V., Sungatullina, G.M., Mizens, G.A., Sungatullin, R.K., Isakova, T.N., Boiko, M.S., Ivanov, A.O., Nurgalieva, N.G., Balabanov, Y.P., Mychko, E.V., Gareev, B.I., Batalin, G.A., 2020b. Multidisciplinary study of the Mechetlino Quarry section (Southern urals, Russia)—The GSSP candidate for the base of the Kungurian Stage (Lower Permian). Palaeoworld 29 (2), 325–352. https://doi.org/10.1016/j.palwor.2019.05.012.
- Chuvashov, B.I., Chernykh, V.V., Shen, S.Z., Henderson, C.M., 2013. Proposal for the Global Stratotype Section and Point (GSSP) for the base-Artinskian Stage (Lower Permian). Permophiles 58, 26–34.
- Cocks, L.R.M., 1985. The Ordovician–Silurian Boundary. Episodes. 8 (2), 98–100. https://doi.org/10.18814/epiiugs/1985/v8i2/004.
- Cooper, R.A., Nowlan, G.S., Williams, S.H., 2001. Global stratotype section and point for base of the Ordovician system. Episodes 24, 19–28. https://doi.org/10.18814/ epiiugs/2001/v24i1/005.
- Cooper, R.A., Sadler, P.M., Hammer, O., Gradstein, F.M., 2012. Chapter 20–The Ordovician Period. In: The Geologic Time Scale. Elsevier, pp. 489–523. https://doi. org/10.1016/B978-0-444-59425-9.00020-2.
- Cramer, B.D., Jarvis, I., 2020. Chapter 11–Carbon isotope stratigraphy. In: Geologic Time Scale 2020. Elsevier, pp. 309–343. https://doi.org/10.1016/B978-0-12-824360-2.00011-5
- Crampton, J.S., Meyers, S.R., Cooper, R.A., Sadler, P.M., Foote, M., Harte, D., 2018. Pacing of Paleozoic macroevolutionary rates by Milankovitch grand cycles. Proc. Natl. Acad. Sci. U.S.A. 115 (22), 5686–5691. https://doi.org/10.1073/pngs.1714342115
- Crick, R.E., Ellwood, B.B., Hladil, J., El Hassani, A., Hrouda, F., Chlupac, I., 2001. Magnetostratigraphy susceptibility of the Pridolian-Lochkovian (Silurian–Devonian) GSSP (Klonk, Czech Republic) and a coeval sequence in Anti-Atlas Morocco. Palaeogeogr. Palaeoclimatol. Palaeoecol. 167 (1–2), 73–100. https://doi.org/ 10.1016/S0031-0182(00)00233-9.
- Cui, Y., Li, M., van Soelen, E.E., Peterse, F., Kürschner, W.M., 2021. Massive and rapid predominantly volcanic CO₂ emission during the end-Permian mass extinction. Proc. Natl. Acad. Sci. U.S.A. 118 (37), e2014701118. 10.1073/pnas.2014701118.
- Da Silva, A.C., De Vleeschouwer, D., Boulvain, F., Claeys, P., Fagel, N., Humblet, M., Mabille, C., Michel, J., Sardar Abadi, M., Pas, D., Dekkers, M.J., 2013. Magnetic susceptibility as a high-resolution correlation tool and as a climatic proxy in Paleozoic rocks Merits and pitfalls: Examples from the Devonian in Belgium. Mar. Petrol. Geol. 46, 173–189. https://doi.org/10.1016/j.marpetgeo.2013.06.012.
- Da Silva, A.C., Hladil, J., Chadimová, L., Slavík, L., Hilgen, F.J., Bábek, O., Dekkers, M.J., 2016. Refining the Early Devonian time scale using Milankovitch cyclicity in Lochkovian-Pragian sediments (Prague Synform, Czech Republic). Earth Planet. Sci. Lett. 455, 125–139. https://doi.org/10.1016/j.epsl.2016.09.009.
- Da Silva, A.C., Sinnesael, M., Claeys, P., Davies, J., de Winter, N.J., Percival, L.M.E., Schaltegger, U., De Vleeschouwer, D., 2020. Anchoring the late Devonian mass extinction in absolute time by integrating climatic controls and radio-isotopic dating. Sci. Rep. 10 (1), 12940. https://doi.org/10.1038/s41598-020-69097-6.
- Dabard, M.P., Loi, A., Paris, F., Ghienne, J.F., Pistis, M., Vidal, M., 2015. Sea-level curve for the Middle to Early Late Ordovician in the Armorican Massif (western France): icehouse third-order glacio-eustatic cycles. Palaeogeogr. Palaeoclimatol. Palaeoecol. 436, 96–111. https://doi.org/10.1016/j.palaeo.2015.06.038.
- Dalziel, I.W.D., 1977. Neoproterozoic–Paleozoic geography and tectonics: review, hypothesis, environmental speculation. Geol. Soc. Am. Bull. 109, 16–42.
- Daniel, G., Stephen, A.L., Jaak, N., Lvak, Seth, Y., Stig, M.B., Warren, D.H., 2007. The Global Stratotype Section and Point (GSSP) for the base of the Katian Stage of the Upper Ordovician Series at Black Knob Ridge, Southeastern Oklahoma, USA. Episodes 30 (4), 258–270.
- Davydov, V.I., Cozar, P., 2019. The formation of the Alleghenian Isthmus triggered the Bashkirian glaciation: constraints from warm-water benthic foraminifera.

- Palaeogeogr. Palaeoclimatol. Palaeoecol. 531, 108403 https://doi.org/10.1016/j.
- Davydov, V.I., Crowley, J.L., Schmitz, M.D., Poletaev, V.I., 2010. High-precision U-Pb zircon age calibration of the global Carboniferous time scale and Milankovitch band cyclicity in the Donets Basin, eastern Ukraine. Geochem. Geophys. Geosyst. 11, 22. https://doi.org/10.1029/2009GC002736.
- Davydov, V.I., Glenister, B.F., Spinosa, C., Ritter, S.M., Chernykh, V.V., Wardlaw, B.R., Snyder, W.S., 1998. Proposal of Aidaralash as Global Stratotype Section and Point (GSSP) for base of the Permian System. Episodes 21, 11–18.
- Davydov, V.I., Korn, D., Schmitz, M.D., Gradstein, F.M., Hammer, O., 2012. The Carboniferous Period. In: Gradstein, F.M., Ogg, J.G., Schmitz, M.D., Ogg, G.M. (Eds.), The Geologic Time Scale 2012. Elsevier, pp. 603–651.
- De Vleeschouwer, D., Parnell, A.C., 2014. Reducing time-scale uncertainty for the Devonian by integrating astrochronology and Bayesian statistics. Geology 42 (6), 491–494. https://doi.org/10.1130/G35618.1.
- De Vleeschouwer, D., Boulvain, F., Da Silva, A.C., Pas, D., Labaye, C., Claeys, P., 2015. The astronomical calibration of the Givetian (Middle Devonian) timescale (Dinant Synclinorium, Belgium). In: DaSilva, A., Whalen, M., Hladil, J., Chadimova, L., Chen, D., Spassov, S., Boulvain, F., Devleeschouwer, X. (Eds.), Magnetic Susceptibility Application: A Window Onto Ancient Environments And Climatic Variations, pp. 245–256. https://doi.org/10.1144/SP414.3.
- De Vleeschouwer, D., Da Silva, A.C., Boulvain, F., Crucifix, M., Claeys, P., 2012b. Precessional and half-precessional climate forcing of Mid-Devonian monsoon-like dynamics. Clim. Past 8 (1), 337–351. https://doi.org/10.5194/cp-8-337-2012.
- De Vleeschouwer, D., Da Silva, A.C., Sinnesael, M., Chen, D.Z., Day, J.E., Whalen, M.T., Guo, Z.H., Claeys, P., 2017. Timing and pacing of the Late Devonian mass extinction event regulated by eccentricity and obliquity. Nat. Commun. 8 (1), 2268. https://doi.org/10.1038/s41467-017-02407-1.
- De Vleeschouwer, D., Konigshof, P., Claeys, P., 2018. Reading time and paleoenvironmental change in the Emsian–Eifelian boundary GSSP section (Wetteldorf, Germany): a combination of cyclostratigraphy and facies analysis. Newsl. Stratigr. 51, 209–226. https://doi.org/10.1127/nos/2017/0397.
- De Vleeschouwer, D., Rakociński, M., Racki, G., Bond, D.P.G., Sobień, K., Claeys, P., 2013. The astronomical rhythm of Late-Devonian climate change (Kowala section, Holy Cross Mountains, Poland). Earth Planet. Sci. Lett. 365, 25–37. https://doi.org/ 10.1016/j.epsl.2013.01.016.
- De Vleeschouwer, D., Whalen, M.T., Day, J.E., Claeys, P., 2012a. Cyclostratigraphic calibration of the Frasnian (Late Devonian) time scale (western Alberta, Canada). Geol. Soc. Am. Bull. 124 (5–6), 928–942. https://doi.org/10.1130/B30547.1.
- Devuyst, F.X., Hance, L., Hou, H.F., Wu, X.H., Tian, S.G., Coen, M., Sevastopulo, G., 2003. A proposed global stratotype section and point for the base of the Visean stage (Carboniferous): the Pengchong section, Guangxi, South China. Episodes 26 (2), 105–115. https://doi.org/10.18814/epiiugs/2003/v26i2/004.
- Ellwood, B.B., Algeo, T.J., El Hassani, A., Tomkin, J.H., Rowe, H.D., 2011a. Defining the timing and duration of the Kacak Interval within the Eifelian/Givetian boundary GSSP, Mech Irdane, Morocco, using geochemical and magnetic susceptibility patterns. Palaeogeogr. Palaeoclimatol. Palaeoecol. 304 (1), 74–84. https://doi.org/ 10.1016/j.palaeo.2010.10.012
- Ellwood, B.B., Hassani, A.E., Tomkin, J.H., Bultynck, P., Silva, A.C.D., Whalen, M.T., Hladil, J., Chadimova, L., Chen, D., Spassov, S., Boulvain, F., Devleeschouwer, X., 2015. A climate-driven model using time-series analysis of magnetic susceptibility (χ) datasets to represent a floating-point high-resolution geological timescale for the Middle Devonian Eifelian stage, magnetic susceptibility application: a window onto ancient environments and climatic variations. Geol. Soc. Lond. Spec. Publ. 414, 209–223. https://doi.org/10.1144/SP414.4.
- Ellwood, B.B., Lambert, L.L., Tomkin, J.H., Bell, G.L., Nestell, M.K., Nestell, G.P., Wardlaw, B.R., 2012. Magnetostratigraphy susceptibility for the Guadalupian series GSSPs (Middle Permian) in Guadalupe Mountains National Park and adjacent areas in West Texas. Geo. Soc. Lond. Spec. Publ. 373 (1), 375–394. https://doi.org/ 10.1144/SP373.1.
- Ellwood, B.B., Tomkin, J.H., El Hassani, A., Bultynck, P., Brett, C.E., Schindler, E., Feist, R., Bartholomew, A.J., 2011b. A climate-driven model and development of a floating point time scale for the entire Middle Devonian Givetian Stage: a test using magnetostratigraphy susceptibility as a climate proxy. Palaeogeogr. Palaeoclimatol. Palaeoecol. 304 (1), 85–95. https://doi.org/10.1016/j.palaeo.2010.10.014.
- Ellwood, B.B., Tomkin, J.H., Richards, B.C., Benoist, S.L., Lambert, L.L., 2007. MSEC data sets record glacially driven cyclicity: examples from the arrow canyon Mississippian-Pennsylvanian GSSP and associated sections. Palaeogeogr. Palaeoclimatol. Palaeoecol. 255 (3-4), 377–390. https://doi.org/10.1016/j.palaeo.2007.08.006.
- Elrick, M., Reardon, D., Labor, W., Martin, J., Desrochers, A., Pope, M., 2013. Orbital-scale climate change and glacioeustasy during the early late Ordovician (pre-Hirnantian) determined from delta 8¹⁸O values in marine apatite. Geology 41 (7), 775–778. https://doi.org/10.1130/G34363.1.
- Eros, J.M., Montañez, I.P., Osleger, D.A., Davydov, V.I., Nemyrovska, T.I., Poletaev, V.I., Zhykalyak, M.V., 2012. Sequence stratigraphy and onlap history of the Donets Basin, Ukraine: insight into Carboniferous icehouse dynamics. Palaeogeogr. Palaeoclimatol. Palaeoecol. 313, 1–25. https://doi.org/10.1016/j. palaeo.2011.08.019.
- Erwin, D.H., 1994. The Permo-Triassic Extinction. Nature 367, 231-236. https://doi.org/10.1038/367231a0.
- Erwin, D., 2006. Dates and rates: temporal resolution in the deep time stratigraphic record. Annu. Rev. Earth Planet. Sci. 34, 569–590. https://doi.org/10.1146/annurev.earth.34.031405.125141.
- Eva, P., Raimund, F., Gerd, F., 1991. Decision on the Devonian–Carboniferous boundary stratotype. Episodes 14 (4), 331–336. https://doi.org/10.18814/epiiugs/1991/v14i4/004.

- Fan, J.X., Shen, S.Z., Erwin, D.H., Sadler, P.M., MacLeod, N., Cheng, Q.M., Hou, X.D., Yang, J., Wang, X.D., Wang, Y., Zhang, H., Chen, X., Li, G.J., Zhang, Y.C., Shi, Y.K., Yuan, D.X., Chen, Q., Zhang, L.N., Li, C., Zhao, Y.Y., 2020. A high-resolution summary of Cambrian to early Triassic marine invertebrate biodiversity. Science 367 (6475), 272–277. doi: 10.1126/science.aax4953.
- Fang, J.C., Wu, H.C., Fang, Q., Shi, M.N., Zhang, S.H., Yang, T.S., Li, H.Y., Cao, L.W., 2020. Cyclostratigraphy of the global stratotype section and point (GSSP) of the basal Guzhangian stage of the Cambrian Period. Palaeogeogr. Palaeoclimatol. Palaeoecol. 540, 109530 https://doi.org/10.1016/j.palaeo.2019.109530.
- Fang, Q., Wu, H.C., Hinnov, L.A., Jing, X.C., Wang, X.L., Jiang, Q.C., 2015. Geologic evidence for chaotic behavior of the planets and its constraints on the third-order eustatic sequences at the end of the Late Paleozoic Ice Age. Palaeogeogr. Palaeoclimatol. Palaeoecol. 440, 848–859. https://doi.org/10.1016/j.palaeo.2015.10.014.
- Fang, Q., Wu, H.C., Hinnov, L.A., Jing, X.C., Wang, X.L., Yang, T.S., Li, H.Y., Zhang, S.H., 2017. Astronomical cycles of Middle Permian Maokou Formation in South China and their implications for sequence stratigraphy and paleoclimate. Palaeogeogr. Palaeoclimatol. Palaeoecol. 474, 130–139. https://doi.org/10.1016/j. palaeo.2016.07.037.
- Fang, Q., Wu, H.C., Hinnov, L.A., Tian, W.Q., Wang, X.L., Yang, T.S., Li, H.Y., Zhang, S. H., 2018b. Abiotic and biotic responses to Milankovitch-forced megamonsoon and glacial cycles recorded in South China at the end of the Late Paleozoic Ice Age. Glob. Planet. Chang. 163, 97–108. https://doi.org/10.1016/j.gloplacha.2018.01.022.
- Fang, Q., Wu, H.C., Hinnov, L.A., Wang, X.L., Yang, T.S., Li, H.Y., Zhang, S.H., 2016. A record of astronomically forced climate change in a late Ordovician (Sandbian) deep marine sequence, Ordos Basin, North China. Sediment. Geol. 341, 163–174. https://doi.org/10.1016/j.sedgeo.2016.06.002.
- Fang, Q., Wu, H.C., Shen, S.Z., Fan, J.X., Hinnov, L.A., Yuan, D.X., Zhang, S.H., Yang, T. S., Chen, J., Wu, Q., 2022. Astronomically paced climate evolution during the Late Paleozoic icehouse-to-greenhouse transition. Glob. Planet. Chang. 213, 103822 https://doi.org/10.1016/j.gloplacha.2022.103822.
- Fang, Q., Wu, H.C., Shen, S.Z., Zhang, S.H., Yang, T.S., Wang, X.D., Chen, J., 2021. Trends and rhythms in climate change during the early Permian icehouse. Paleoceanogr. Paleoclimatol. 36 (12) https://doi.org/10.1029/2021PA004340 e2021PA004340.
- Fang, Q., Wu, H.C., Wang, X.L., Yang, T.S., Li, H.Y., Zhang, S.H., 2018a. Astronomical cycles in the Serpukhovian-Moscovian (Carboniferous) marine sequence, South China and their implications for geochronology and icehouse dynamics. J. Asian Earth Sci. 156, 302–315. https://doi.org/10.1016/j.jseaes.2018.02.001.
- Fang, Q., Wu, H.C., Wang, X.L., Yang, T.S., Li, H.Y., Zhang, S.H., 2019. An astronomically forced cooling event during the Middle Ordovician. Glob. Planet. Chang. 173, 96–108. https://doi.org/10.1016/j.gloplacha.2018.12.010.
- Farhat, M., Auclair-Desrotour, P., Boué, G., Laskar, J., 2022. The resonant tidal evolution of the Earth-Moon distance. Astron. Astrophys. 665, L1 https://doi.org/10.1051/ 0004-6361/202243445.
- Fielding, C.R., 2021. Late Palaeozoic cyclothems-a review of their stratigraphy and sedimentology. Earth-Sci. Rev. 217, 103612 https://doi.org/10.1016/j. earscirev.2021.103612.
- Fielding, C.R., Frank, T.D., Birgenheier, L.P., Rygel, M.C., Jones, A.T., Roberts, J., 2008. Stratigraphic imprint of the Late Palaeozoic Ice Age in eastern Australia: a record of alternating glacial and nonglacial climate regime. J. Geol. Soc. London 165 (1), 129–140. https://doi.org/10.1144/0016-76492007-036.
- Fischer, A.G., Silva, I.P., de Boer, P.L., 1990. Cyclostratigraphy. In: Ginsburg, R.N., Beaudoin, B. (Eds.), Cretaceous Resources, Events and Rhythms: Background and Plans for Research. Springer, Dordrecht, pp. 139–172. https://doi.org/10.1007/978-94-015-6861-6 8.
- Gambacorta, G., Menichetti, E., Trincianti, E., Torricelli, S., 2018. Orbital control on cyclical primary productivity and benthic anoxia: astronomical tuning of the Telychian Stage (Early Silurian). Palaeogeogr. Palaeoclimatol. Palaeoecol. 495, 152–162. https://doi.org/10.1016/j.palaeo.2018.01.003.
- Gannon, P.J., Smith, M.E., Umhoefer, P.J., Leary, R.J., 2022. High-resolution Late Paleozoic cyclostratigraphy and tectonic evolution of the Keeler Basin, California, southwest Laurentia. Geol. Soc. Am. Bull. 134 (3–4), 1065–1078. https://doi.org/ 10.1130/B36027.1.
- Ghienne, J.F., Desrochers, A., Vandenbroucke, T.R.A., Achab, A., Asselin, E., Dabard, M.-P., Farley, C., Loi, A., Paris, F., Wickson, S., Veizer, J., 2014. A Cenozoic-style scenario for the end-Ordovician glaciation. Nat. Commun. 5 (1), 4485. https://doi.org/10.1038/ncomms5485.
- Gilbert, K., Raimund, F., Michael, R.H., 1987. Decision on the boundary stratotype for the Middle/Upper Devonian series boundary. Episodes 10 (2), 97–101. https://doi. org/10.18814/epiiugs/1987/v10i2/004.
- Glenister, B.F., Wardlaw, B.R., Lambert, L.L., Spinosa, C., Bowring, S.A., Erwin, D.H., Menning, M., Wilde, G.L., 1999. Proposal of Guadalupian and component Roadian, Wordian and Capitanian stages as international standards for the Middle Permian Series. Permophiles 34, 3–11.
- Goldhammer, R.K., Lehmann, P.J., Dunn, P.A., 1993. The origin of high-frequency platform carbonate cycles and third-order sequences (Lower Ordovician El Paso Gp, West Texas); constraints from outcrop data and stratigraphic modeling. J. Sediment. Res. 63 (3), 318–359. https://doi.org/10.1306/D4267AFA-2B26-11D7-8648000102C1865D.
- Goldman, D., Sadler, P.M., Leslie, S.A., Melchin, M.J., Agterberg, F.P., Gradstein, F.M., 2020. Chapter 20–The Ordovician Period. In: Gradstein, F.M., Ogg, J.G., Schmitz, M. D., Ogg, G.M. (Eds.), Geologic Time Scale 2020. Elsevier, pp. 631–694. https://doi.org/10.1016/B978-0-12-824360-2.00020-6.

- Gong, Y.M., Droser, M.L., 2001. Periodic anoxic shelf in the Early–Middle Ordovician transition: ichnosedimentologic evidence from west-Central Utah, USA. Sci. China Ser. D. Earth Sci. 44 (11), 979–989. https://doi.org/10.1007/BF02875391.
- Gong, Y.M., Li, B.H., Wang, C.Y., Wu, Y., 2001. Orbital cyclostratigraphy of the Devonian Frasnian–Famennian transition in South China. Palaeogeogr. Palaeoclimatol. Palaeoecol. 168, 237–248. https://doi.org/10.1016/S0031-0182(00)00257-1.
- Gong, Y.M., Xu, R., Tang, Z.D., Li, B.H., 2005. The Upper Devonian orbital cyclostratigraphy and numerical dating conodont zones from Guangxi, South China. Sci. China Ser. D. Earth Sci. 48, 32–41. https://doi.org/10.1360/03yd0025.
- Goodwin, P.W., Anderson, E.J., Goodman, W.M., Saraka, L.J., 1986. Punctuated aggradational cycles: implications for stratigraphic analysis. Paleoceanography 1 (4), 417–429. https://doi.org/10.1029/PA001i004p00417.
- Grader, G.W., Isaacson, P.E., Díaz-Martínez, E., Pope, M.C., 2008. In: Fielding, C.R., Frank, T.D., Isbell, J.L. (Eds.), Time and Space. Geol. Soc. Am. Spec. Pap.441, pp. 143–159. https://doi.org/10.1130/2008.2441(10.
- Gradstein, F.M., Ogg, J.G., Schmitz, M.D., Ogg, G.M., 2012. The Geologic Time Scale 2012. Elsevier. https://doi.org/10.1016/C2011-1-08249-8.
- Gradstein, F.M., Ogg, J.G., Schmitz, M.D., Ogg, G.M., 2020. The Geologic Time Scale 2020. Elsevier. https://doi.org/10.1016/C2020-1-02369-3.
- Greb, S.F., Pashin, J.C., Martino, R.L., Eble, C.F., 2008. Appalachian sedimentary cycles during the Pennsylvanian: Changing influences of sea level, climate, and tectonics.
 In: Fielding, C.R., Frank, T.D., Isbell, J.L. (Eds.), Resolving the Late Paleozoic Ice Age in Time and Space. Geol. Soc. Am. Spec. Pap. 441, pp. 235–248.
- Haq, B.U., Schutter, S.R., 2008. A chronology of Paleozoic Sea-level changes. Science 322 (5898), 64–68. https://doi.org/10.1126/science.1161648.
- Harland, W.B., Armstrong, R.L., Cox, A.V., Craig, L.E., Smith, A.G., Smith, D.G., 1990.
 A Geological Time Scale. Cambridge University Press.
- Harper, D.A.T., Hammarlund, E.U., Rasmussen, C.M.Ø., 2014. End Ordovician extinctions: a coincidence of causes. Gondwana Res. 25 (4), 1294–1307. https://doi. org/10.1016/j.gr.2012.12.021.
- Hays, J.D., Imbrie, J., Shackleton, N.J., 1976. Variations in the Earth's orbit: Pacemaker of the ice ages. Science 194 (4270), 1121–1132. https://doi.org/10.1126/ science.194.4270.1121.
- Heckel, P.H., 1986. Sea-level curve for Pennsylvanian eustatic marine transgressive-regressive depositional cycles along midcontinent outcrop belt, North America. Geology 14, 330–334. https://doi.org/10.1130/0091-7613(1986)14<330: SCFPEM>2.0.CO:2.
- Heckel, P.H., 1994. Evaluation of evidence for glacio-eustatic control over marine Pennsylvanian cyclothems in North America and consideration of possible tectonic effects. In: Dennison, J.M., Ettensohn, F.R. (Eds.), Tectonic and Eustatic Controls on Sedimentary Cycles. SEPM. 4, pp. 65–87. https://doi.org/10.2110/csp.94.04.0065.
- Heckel, P.H., 2008. Pennsylvanian cyclothems in Midcontinent North America as far-field effects of waxing and waning of Gondwana ice sheets. Geol. Soc. Am. Spec. Pap. 441 (19), 275–289. https://doi.org/10.1130/2008.2441(19).
- Heckel, P.H., 2013. Pennsylvanian stratigraphy of Northern Midcontinent Shelf and biostratigraphic correlation of cyclothems. Stratigraphy 10 (1–2), 3–40.
- Heckel, P.H., Alekseev, A.S., Barrick, J.E., Boardman, D.R., Goreva, N.V., Isakova, T.N., Nemyrovska, T.I., Ueno, K., Villa, E., Work, D.M., 2008. Choice of conodont Idiognathodus simulator (sensu stricto) as the event marker for the base of the global Gzhelian Stage (Upper Pennsylvanian Series, Carboniferous System). Episodes 31 (3), 319–325. https://doi.org/10.18814/epiiugs/2008/v31i3/006.
- Heckel, P.H., Alekseev, A.S., Barrick, J.E., Boardman, D.R., Goreva, N.V., Nemyrovska, T. I., Ueno, K., Villa, E., Work, D.M., 2007. Cyclothem ["digital"] correlation and biostratigraphy across the global Moscovian–Kasimovian–Gzhelian stage boundary interval (Middle–Upper Pennsylvanian) in North America and eastern Europe. Geology 35 (7), 607–610. https://doi.org/10.1130/G23564A.1.
- Henderson, C.M., Shen, S.Z., Gradstein, F.M., Agterberg, F.P., 2020. Chapter 24–The Permian Period. In: Geologic Time Scale 2020. Elsevier, pp. 875–902. https://doi. org/10.1016/B978-0-12-824360-2.00024-3.
- Hilgen, F., Schwarzacher, W., Strasser, A., 2004. Concept and definitions in Cyclostratography (Second report of the Cyclostratigraphic Working Group). In: Fischer, A.G., Silva, I.P., Weissert, H., Ferreri, V., Argenio, B.D. (Eds.), Cyclostratigraphy: Approaches and Case Histories. SEPM. Spec. Publ, p. 81. https://doi.org/10.2110/pec.04.81.0303.
- Hinnov, L.A., 2013. Cyclostratigraphy and its revolutionizing applications in the earth and planetary sciences. Geol. Soc. Am. Bull. 125 (11–12), 1703–1734. https://doi. org/10.1130/B30934.1.
- Hinnov, L.A., 2018. Cyclostratigraphy and Astrochronology in 2018. Chapter 1. Stratigraphy & Timescales. Elsevier, pp. 1–80. https://doi.org/10.1016/bs.sats/2018.08/004
- Hinnov, L.A., Hilgen, F.J., 2012. Chapter 4–Cyclostratigraphy and astrochronology. In: Gradstein, F.M., Ogg, J.G., Schmitz, M.D., Ogg, G.M. (Eds.), Geologic Time Scale. Elsevier, pp. 63–83. https://doi.org/10.1016/B978-0-444-59425-9.00004-4.
- Hu, K.Y., Qi, Y.P., Qie, W.K., Wang, Q.L., 2019. Carboniferous conodont zonation of China. Newsl. Stratigr. 53, 141–190. https://doi.org/10.1127/nos/2019/0498.
- Huang, C.J., Gong, Y.M., 2016. Timing and patterns of the Frasnian-Famennian event: evidences from high-resolution conodont biostratigraphy and event stratigraphy at the Yangdi section, Guangxi, South China. Palaeogeogr. Palaeoclimatol. Palaeoecol. 448, 317–338. https://doi.org/10.1016/j.palaeo.2015.10.031.
- Huang, C.J., 2018. In: Chapter 2: Astronomical Time Scale for the Mesozoic, Stratigraphy and Timescales, 3, pp. 81–150. https://doi.org/10.1016/bs.sats.2018.08.005.
- Huang, C.J., Tong, J.N., Hinnov, L., Chen, Z.Q., 2011. Did the great dying of life take 700 k.y..? Evidenceyfrom global astronomical correlation of the Permian-Triassic boundary interval. Geology 39 (8), 779–782. https://doi.org/10.1130/G32126.1.
- Huang, H., Gao, Y., Jones, M.M., Tao, H.F., Carroll, A.R., Ibarra, D.E., Wu, H.C., Wang, C. S., 2020. Astronomical forcing of Middle Permian terrestrial climate recorded in a

- large paleolake in northwestern China. Palaeogeogr. Palaeoclimatol. Palaeoecol. 550, 109735 https://doi.org/10.1016/j.palaeo.2020.109735.
- Huang, H., Gao, Y., Ma, C., Niu, L., Dong, T., Tian, X., Cheng, H., Hei, C.L., Tao, H.F., Wang, C.S., 2021. Astronomical constraints on the development of alkaline lake during the Carboniferous–Permian Period in North Pangea. Glob. Planet. Chang. 207, 103681 https://doi.org/10.1016/j.gloplacha.2021.103681.
- Huang, W.T., Wu, H.C., Fang, Q., Zhang, S.H., Yang, T.S., Li, H.Y., Shi, M.N., 2022. Orbitally forced organic matter accumulation recorded in an Early Permian midlatitude palaeolake. Palaeogeogr. Palaeoclimatol. Palaeoecol. 606, 111259 https:// doi.org/10.1016/j.palaeo.2022.111259.
- Imbrie, J., Boyle, E.A., Clemens, S.C., Duffy, A., Howard, W.R., Kukla, G., Kutzbach, J., Martinson, D.G., McIntyre, A., Mix, A.C., Molfino, B., Morley, J.J., Peterson, L.C., Pisias, N.G., Prell, W.L., Raymo, M.E., Shackleton, N.J., Toggweiler, J.R., 1992. On the structure and origin of major glaciation cycles 1. Linear responses to Milankovitch forcing. Paleoceanography 7 (6), 701–738. https://doi.org/10.1029/92PA02253.
- Imbrie, J., Imbrie, K.P., 1979. In: Ice Ages: Solving the Mystery. Harvard University Press, Cambridge.
- Isbell, J.L., Miller, M.F., Wolfe, K.L., Lenaker, P.A., 2003. Timing of late Paleozoic glaciation in Gondwana: was glaciation responsible for the development of Northern Hemisphere cyclothems? Geol. Soc. Am. Spec. Pap. 370, 5–24. https://doi.org/ 10.1130/0-8137-2370-1.5.
- Ivo, C., František, V., 2003. Thirty years of the first international stratotype: the Silurian–Devonian boundary at Klonk and its present status. Episodes 26 (1), 10–15. https://doi.org/10.18814/epiiugs/2003/v26i1/002.
- Ivo, C., William Jr., A.O., 1989. Decision on the Lochkovian–Pragian Boundary Stratotype (Lower Devonian). Episodes 12 (2), 109–114. https://doi.org/10.18814/epiiugs/1989/v12i2/014.
- Izart, A., Briand, C., Vaslet, D., Vachard, D., Coquel, R., Maslo, A., 1996. Stratigraphy and sequence stratigraphy of the Moscovian in the Donets basin. Tectonophysics 268 (1-4), 189-209. https://doi.org/10.1016/S0040-1951(96)00224-7.
- Izart, A., Le Nindre, Y., Stephenson, R., Vaslet, D., Stovba, S., 2003a. Quantification of the control of sequences by tectonics and eustacy in the Dniepr-Donets Basin and on the Russian Platform during Carboniferous and Permian. Bull. Soc. Geol. Fr. 174 (1), 93–100. https://doi.org/10.2113/174.1.93.
- Izart, A., Stephenson, R., Vai, G.B., Vachard, D., Le Nindre, Y., Vaslet, D., Fauvel, P.-J., Süss, P., Kossovaya, O., Chen, Z., Maslo, A., Stovba, S., 2003b. Sequence stratigraphy and correlation of late Carboniferous and Permian in the CIS, Europe, Tethyan area, North Africa, Arabia, China, Gondwanaland and the USA. Palaeogeogr. Palaeoclimatol. Palaeoecol. 196 (1–2), 59–84. https://doi.org/10.1016/S0031-0182 (03)00313-4.
- Jaeger, H., 1977. Graptolites. In: Martinsson, A. (Ed.), The Silurian–Devonian boundary. IUGS Ser. A, no. 5, pp. 337–345.
- Jia, D.L., Tian, J.C., Lin, X.B., Yang, G.H., Feng, W.X., Zhang, X., Tang, Y., Yang, C.Y., 2018. Milankovitch cycles in the Silurian Kepingtage Formation in Shuntuoguole area, Tarim Basin. Oil Gas Geol. 39 (04), 749–758. doi: 10.11743/ogg20180412.
- Jin, S.D., Deng, H.C., Zhu, X., Liu, Y., Liu, S.B., Fu, M.Y., 2020. Orbital control on cyclical organic matter accumulation in early Silurian Longmaxi Formation shales. Geosci. Front. 11 (2), 533–545. https://doi.org/10.1016/j.gsf.2019.06.005.
- Front. 11 (2), 533–545. https://doi.org/10.1016/j.gsf.2019.06.005.

 Jin, Y.G., Shen, S.Z., Henderson, C.M., Wang, X.D., Wang, W., Wang, Y., Cao, C.Q., Shang, Q.H., 2006a. The Global Stratotype Section and Point (GSSP) for the boundary between the Capitanian and Wuchiapingian Stage (Permian). Episodes 29 (4) 253–262. https://doi.org/10.18814/epiiuss/2006/v2914/003
- (4), 253–262. https://doi.org/10.18814/epiiugs/2006/v29i4/003.
 Jin, Y.G., Wang, Y., Henderson, C., Wardlaw, B.R., Shen, S.Z., Cao, C.Q., 2006b. The Global Boundary Stratotype Section and Point (GSSP) for the base of Changhsingian Stage (Upper Permian). Episodes 29 (3), 175–182. https://doi.org/10.18814/epiiugs/2006/v29i3/003.
- Jirásek, J., Opluštil, S., Sivek, M., Schmitz, M.D., Abels, H.A., 2018. Astronomical forcing of Carboniferous paralic sedimentary cycles in the Upper Silesian Basin, Czech Republic (Serpukhovian, latest Mississippian): New radiometric ages afford an astronomical age model for european biozonations and substages. Earth-Sci. Rev. 177, 715–741. https://doi.org/10.1016/j.earscirev.2017.12.005.
- Joachimski, M.M., Breisig, S., Buggisch, W., Talent, J.A., Mawson, R., Gereke, M., Morrow, J.R., Day, J., Weddige, K., 2009. Devonian climate and reef evolution: Insights from oxygen isotopes in apatite. Earth Planet. Sci. Lett. 284 (3), 599–609. https://doi.org/10.1016/j.epsl.2009.05.028.
- Joachimski, M.M., Buggisch, W., 2002. Conodont apatite 8¹⁸O signatures indicate climatic cooling as a trigger of the Late Devonian mass extinction. Geology 30 (8), 711–714. https://doi.org/10.1130/0091-7613(2002)030<0711:CAOSIC>2.0.CO;2.
- Kabanov, P.B., Alekseev, A.S., Gibshman, N.B., Gabdullin, R.R., Bershov, A.V., 2016. The upper Visean–Serpukhovian in the type area for the Serpukhovian Stage (Moscow Basin, Russia): Part 1. Sequences, disconformities and biostratigraphical summary. Geol. J. 51, 163–194. https://doi.org/10.1002/gj.2612.
- Kaiser, S.I., 2009. The Devonian/Carboniferous boundary stratotype section (La Serre, France) revisited. Newsl. Stratigr. 43 (2), 195–205. https://doi.org/10.1127/0078-0421/2009/0043-0195.
- Kaiser, S.I., Aretz, M., Becker, R.T., 2016. The global Hangenberg Crisis (Devonian-Carboniferous transition): review of a first order mass extinction. In: Becker, R.T., Königshof, P., Brett, C.E. (Eds.), Devonian Climate, Sea Level and Evolutionary Events. Geol. Soc. Spec. Publ. 423, pp. 387–437. https://doi.org/ 10.1144/SP423.9.
- Kaiser, S.I., Becker, R.T., Steuber, T., Aboussalam, S.Z., 2011. Climate-controlled mass extinctions, facies, and sea-level changes around the Devonian–Carboniferous boundary in the eastern Anti-Atlas (SE Morocco). Palaeogeogr. Palaeoclimatol. Palaeoecol. 310 (3–4), 340–364. https://doi.org/10.1016/j.palaeo.2011.07.026.

- Kaufmann, B., 2006. Calibrating the Devonian Time Scale: a synthesis of U-Pb ID-TIMS ages and conodont stratigraphy. Earth-Sci. Rev. 76 (3), 175–190. https://doi.org/ 10.1016/j.earscirev.2006.01.001.
- Kaufmann, B., Trapp, E., Mezger, K., 2004. The Numerical Age of the Upper Frasnian (Upper Devonian) Kellwasser Horizons: a New U-Pb Zircon date from Steinbruch Schmidt (Kellerwald, Germany). J. Geol. 112 (4), 495–501. https://doi.org/ 10.1086/421077.
- Khodjanyazova, R.R., Davydov, V.I., Montañez, I.P., Schmitz, M.D., 2014. Climate- and eustasy-driven cyclicity in Pennsylvanian fusulinid assemblages, Donets Basin (Ukraine). Palaeogeogr. Palaeoclimatol. Palaeoecol. 396, 41–61. https://doi.org/10.1016/j.palaeo.2013.12.038.
- Kim, J.C., Lee, Y.I., 1998. Cyclostratigraphy of the lower Ordovician Dumugol Formation, Korea: meter-scale cyclicity and sequence-stratigraphic interpretation. Geosci. J. 2 (3), 134–147. https://doi.org/10.1007/BF02910257.
- Klapper, G., Feist, R., Becker, R.T., House, M.R., 1993. Definition of the Frasnian/ Famennian Stage boundary. IUGS 16 (4), 433–441. https://doi.org/10.18814/ epiiugs/1993/y16i4/003.
- Klapper, G., Kirchgasser, W.T., 2016. Frasnian late Devonian conodont biostratigraphy in New York: graphic correlation and taxonomy. J. Paleontol. 90 (3), 525–554. https://doi.org/10.1017/jpa.2015.70.
- Kochhann, M.V.L., Cagliari, J., Kochhann, K.G.D., Franco, D.R., 2020. Orbital and millennial-scale cycles paced climate variability during the late Paleozoic Ice Age in the southwestern Gondwana. Geochem. Geophy. Geosy. 21 https://doi.org/ 10.1029/2019GC008676 e2019GC008676.
- Kodama, K.P., 2019. Rock magnetic Cyclostratigraphy of the Carboniferous Mauch Chunk Formation, Pottsville, PA, United States. Front. Earth Sci. 7, 285. https://doi. org/10.3389/feart.2019.00285.
- Kump, L.R., 2018. Prolonged late Permian–Early Triassic hyperthermal: failure of climate regulation? Philos. T. R. Soc. A. 376 (2130), 20170078. https://doi.org/ 10.1098/rsta.2017.0078.
- Lanci, L., Galeotti, S., Ratcliffe, K., Tohver, E., Wilson, A., Flint, S., 2022. Astronomically forced cycles in Middle Permian fluvial sediments from Karoo Basin (South Africa). Palaeogeogr. Palaeoclimatol. Palaeoecol. 596, 110973 https://doi.org/10.1016/j.palaeo.2022.110973.
- Lantink, M.L., Davies, J.H., Ovtcharova, M., Hilgen, F.J., 2022. Milankovitch cycles in banded iron formations constrain the Earth-Moon system 2.46 billion years ago, 119 (40). https://doi.org/10.1073/pnas.2117146119 e2117146119.
- Lane, H.R., Brenckle, P.L., Baesemann, J., Richards, B., 1999. The IUGS boundary in the middle of the Carboniferous: Arrow Canyon, Nevada, USA. Episodes 22 (4), 272–283.
- Laskar, J., 2020. Chapter 4–Astrochronology. In: Gradstein, F.M., Ogg, J.G., Schmitz, M. D., Ogg, G.M. (Eds.), Geologic Time Scale 2020. Elsevier, pp. 139–158. https://doi.org/10.1016/B978-0-12-824360-2.00004-8.
- Laskar, J., Fienga, A., Gastineau, M., Manche, H., 2011. La2010: a new orbital solution for the long term motion of the Earth. Astron. Astrophys. 532, A89. https://doi.org/ 10.1051/0004-6361/201116836.
- Laskar, J., Robutel, P., Joutel, F., Gastineau, M., Correia, A.C.M., Levrard, B., 2004.
 A long-term numerical solution for the insolation quantities of the Earth. Astron.
 Astrophys. 428 (1), 261–285. https://doi.org/10.1051/0004-6361:20041335.
- Lever, H., 2004. Climate changes and cyclic sedimentation in the Mid-Late Permian: Kennedy Group, Carnarvon Basin, Western Australia. Gondwana Res. 7 (1), 135–142. https://doi.org/10.1016/S1342-937X(05)70312-9.
- Li, M.S., Kump, L.R., Hinnov, L.A., Mann, M.E., 2018. Tracking variable sedimentation rates and astronomical forcing in Phanerozoic paleoclimate proxy series with evolutionary correlation coefficients and hypothesis testing. Earth Planet. Sci. Lett. 501, 165–179. https://doi.org/10.1016/j.epsl.2018.08.041.
- Li, M.S., Ogg, J., Zhang, Y., Huang, C.J., Hinnov, L., Chen, Z.Q., Zou, Z.Y., 2016. Astronomical tuning of the end-Permian extinction and the Early Triassic Epoch of South China and Germany. Earth Planet. Sci. Lett. 441, 10–25. https://doi.org/ 10.1016/j.epsl.2016.02.017.
- Lindskog, A., Costa, M.M., Rasmussen, C.M.O., Connelly, J.N., Eriksson, M.E., 2017. Refined Ordovician timescale reveals no link between asteroid breakup and biodiversification. Nat. Commun. 8 (1), 14066. https://doi.org/10.1038/ programs/14066.
- Ling, M.X., Zhan, R.B., Wang, G.X., Wang, Y., Amelin, Y., Tang, P., Liu, J.B., Jin, J., Huang, B., Wu, R.C., Xue, S., Fu, B., Bennett, V.C., Wei, X., Luan, X.C., Finnegan, S., Harper, D.A.T., Rong, J.Y., 2019. An extremely brief end Ordovician mass extinction linked to abrupt onset of glaciation. Solid Earth Sci. 4 (4), 190–198. https://doi.org/ 10.1016/j.sesci.2019.11.001.
- Linnemann, U., Ovtcharova, M., Schaltegger, U., Gärtner, A., Hautmann, M., Geyer, G., Vickers-Rich, P., Rich, T., Plessen, B., Hofmann, M., Zieger, J., Krause, R., Kriesfeld, L., Smith, J., 2019. New high-resolution age data from the Ediacaran-Cambrian boundary indicate rapid, ecologically driven onset of the Cambrian explosion. Terra Nova 31 (1), 49–58. https://doi.org/10.1111/ter.12368.
- Liu, Z.H., 2012. Orbital cycles analysis and its genesis significance for the sequence hierarchy: a case study of Carboniferous Karashayi Formation, Central Tarim basin. J. Earth Sci. 23 (4), 516–528. https://doi.org/10.1007/s12583-012-0272-3.
- Long, D.G., 2007. Tempestite frequency curves: a key to late Ordovician and early Silurian subsidence, sea-level change, and orbital forcing in the Anticosti foreland basin, Quebec, Canada. Can. J. Earth Sci. 44 (3), 413–431. https://doi.org/10.1139. e06-009
- Lu, Y.B., Huang, C.J., Jiang, S., Zhang, J.Y., Lu, Y.C., Liu, Y., 2019. Cyclic late Katian through Hirnantian glacioeustasy and its control of the development of the organicrich Wufeng and Longmaxi shales, South China. Palaeogeogr. Palaeoclimatol. Palaeoecol. 526, 96–109. https://doi.org/10.1016/j.palaeo.2019.04.012.

- Ma, K.Y., Hinnov, L., Zhang, X.S., Gong, Y.M., 2020. Astronomical time calibration of the Upper Devonian Lali section, South China. Glob. Planet. Chang. 193 https://doi.org/ 10.1016/j.gloplacha.2020.103267.
- Ma, K.Y., Hinnov, L., Zhang, X.S., Gong, Y.M., 2022. Astronomical climate changes trigger Late Devonian bio- and environmental events in South China. Glob. Planet. Chang. 215, 103874 https://doi.org/10.1016/j.gloplacha.2022.103874.
- Ma, K.Y., Li, R.C., Hinnov, L.A., Gong, Y.M., 2019a. Conodont biostratigraphy and astronomical tuning of the Lower-Middle Ordovician Liangjiashan (North China) and Huanghuachang (South China) marine sections. Palaeogeogr. Palaeoclimatol. Palaeoecol. 528, 272–287. https://doi.org/10.1016/j.palaeo.2019.05.003.
- Ma, X.Y., Deng, S.H., Lu, Y.Z., Wu, H.C., Luo, Z., Fan, R., Li, X., Fang, Q., 2019b. Astrochronology of the Upper Ordovician Pagoda Formation, South China and its geological implications. Earth Sci. Front. 26 (02), 281–291. https://doi.org/ 10.13745/j.esf.sf.2019.3.8.
- Malinverno, A., Erba, E., Herbert, T.D., 2010. Orbital tuning as an inverse problem: chronology of the Early Aptian oceanic anoxic event 1a (Selli Level) in the Cismon APTICORE. Paleoceanogr. Paleoclimatol. 25 (2), PA2203. https://doi.org/10.1029/ 2009pa001769
- Manger, W.L., 2017. Journey to the Mississippian–Pennsylvanian Boundary GSSP: a long and winding road. Stratigraphy 14 (1–4), 247–258. https://doi.org/10.29041/
- Marshall, J.E.A., 2000. In: Palynofacies and orbital cyclicity: an example from the Silurian of Saudi Arabia. Gulf PetroLink, pp. 216–231. http://eprints.soton.ac. uk/id/eprint/12692.
- Martin, L.G., Montañez, I.P., Bishop, J.W., 2012. A paleotropical carbonate-dominated archive of Carboniferous icehouse dynamics, Bird Spring Fm., Southern Great Basin, USA. Palaeogeogr. Palaeoclimatol. Palaeoecol. 329–330, 64–82. https://doi.org/ 10.1016/j.palaeo.2012.02.018.
- Maurice, S., Johannes, N.T., 1999. The Devonian–Carboniferous boundary in South Africa and the age of the earliest episode of the Dwyka glaciation: new palynological result. IUGS 22 (1), 41–44. https://doi.org/10.18814/epiiugs/1999/v22i1/007.
- Mauviel, A., Sinnesael, M., Desrochers, A., 2020. The stratigraphic and geochemical imprints of late Ordovician glaciation on far-field neritic carbonates, Anticosti Island, eastern Canada. Palaeogeogr. Palaeoclimatol. Palaeoecol. 543, 109579 https://doi.org/10.1016/j.palaeo.2019.109579.
- Meyers, S.R., 2015. The evaluation of eccentricity-related amplitude modulation and bundling in paleoclimate data: an inverse approach for astrochronologic testing and time scale optimization. Paleoceanogr. Paleoclimatol. 30 (12), 1625–1640. https:// doi.org/10.1002/2015pa002850.
- Meyers, S.R., Malinverno, A., 2018. Proterozoic Milankovitch cycles and the history of the solar system. Proc. Natl. Acad. Sci. U.S.A. 115 (25), 6363–6368. https://doi.org/ 10.1073/pnas.1717689115.
- McGhee, G.R., 1996. The Late Devonian Mass Extinction. In: Columbia University Press, New York, pp. 1–303. https://doi.org/10.1038/npg.els.0004177.
- McGhee, G.R., Clapham, M.E., Sheehan, P.M., Bottjer, D.J., Droser, M.L., 2013. A new ecological-severity ranking of major Phanerozoic biodiversity crises. Palaeogeogr. Palaeoclimatol. Palaeoecol. 370, 260–270. https://doi.org/10.1016/j. palaeo. 2012.12.019
- McGhee, G.R., Sheehan, P.M., Bottjer, D.J., Droser, M.L., 2012. Ecological ranking of Phanerozoic biodiversity crises: the Serpukhovian (early Carboniferous) crisis had a greater ecological impact than the end-Ordovician. Geology 40 (2), 147–150. https://doi.org/10.1130/G32679.1.
- McLaughlin, P.I., Emsbo, P., Desrochers, A., Bancroft, A., Brett, C.E., Riva, J.F., Premo, W., Neymark, L., Achab, A., Asselin, E., Emmons, M.M., Melchin, M., 2016. Refining 2 km of Ordovician chronostratigraphy beneath Anticosti Island utilizing integrated chemostratigraphy. Can. J. Earth Sci. 53 (8), 865–874. https://doi.org/ 10.1139/cies-2015-0242.
- Mei, S.L., Henderson, C.M., 2001. Evolution of Permian conodont provincialism and its significance in global correlation and paleoclimate implication. Palaeogeogr. Palaeoclimatol. Palaeoecol. 170 (3-4), 237–260. https://doi.org/10.1016/S0031-0182(01)00258-9.
- Melchin, M.J., Sadler, P.M., Cramer, B.D., 2020. Chapter 21-the Silurian Period. In: Gradstein, F.M., Ogg, J.G., Schmitz, M.D., Ogg, G.M. (Eds.), Geologic Time Scale 2020. Elsevier, pp. 69–732.
- Melchin, M.J., Sadler, P.M., Cramer, B.D., Cooper, R.A., Gradstein, F.M., Hammer, O., 2012. Chapter 21–The Silurian Period. In: Gradstein, F.M., Ogg, J.G., Schmitz, M.D., Ogg, G.M. (Eds.), The Geologic Time Scale. Elsevier, Boston, pp. 525–558. https:// doi.org/10.1016/B978-0-444-59425-9.00021-4.
- Meyers, S.R., 2019. Cyclostratigraphy and the problem of astrochronologic testing. Earth-Sci. Rev. 190, 190–223. https://doi.org/10.1016/j.earscirev.2018.11.015.
- Meyers, S.R., Sageman, B.B., 2007. Quantification of deep-time orbital forcing by average spectral misfit. Am. J. Sci. 307 (5), 773–792. https://doi.org/10.2475/ 05.2007.01.
- Milanković, M., 1941. Kanon der Erdbestrahlung und seine Anwendung auf das Eiszeitenproblem. na.
- Mitchell, C.E., Chen, X., Bergstr, S.M., Zhang, Y.D., Wang, Z.H., Webby, B.D., Finney, S. C., 1997. Definition of a global boundary stratotype for the Darriwilian stage of the Ordovician System. Episodes 20 (3), 158–166. https://doi.org/10.18814/epiiugs/1997/v20i3/003.
- Mitchell, R.N., Kirscher, Uwe, 2023. Mid-Proterozoic day length stalled by tidal resonance. Nat. Geosci. https://doi.org/10.1038/s41561-023-01202-6.
- Montañez, I.P., Poulsen, C.J., 2013. The late Paleozoic ice age: an evolving paradigm. Annu. Rev. Earth Planet. Sci. 41, 629–656. https://doi.org/10.1146/annurev.earth.031208.100118.

- Munnecke, A., Calner, M., Harper, D., Servais, T., 2010. Ordovician and Silurian sea-water chemistry, sea level, and climate: a synopsis. Palaeogeogr. Palaeoclimatol. Palaeoecol. 389–413 https://doi.org/10.1016/j.palaeo.2010.08.001.
- Murphy, J., Nance, R., Cawood, P., 2009. Contrasting Modes of Supercontinent Formation and the Conundrum of Pangea. Gondwana Res. 15, 408–420. https://doi. org/10.1016/j.gr.2008.09.005.
- Myrow, P.M., Ramezani, J., Hanson, A.E., Bowring, S.A., Racki, G., Rakociński, M., 2014. High-precision U-Pb age and duration of the latest Devonian (Famennian) Hangenberg event, and its implications. Terra Nova 26 (3), 222–229. https://doi. org/10.1111/ter.12090.
- Nemyrovska, T.I., 1999. Bashkirian conodonts of the Donets Basin, Ukraine. Scr. Geol. 119. 1–115.
- Normore, L.S., Zhen, Y.Y., Dent, L.M., Crowley, J.L., Percival, I.G., Wingate, M.T.D., 2018. Early Ordovician CA-IDTIMS U-Pb zircon dating and conodont biostratigraphy, Canning Basin, Western Australia. Aust. J. Earth Sci. 65 (1), 61–73. https://doi.org/10.1080/08120099.2018.1411292.
- Ogg, J.G., Chen, Z.Q., 2020. The Triassic Period. In Geologic Time Scale 2020. Elsevier, pp. 903–953.
- Ogg, J.G., Ogg, G.M., Gradstein, F.M., 2016. 7–Silurian. In: Ogg, J.G., Ogg, G.M., Gradstein, F.M. (Eds.), A Concise Geologic Time Scale. Elsevier, pp. 71–84. https://doi.org/10.1016/C2009-0-64442-1.
- Paproth, E., Feist, R., Flajs, G., 1991. Decision on the Devonian–Carboniferous Boundary Stratotype. Episodes 14 (4), 331–336. https://doi.org/10.18814/epiiugs/1991/ v14i4/004.
- Pas, D., Da Silva, A.C., Over, D.J., Brett, C.E., Brandt, L., Over, J.S., Hilgen, F.J., Dekkers, M.J., 2020. Cyclostratigraphic calibration of the Eifelian Stage (Middle Devonian, Appalachian Basin, Western New York, USA). Geol. Soc. Am. Bull. 133 (1–2), 277–286. https://doi.org/10.1130/B35589.1.
- Pas, D., Hinnov, L., Day, J.E., Kodama, K., Sinnesael, M., Liu, W., 2018. Cyclostratigraphic calibration of the Famennian stage (Late Devonian, Illinois Basin, USA). Earth Planet. Sci. Lett. 488, 102–114. https://doi.org/10.1016/j.epsl.2018.02.010.
- Payne, J.L., Lehrmann, D.J., Wei, J.Y., Orchard, M.J., Schrag, D.P., Knoll, A.H., 2004. Large perturbations of the carbon cycle during recovery from the end-Permian extinction. Science 305, 506–509. https://doi.org/10.1126/science.1097023.
- Peng, X.F., Feng, Q.L., Li, Z.B., Meng, Y.Y., 2008. High-resolution cyclostratigraphy of geochemical records from Permo-Triassic boundary section of Dongpan, southwestern Guangxi, South China. Sci. China Earth Sci. 51 (2), 187–193. https:// doi.org/10.1007/s11430-008-0001-z.
- Pfeifer, L., Hinnov, L., Zeeden, C., Rolf, C., Laag, C., Soreghan, G., 2020. Rock magnetic Cyclostratigraphy of Permian Loess in Eastern Equatorial Pangea (Salagou Formation, South-Central France). Front. Earth Sci. 8, 241. https://doi.org/10.3389/ feart.2020.00241.
- Pointon, M.A., Chew, D.M., Ovtcharova, M., Sevastopulo, G.D., Crowley, Q.G., 2012. New high-precision U-Pb dates from western European Carboniferous tuffs; implications for time scale calibration, the periodicity of late Carboniferous cycles and stratigraphical correlation. J. Geol. Soc. Lond. 169, 713–721. https://doi.org/ 10.1144/jcs2011-092.
- Poty, E., Devuyst, F.X., Hance, L., 2006. Upper Devonian and Mississippian foraminiferal and rugose coral zonations of Belgium and northern France: a tool for Eurasian correlations. Geol. Mag. 143 (6), 829–857. https://doi.org/10.1017/ S0016756806002457.
- Poussart, P.F., Weaver, A.J., Barnes, C.R., 1999. Late Ordovician glaciation under high atmospheric CO₂: a coupled model analysis. Paleoceanography 14 (4), 542–558. https://doi.org/10.1029/1999PA900021.
- Qi, Y.P., Lambert, L.L., Nemyrovska, T.I., Wang, X.D., Hu, K.Y., Wang, Q.L., 2016. Late Bashkirian and early Moscovian conodonts from the Naqing section, Luodian, Guizhou, South China. Palaeoworld 25 (2), 170–187. https://doi.org/10.1016/j. palwor.2015.02.005.
- Racki, G., Baliński, A., Wrona, R., Krzysztof, M., Drygant, D., Szaniawski, H., 2012. Faunal dynamics across the Silurian—Devonian positive isotope excursions (δ^{13} C, δ^{18} O) in Podolia, Ukraine: comparative analysis of the Ireviken and Klonk events. Acta Palaeontol. Pol. 57, 795–832. https://doi.org/10.4202/app.2011.0206.
- Radzevičius, S., Spiridonov, A., Brazauskas, A., 2014. Application of Wavelets to the Cyclostratigraphy of the Upper Homerian (Silurian) Geluva Regional Stage in the Viduklė-61 Deep Well (Western Lithuania). In: Rocha, R., Pais, J., Kullberg, J., Finney, S. (Eds.), STRATI 2013. Springer Geology. Springer, Cham, pp. 437–440. https://doi.org/10.1007/978-3-319-04364-7_84.
- Radzevičius, S., Tumakovaitė, B., Spiridonov, A., 2017. Upper Homerian (Silurian) high-resolution correlation using cyclostratigraphy: an example from western Lithuania. Acta Palaeontol. Pol. 67, 307–322. https://doi.org/10.1515/agp-2017-0011.
- Rampino, M.R., Prokoph, A., Adler, A., 2000. Tempo of the end-Permian event: high-resolution cyclostratigraphy at the Permian–Triassic boundary. Geology 28, 643–646. https://doi.org/10.1130/0091-7613(2000)28<643:TOTEEH>2.0.CO;2.
- Rasmussen, C., Sinnesael, M., Thibault, N., Stouge, S., Andersen, M. L.S., Schovsbo, N., 2019. An imprint of astronomical climate forcing in the Baltoscandian Middle Ordovician 'orthoceratite limestone'? Geophys. Res. Abstr. 21, EGU2019–14038.
- Rasmussen, J.A., Thibault, N., Rasmussen, C.M., 2021. Middle Ordovician astrochronology decouples asteroid breakup from glacially-induced biotic radiations. Nat. Commun. 12 (1), 1–14. https://doi.org/10.1038/s41467-021-26396-4
- Richards, B.C., Aretz, M., 2009. Report of the task group to establish a GSSP for the Tournaisian–Visean boundary. Newslett. Carbonifer. Stratigr. 2, 9–10.
- Rodrigues, P., Hinnov, L.A., Franco, D.R., 2019. A new appraisal of depositional cyclicity in the Neoarchean-Paleoproterozoic Dales Gorge Member (Brockman Iron

- Formation, Hamersley Basin, Australia). Precambrian Res. 328, 27–47. https://doi.org/10.1016/j.precamres.2019.04.007.
- Roden, M.K., Parrish, R.R., Miller, D.S., 1990. The Absolute Age of the Eifelian Tioga Ash Bed, Pennsylvania. J. Geol. 98 (2), 282–285. https://doi.org/10.1086/629399.
- Rodionov, V.P., Dekkers, M.J., Khramov, A.N., Gurevich, E.L., Krijgsman, W., Duermeijer, C.E., Heslop, D., 2003. Paleomagnetism and cyclostratigraphy of the Middle Ordovician Krivolutsky suite, Krivaya Luka section, southern Siberian platform: record of non-synchronous NRM-components or a non-axial geomagnetic field? Stud. Geophys. Geod. 47 (2), 255–274. https://doi.org/10.1023/A: 1023767523451.
- Rogers, J.J., Santosh, M., 2004. Continents and Supercontinents. Oxford University Press. Rong, J.Y., Huang, B., 2014. Study of Mass Extinction over the past thirty years: a synopsis (in Chinese). Sci. Sin. Terrae 44, 377–404.
- Saltzman, M.R., Edwards, C.T., Leslie, S.A., Dwyer, G.S., Bauer, J.A., Repetski, J.E., Harris, A.G., Bergström, S.M., 2014. Calibration of a conodont apatite-based Ordovician ⁸⁷Sr, ⁸⁶Sr curve to biostratigraphy and geochronology: implications for stratigraphic resolution. Geol. Soc. Am. Bull. 126 (11–12), 1551–1568. https://doi. org/10.1130/B31038.1.
- Schmitz, M.D., Davydov, V.I., 2012. Quantitative radiometric and biostratigraphic calibration of the Pennsylvanian–Early Permian (Cisuralian) time scale and pan-Euramerican chronostratigraphic correlation. Geol. Soc. Am. Bull. 124 (3–4), 549–577. https://doi.org/10.1130/B30385.1.
- Scotese, C., 2009. Late Proterozoic plate tectonics and palaeogeography: a tale of two supercontinents, Rodinia and Pannotia. Geo. Soc. Lond. Spec. Publ. 326, 67–83. https://doi.org/10.1144/SP326.
- Scotese, C.R., 2021. An atlas of Phanerozoic paleogeographic maps: the seas come in and the seas go out. Annu. Rev. Earth Planet. Sci. 49, 679–728. https://doi.org/10.1146/ annurev-earth-081320-064052.
- Scotese, C.R., Song, H., Mills, B.J.W., van der Meer, D.G., 2021. Phanerozoic paleotemperatures: the earth's changing climate during the last 540 million years. Earth-Sci. Rev. 103503 https://doi.org/10.1016/j.earscirev.2021.103503.
- Sedgwick, A., 1838. In: A synopsis of the English series of stratified rocks inferior to the old red sandstone, pp. 675–685.
- Sepkoski, J., Sheehan, P., 1983. Diversification, Faunal Change, and Community
 Replacement during the Ordovician Radiations. In: Biotic Interactions in Recent and
 Fossil Benthic Communities. Springer, Boston, MA, pp. 673–717.
- Sepkoski, J., 1995. In: The Ordovician Radiation: Diversification and extinction shown by global–genus level taxonomic data. Ordovician Odyssey: Short papers for the Seventh International Symposium on the Ordovician System, pp. 393–396.
- Sepkoski, J., 1996. In: Patterns of Phanerozoic Extinction: a Perspective from Global Data Bases, pp. 35–51.
- Shen, S.Z., Crowley, J.L., Wang, Y., Bowring, S.A., Erwin, D.H., Sadler, P.M., Cao, C.Q., Rothman, D.H., Henderson, C.M., Ramezani, J., Zhang, H., Shen, Y.N., Wang, X.D., Wang, W., Lin, M., Li, W.Z., Tang, Y.G., Liu, X.L., Liu, L.J., Jin, Y.G., 2011. Calibrating the End-Permian mass extinction. Science 334, 1367–1372. https://doi.org/10.1126/science.1213454.
- Sinnesael, M., Loi, A., Dabard, M.P., Vandenbroucke, T.R.A., Claeys, P., 2022.

 Cyclostratigraphy of the Middle to Upper Ordovician successions of the Armorican Massif (western France) using portable X–ray fluorescence. Geochronology 4, 251–267. https://doi.org/10.5194/gchron-4-251-2022.
- Sinnesael, M., Mauviel, A., Desrochers, A., McLaughlin, P., De Weirdt, J., Vandenbroucke, T., Claeys, P., 2017. Cyclostratigraphy of the Upper Ordovician Vaureal Formation, Anticosti Island, eastern Canada. In: Geological Society of America Annual Meeting 2017.
- Sinnesael, M., Zivanovic, M., De Vleeschouwer, D., Claeys, P., 2018. Spectral moments in cyclostratigraphy: advantages and disadvantages compared to more classic approaches. Paleoceanogr. Paleoclimatol. 33 (5), 493–510. https://doi.org/ 10.1029/2017na003293
- Sinnesael, M., McLaughlin, P.I., Desrochers, A., Mauviel, A., De Weirdt, J., Claeys, P., Vandenbroucke, T.R.A., 2021. Precession-driven climate cycles and time scale prior to the Hirnantian glacial maximum. Geology 49 (11), 1295–1300. https://doi.org/ 10.1130/C40083.1
- Song, H.J., Wignall, P.B., Tong, J.N., Yin, H.F., 2013. Two pulses of extinction during the Permian–Triassic crisis. Nat. Geosci. 6, 52–56. https://doi.org/10.1038/NGE01649.
- Sørensen, A.L., Nielsen, A.T., Thibault, N., Zhao, Z.F., Schovsbo, N.H., Dahl, T.W., 2020. Astronomically forced climate change in the Late Cambrian. Earth Planet. Sci. Lett. 548 https://doi.org/10.1016/j.epsl.2020.116475.
- Spiridonov, A., Brazauskas, A., Radzevičius, S., 2016. Dynamics of abundance of the midto late Pridoli conodonts from the eastern part of the Silurian Baltic basin: multifractals, state shifts, and oscillations. Am. J. Sci. 316 (4), 363–400. https://doi. org/10.2475/04.2016.03.
- Sproson, A.D., 2020. Pacing of the latest Ordovician and Silurian carbon cycle by a \sim 4.5 Myr orbital cycle. Palaeogeogr. Palaeoclimatol. Palaeoecol. 540, 109543 https://doi.org/10.1016/j.palaeo.2019.109543.
- Sutcliffe, O.E., Dowdeswell, J.A., Whittington, R.J., Theron, J.N., Craig, J., 2000. Calibrating the late Ordovician glaciation and mass extinction by the eccentricity cycles of Earth's orbit. Geology 28 (11), 967–970. https://doi.org/10.1130/0091-7613(2000)28-967:CTLOGA>2.0.CO:2.
- Svensen, H.H., Hammer, Ø., Corfu, F., 2015. Astronomically forced cyclicity in the Upper Ordovician and U-Pb ages of interlayered tephra, Oslo Region, Norway. Palaeogeogr. Palaeoclimatol. Palaeoecol. 418, 150–159. https://doi.org/10.1016/j. palaeo.2014.11.001.
- Tabor, N.J., Montañez, I.P., Scotese, C.R., Poulsen, C.J., Mack, G.H., 2008. Paleosol archives of environmental and climatic history in paleotropical western Pangea during the latest Pennsylvanian through early Permian. Geol. Soc. Am. Bull. Spec. Pap. 441, 291–303. https://doi.org/10.1130/2008.2441(20).

- Taylor, T.N., Taylor, E.L., Krings, 2009. Paleobotany: The Biology and Evolution of Fossil Plants. In: Academic Press, p. 1252.
- Trotter, J.A., Williams, I.S., Barnes, C.R., Christophe, L., Nicoll, R.S., 2008. Did cooling oceans trigger Ordovician biodiversification? Evidence from conodont thermometry. Science 321 (5888), 550–554. https://doi.org/10.1126/science.1155814.
- Ueno, K., Hayakawa, N., Nakazawa, T., Wang, Y., Wang, X.D., 2013.
 Pennsylvanian–early Permian cyclothemic succession on the Yangtze Carbonate Platform, South China. Geo. Soc. Lond. Spec. Publ. 376 (1), 235–267. https://doi.org/10.1144/SP376.5.
- Villa, E., Alekseev, A.S., Barrick, J.E., Boardman, D.R., Djenchuraeva, A.V., Fohrer, B., Forke, H., Goreva, N.V., Heckel, P.H., Isakova, T.N., 2009. Selection of the conodont Idiognathodus simulator (Ellison) as the event marker for the base of the global Gzhelian Stage (Upper Pennsylvanian, Carboniferous). Palaeoworld 18, 114–119. https://doi.org/10.1016/j.palwor.2009.04.002.
- Wahlman, G.P., 2013. Pennsylvanian to Lower Permian (Desmoinesian-Wolfcampian) fusulinid biostratigraphy of Midcontinent North America. Stratigraphy 10 (1-2), 73-104.
- Walliser, O.H., Bultynck, P., Weddige, K., Becker, R.T., House, M.R., 1995. Definition of the Eifelian–Givetian Stage boundary. Episodes 18 (3), 107–115. https://doi.org/ 10.18814/epiiugs/1995/v18i3/002.
- Waltham, D., 2015. Milankovitch period uncertainties and their impact on cyclostratigraphy. J. Sediment. Res. 85, 990–998. https://doi.org/10.2110/ isr 2015.66
- Wang, X., Zhang, X., Gao, F., Zhang, M., 2020. Astronomical cycles of the Late Permian Lopingian in South China and their implications for third-order sea-level change. J. Ocean U. China 19 (6), 1331–1344.
- Wang, X.F., Svend, S., Chen, X.H., Li, Z.H., Wang, C.S., Stan, C.F., Zeng, Q.L., Zhou, Z.Q., Chen, H.M., Bernd, D.E., 2009. The Global Stratotype Section and Point for the base of the Middle Ordovician Series and the Third Stage (Dapingian). Episodes 32 (2), 96–113. https://doi.org/10.18814/epiiugs/2009/v32i2/003.
- Wanless, H.R., Shepard, F.P., 1936. Sea level and climatic changes related to late Paleozoic cycles. Geol. Soc. Am. Bull. 47 (8), 1177–1206. https://doi.org/10.1130/ GSAB-47-1177.
- Waters, C.N., Condon, D.J., 2012. Nature and timing of late Mississippian to Mid-Pennsylvanian glacio-eustatic sea-level changes of the Pennine Basin,UK. J. Geol. Soc. London 169, 37–51. https://doi.org/10.1144/0016-76492011-047.
- Weedon, G.P., 2003. Time-Series Analysis and Cyclostratigraphy: Examining Stratigraphic Records of Environmental Cycles. Cambridge University Press.
- Wei, R., Zhang, R., Li, M., Wang, X., Jin, Z., 2023. Obliquity forcing of lake-level changes and organic carbon burial during the late Paleozoic ice age. Glob. Planet. Change 223, 104092. https://doi.org/10.1016/j.gloplacha.2023.104092.
- Westphal, H., Hilgen, F., Munnecke, A., 2010. An assessment of the suitability of individual rhythmic carbonate successions for astrochronological application. Earth-Sci. Rev. 99 (1–2), 19–30. https://doi.org/10.1016/j.earscirev.2010.02.001.
- Williams, G., 1991. Milankovitch–band cyclicity in bedded halite deposits contemporaneous with late Ordovician-early Silurian glaciation, Canning Basin, Western Australia. Earth Planet. Sci. Lett. 103, 143–155. https://doi.org/10.1016/ 0012-821X(91)90156-C.
- Wu, H.C., Fang, Q., Wang, X.D., Hinnov, L.A., Qi, Y.P., Shen, S.Z., Yang, T.S., Li, H.Y., Chen, J.T., Zhang, S.H., 2019. An ~34 my astronomical time scale for the uppermost Mississippian through Pennsylvanian of the Carboniferous System of the Paleo-Tethyan realm. Geology 47 (1), 83–86. https://doi.org/10.1130/G45461.1.
- Wu, H.C., Zhang, S.H., Hinnov, L.A., Jiang, G.Q., Feng, Q.L., Li, H.Y., Yang, T.S., 2013. Time-calibrated Milankovitch cycles for the late Permian. Nat. Commun. 4 (1), 1–8. https://doi.org/10.1038/ncomms3452.
- Wu, Q., Ramezani, J., Zhang, H., Wang, T.T., Yuan, D.X., Mu, L., Zhang, Y.C., Li, X.H., Shen, S.Z., 2017. Calibrating the Guadalupian series (middle Permian) of South China. Palaeogeogr. Palaeoclimatol. Palaeoecol. 466, 361–372. https://doi.org/ 10.1016/j.palaeo.2016.11.011.
- Yao, X., Hinnov, L.A., 2019. Advances in characterizing the cyclostratigraphy of binary chert–mudstone lithologic successions, Permian (Roadian-lower Capitanian), Chaohu, lower Yangtze,South China. Palaeogeogr. Palaeoclimatol. Palaeoecol. 528 https://doi.org/10.1016/j.palaeo.2019.05.004.

- Yao, X., Zhou, Y.Q., Hinnov, L.A., 2015. Astronomical forcing of a Middle Permian chert sequence in Chaohu, South China. Earth Planet. Sci. Lett 422, 206–221. https://doi. org/10.1016/j.epsl.2015.04.017.
- Xue, W.Q., Li, B., Yan, J.X., Ellwood, B.B., Tomkin, J.H., Wang, Y., Zhu, Z.M., 2015. High-resolution floating point time scale (FPTS) of Permian Capitanian Stage in South China. Chinese J. Geophys-Ch. 58 (10), 3719–3734. https://doi.org/10.1002/ cip2.20199
- Yolkin, E.A., Sennikov, N.V., Bakharev, N.K., Izokh, N.G., Yazikov, A.Y., 1997a.
 Periodicity of deposition in the Silurian and relationships of global geological events in the middle Paleozoic of the southwestern margin of the Siberian continent. Russ. Geol. Geophys. 38, 636–647.
- Yolkin, E.A., Kim, A.I., Weddige, K., Talent, J.A., House, M.R., 1997b. Definition of the Pragian/Emsian Stage boundary. Int. Union Geol. Sci. 20 (4), 235–240. https://doi. org/10.18814/epiiugs/1997/v20i4/005.
- Young, S.A., Saltzman, M.R., Foland, K.A., Linder, J.S., Kump, L.R., 2009. A major drop in seawater 875r/86Sr during the Middle Ordovician (Darriwillan): links to volcanism and climate? Geology 37 (10), 951–954. https://doi.org/10.1130/ G30152A 1
- Zeebe, R.E., 2017. Numerical solutions for the orbital motion of the solar system over the past 100 Myr: limits and new results. Astrono. J. 154 (5), 193. https://doi.org/
- Zeebe, R.E., Lourens, L.J., 2022. Geologically constrained astronomical solutions for the Cenozoic era. Earth Planet. Sci. Lett. 592, 117595 https://doi.org/10.1016/j. epsl.2022.117595.
- Zhang, T., Li, Y.F., Fan, T.L., Da Silva, A.C., Shi, J.Y., Gao, Q., Kuang, M.Z., Liu, W.W., Gao, Z.Q., Li, M.S., 2022. Orbitally-paced climate change in the early Cambrian and its implications for the history of the Solar System. Earth Planet. Sci. Lett. 583 https://doi.org/10.1016/j.epsl.2022.117420.
- Zhang, X., Zhang, T.S., Zhao, X.M., Zhu, H.H., Mihai, E.P., Chen, L., Yong, J.J., Xiao, Q., Li, H.J., 2021. Effects of astronomical orbital cycle and volcanic activity on organic carbon accumulation during late Ordovician–early Silurian in the Upper Yangtze area, South China. Petrol. Explor. Dev. 48 (4), 850–863. https://doi.org/10.1016/S1876-3804(21)60071-X.
- Zhang, Y.B., Zhao, Z.J., Yuan, S.Q., Zheng, M., 2011. Application of spectral analysis to identify milankovitch cycles and high-frequency sequences-take the Lower Ordovician Yingshan Formation of Mid-Tarim Basin as an example. J. Jilin Univ. (Earth Sci. Ed.) 41 (02), 400–410. https://doi.org/10.13278/j.cnki. jjuese.2011.02.029.
- Zhao, Z.F., Thibault, N.R., Dahl, T.W., Schovsbo, N.H., Sorensen, A.L., Rasmussen, C.M. O., Nielsen, A.T., 2022. Synchronizing rock clocks in the late Cambrian. Nat. Commun. 13 (1), 1990. https://doi.org/10.1038/s41467-022-29651-4.
- Zhao, Z.J., Chen, X., Pan, M., Wu, X.N., Zheng, X.P., Pan, W.Q., 2010. Milankovitch cycles in the Upper Ordovician Lianglitage Formation in the Tazhong—Bachu Area, Tarim Basin. Acta Geol. Sin. 84 (04), 518–536.
- Zhong, Y.Y., Chen, D.Y., Fan, J.X., Wu, H.C., Fang, Q., Shi, M.N., 2019.
 Cyclostratigraphic Calibration of the Upper Ordovician (Sandbian–Katian) Pagoda and Linhsiang Formations in the Yichang Area, South China. Acta Geol. Sin-Engl. 93 (S3) 177–180
- Zhong, Y.Y., Wu, H.C., Fan, J.X., Fang, Q., Shi, M.N., Zhang, S.H., Yang, T.S., Li, H.Y., Cao, L.W., 2020. Late Ordovician obliquity-forced glacio-eustasy recorded in the Yangtze Block, South China. Palaeogeogr. Palaeoclimatol. Palaeoecol. 540, 109520 https://doi.org/10.1016/j.palaeo.2019.109520.
- Zhong, Y.Y., Wu, H.C., Zhang, Y.D., Zhang, S.H., Yang, T.S., Li, H.Y., Cao, L.W., 2018. Astronomical calibration of the Middle Ordovician of the Yangtze Block, South China. Palaeogeogr. Palaeoclimatol. Palaeoecol. 505, 86–99. https://doi.org/10.1016/j.palaeo.2018.05.030.
- Zhou, M., Wu, H., Hinnov, L.A., Fang, Q., Zhang, S., Yang, T., Shi, M., 2022. Empirical reconstruction of Earth-Moon and Solar System dynamical parameters for the past 2.5 billion years from cyclostratigraphy. Geophys. Res. Lett. 49 https://doi.org/10.1029/2022GL098304 e2022GL098304.
- Zhu, M.Y., Yang, A.H., Yuan, J.L., Li, G.X., Zhang, J.M., Zhao, F.C., Ahn, S.-Y., Miao, L.Y., 2018. Cambrian integrative stratigraphy and timescale of China. Sci. China Earth Sci. 62, 1–36.